

MODUL PHYSIK590: MASTERARBEIT

Masterarbeit im Fach Physik

Coupled Anisotropic Heisenberg Chains in a Transverse Field

Specific Heat and Phasediagram of Cs_2CoCl_4

von
Benjamin Buldmann

Augst 22, 2012

1. Gutachter: Prof. Dr. A. Rosch
2. Gutachter: Priv.-Doz. Dr. T. Lorenz

angefertigt am
Institut für Theoretische Physik der Universität zu Köln

vorgelegt der
Mathematisch-Naturwissenschaftlichen Fakultät der
Universität zu Köln

Abstract

In the presented work the Cs_2CoCl_4 system, which can be seen as a compound of weakly coupled spin chains, was used as a starting point for several theoretical considerations.

First of all the concept of local interactions of spins on a one dimensional chain will be developed. This considerations will be related to several Heisenberg chains containing an anisotropy term Δ . The influence of such a term as well as the effect of an external magnetic field will be considered. It is fundamentally important to distinguish between models containing a longitudinal or a transversal field. The emerging ground states, that are totally different, will be discussed. Beside several works on longitudinal fields only a few consider transversal fields. One reason could be the complication brought into the model, as the field does not commute with the spin-spin interaction term. This work will try to contribute to further insight in the case of transversal fields.

The system under consideration is not exactly solvable. This means it is necessary to develop certain approximations such as a Mean field approach. In the second chapter of this work an advanced application of the principle of Mean field theory will developed. It will be used to describe the behaviour of spins in a chain as well as to describe the effect occurring through the coupling of those chains. In there two particle terms are decoupled using the evaluation of expectations values with respect to a chosen reference Hamilton \mathcal{H}_0 . With the definition of such a reference system new parameters are introduced. They can be found using a minimum condition of the Mean field free energy F_{MF} . From this, self consistent equations arise, which will be solved iteratively and equivalently by minimization of the free energy with respect to such parameters. The values obtained by the mentioned techniques can be used e.g. to calculate thermodynamic quantities.

Basically in the same way, self consistent equations will be derived in the case of coupled chains. In contrast to further works on this material, different chain types will be considered where the type relation is defined through the orientation of corresponding easy planes. The self consistent equations derived by this will be solved iteratively. This solution provides an numerical approach to the spin configuration of the system.

From this point on one can calculate the staggered and uniform magnetization of the system. Furthermore one can calculate phase transitions, which are related to the magnetic configuration. It will be shown, that the material shows first and second order quantum phase transitions.

Contents

1	Introduction	7
2	Theoretical considerations	9
2.1	Anisotropic Heisenberg model in a transverse field	9
3	Mean Field Concept	13
3.1	Physical input and geometry of Cs_2CoCl_4	13
3.2	Concept of Mean Field Theory	21
3.3	Mean field approach in one dimension	24
3.3.1	Operator Identities	24
3.3.2	Mean-field approach	25
3.3.3	Exact solution of the effective 1d model	27
3.3.4	Self consistent equations	29
3.4	Mean field approach for coupled chains	30
3.4.1	Introduction to the 3d Problem	30
3.4.2	Construction of the Effective Hamiltonian	30
3.4.3	Classical analysis of the effective Hamiltonian \mathcal{H}_{eff}	34
3.4.4	Explicit derivation of the Mean field equations	37
4	Numerical solutions	41
4.1	Experimental results of measurements on Cs_2CoCl_4	41
4.1.1	Specific heat measurements	41
4.1.2	Phase diagram of Cs_2CoCl_4	43
4.2	Verification of the one dimensional model	44
4.2.1	Exact diagonalization	44
4.2.2	Low temperature and high field	46
4.2.3	High temperature limit	47
4.3	Calculation of C_V for the 1d system	50
4.3.1	1d c++ Program	50
4.3.2	Exact diagonalization vs. Mean field	51
4.4	Specific heat for coupled chains in the 3d setting	54
4.5	Phase diagram for coupled chains	55
4.5.1	Staggered magnetization and Iteration	56
4.5.2	Free energy	59
4.5.3	Phase diagrams	61
4.5.4	Scaling estimates	65
5	Summary	69

1 Introduction

Concerning the theoretical part of this work two basic aspect should be mentioned: The principle of local interactions and the theory of Mean field (Mf) fields in combination with a minimum condition for an estimate of the free energy.

In the 1930's Heisenberg¹ and Dirac² independently introduced the description of ferromagnetism in terms of local spin interactions. They invented the picture of chain interactions via nearest neighbour interactions. Using this description there were huge efforts and successes concerning the description of many body systems through a local interaction approximation. Famous effects like superconductivity, quantum Hall Effect or the Kondo Effect can be derived using this approach. The second theoretical aspect, that has to be mentioned here is the idea of treating a system in a Mf approach. It is not a recent aspect, as in the 1970's several publications related to this topic were published. Eugene³ wrote a book were he introduced the Mf theory of magnetic phase transitions. Additionally to the MF approach, a variational principle providing a formal estimate for an upper bound of the free energy, developed by Feynman⁴ is used.

On the other hand the material Cs_2CoCl_4 was studied in the 1970's, for example by Alga *et al.*⁵, who did specific heat measurements on Cs_2CoCl_4 . From these measurements it was concluded that this material can be described using an anisotropic Hamiltonian built of local spin-spin interactions. Similar conclusions were drawn by investigation of other tetrahedral cobalt salts, which have been studied earlier, but all of them not in a external magnetic field. The field direction is a crucial detail, either the field is in the anisotropy direction or it is not. In the first case, the field term commutes with the spin-spin interaction. This case was studied extensively in the 1970's by Yang *et al.*⁶. Due to the commuting character of the field this model can be solved exactly using the Bethe ansatz⁷.

In this work the other case is studied in which the field does not commute, as it is applied in the anisotropy direction. Those systems behave drastically different compared to the case of longitudinal fields. In the early 1980's Kurmann *et al.*^{8,9} theoretically considered XXZ models in a transverse field. From these considerations two main aspects concerning this work follow. Firstly the field in the xy -plane induces long range order, namely antiferromagnetic order perpendicular to the field, where the corresponding ground state is called spin flop state. Secondly the field causes a gap in the excitations spectrum. For a specific external magnetic field the gap closes and the long range order is destroyed at a Mf-type phase transition. This critical field is below that where the system is fully polarized. Altogether these systems can show a quantum phase transition through a quantum critical point, where the external field acts the tuning parameter.

1 Introduction

In the following theoretical approach the mentioned anisotropic Heisenberg chains are fundamentally considered and classified with respect to the several symmetries they hold. By means of numerical calculations, the magnetic configuration of the single spin chains and of coupled chains is found. Using these results, thermodynamic properties such as, specific heat or the magnetization is calculated. In the case of coupled chains, quantum phase transitions could be calculated and thus a phase diagram constructed. Most of these results are comparable to measurements done recently.

2 Theoretical considerations

2.1 Anisotropic Heisenberg model in a transverse field

In this section several aspects concerning the Heisenberg model will be briefly discussed. The specific model, which is taken under further analysis in this work, will be classified with respect to models occurring in the context of Heisenberg chains. The effects will be described, which are caused by the assumptions taken. In the last part of this section, the specific model mentioned above will be described concerning quantum phases.

Beside other well studied models the spin-1/2 Heisenberg chain is one of the most studied and understood models providing quantum phase transitions. The most general Heisenberg chain model under consideration can be defined through:

$$\mathcal{H} = \sum_{ij} \sum_a J_{ij}^a S_i^a S_j^a, \quad (2.1)$$

where the summation $\sum_a, a \in \{x, y, z\}$ runs over all three spin components, \sum_{ij} over all sites and couples the spins sitting on the lattice site i and j . The term S_i^a denotes the usual spin operator at a given site i . J_{ij}^a is the anisotropic spin-spin interaction constant, also called exchange energy. If all $J_{ij}^a < 0$, the coupling is called ferromagnetic and if all $J_{ij}^a > 0$, it is called antiferromagnetic. This corresponds to the preferred ground state of the specific model. It is obvious, that for $J_{ij}^a < 0$, the spins prefer to be parallel to minimize the energy and it turns out that they form ferromagnetic order. The sum \sum_{ij} reduces mostly to the summation over nearest neighbouring lattice sites denoted by $\sum_{\langle ij \rangle}$. This corresponds to an exchange energy J_{ij} , which is finite only for nearest neighbours. More commonly the model is represented by $\mathcal{H} = \sum_{i,a} J^a S_i^a S_{i+1}^a$. In the case of the spin 1/2 Heisenberg model they are connected to the Pauli spin matrices σ^a via:

$$S_i^a = \frac{\sigma_i^a}{2} \quad \sigma^a \in \{\sigma^x, \sigma^y, \sigma^z\} = \left\{ \begin{bmatrix} 0 & 1 \\ 1 & 0 \end{bmatrix}, \begin{bmatrix} 0 & -i \\ i & 0 \end{bmatrix}, \begin{bmatrix} 1 & 0 \\ 0 & -1 \end{bmatrix} \right\}. \quad (2.2)$$

where \hbar is set to one. This model can be used to describe a huge field of different states of matter, such like ferro- or antiferromagnetism on lattices. The fact that for example ferromagnetism can be described by an effective Hamiltonian containing only the local spin-spin interactions was firstly shown by Heisenberg¹ and Dirac². The term effective Hamiltonian describes the aspect that the global Coulomb interactions of electrons, can be described by the local interactions of neighbouring spins.

As long as the J^a are arbitrary the model is often called the XYZ model. But one can introduce several restrictions, $J^x = J^y \neq J^z$ or $J^x = J^y = J^z$, which correspond to

2 Theoretical considerations

XXZ respectively XXX models¹⁰. If one chooses $J^x = J^y = 0$ one ends up with the well studied Ising Model¹¹. The particular choice in this work is a XXZ model, where the anisotropy is partially broken by $J^x = J = J^y$ and $J^z = J\Delta$. This is motivated through the claim¹² that the properties of the material Cs_2CoCl_4 are reproduced by taking the following Hamiltonian:

$$\mathcal{H} = J \sum_i (S_i^x S_{i+1}^x + S_i^y S_{i+1}^y + \Delta S_i^z S_{i+1}^z) = J \sum_i \mathbf{S}_i^\top \hat{J} \mathbf{S}_{i+1} \quad (2.3)$$

in the field less case, where the objects $\mathbf{S}_i \equiv \{S_i^x, S_i^y, S_i^z\}^\top$ and $\hat{J} \equiv \begin{bmatrix} 1 & 0 & 0 \\ 0 & 1 & 0 \\ 0 & 0 & \Delta \end{bmatrix}$ are introduced.

The several models refer to different symmetries. Concerning symmetries the rotational invariant XXX model is in $SU(2)$. Breaking this symmetry by going to the XXZ model one has rotational freedom in the xz plane referring to an $U(1)$ symmetry¹². Concerning an external magnetic field, basically one has two distinct options. Firstly a so called longitudinal field in the same direction than the anisotropy and secondly a transversal field not in the anisotropy direction. In general the Hamiltonian would read as:

$$\mathcal{H} = J \sum_i \mathbf{S}_i \hat{J} \mathbf{S}_{i+1} - B \sum_i S_i^x \quad (2.4)$$

where the field should be specified according to the assumption taken in to account. The case of longitudinal fields was studied intensively and is presented for example in the book *Quantum Many-Body Systems in One Dimension* by Ha¹³ or in the papers of Yang *et al.*^{6,14}. The basic aspect of the application of longitudinal fields is that no further spatial symmetry is broken. In this case, the longitudinal field commutes with the XXZ Hamiltonian and thus the model is exactly solvable using the Bethe ansatz⁷. The model under consideration is Eq.(2.4) an additional transversal field in the x direction. In general this particular choice breaks the rotational symmetry in the xy -plane. By this the exact integrability of the XXZ model is lost and one ends up with the following model:

$$\begin{aligned} \mathcal{H} &= J \sum_i \mathbf{S}_i \hat{J} \mathbf{S}_{i+1} - B_x \sum_i S_i^x \\ &= J \sum_i (S_i^x S_{i+1}^x + S_i^y S_{i+1}^y + \Delta S_i^z S_{i+1}^z) - B_x \sum_i S_i^x \end{aligned} \quad (2.5)$$

In 2002, Krivnov *et al.* stated, that due to its mathematical complexity this model has not been studied much⁷ and following they considered such models in much detail. The following description of the qualitative aspects and phases of these models is inspired by those publications.

Phases of the anisotropic Heisenberg chain in a transverse field

In the model Eq.(2.5), one has two parameters to vary, the anisotropy Δ and the external transversal field B_x . Concerning these parameters the ground state properties of this model will be described.

$B_x = 0$

If the field is $B_x = 0$ one has a XXZ model, depending on Δ which is exactly solvable using a Bethe ansatz. For $\Delta > 1$ the model is a Ising like model for which the ground has Néel long range order along the z -axes¹⁵. Néel long-range order describes order of alternating spin orientation, e.g. $S_i^z = (-1)^i \langle S^z \rangle$. This fact is obvious, as the dominant term in Eq. (2.5) is minimized for $S_{i+1}^z = -S_i^z$. In this phase one can define a finite quantity, the staggered magnetization:

$$\mathbf{M}_{st} \equiv \langle \mathbf{S}_{st} \rangle \quad \text{with } \mathbf{S}_{st} = \frac{1}{L} \sum_i (-1)^i \mathbf{S}_i \quad (2.6)$$

which is conserved on long range. It turns out that the excitation spectrum is gapped⁷.

For $\Delta < -1$ the opposite kind of order sets in, namely a ferromagnetic phase characterized by finite uniform magnetization:

$$\mathbf{M}_{un} \equiv \langle \mathbf{S}_{un} \rangle \quad \text{with } \mathbf{S}_{un} = \frac{1}{L} \sum_i \mathbf{S}_i. \quad (2.7)$$

The ground state is the classical ferromagnet¹⁵, where every spin is aligned parallel to each other. In this phase one has a gap in the excitation spectrum, lying above the ferromagnetic ground state.

In the intermediate regime, where $-1 < \Delta \leq 1$ the system is in the so-called Luttinger liquid phase, in which the correlations decay algebraically and the spectrum is linear⁷.

 $B_x \neq 0$

In the other case, where $B_x \neq 0$, the model becomes more complicated, because the total spin projection S^z is not a good quantum number anymore. In the case of large Δ , for $|\Delta| \rightarrow \infty$ the model reduces again to a 1d Ising model in a transverse field.⁷ This model can be solved exactly (e.g. see Sachdev¹⁶) by transforming it into the system of non-interacting fermions, called Jordan Wigner transformation¹⁷.

There is a critical field, $B_x^{crit} = |\Delta|/2$, at which the system undergoes a phase transition, the gap closes and the long range order in the z direction vanishes. This phase transition is suggested to happen for any $\Delta > 0$ at some critical $B_x^{crit}[\Delta]$ ¹⁸. Similar to the $B_x = 0$ case there is for $B_x < B_x^{crit}[\Delta]$: Néel order for $\Delta > 1$ and ferromagnetic ordering for $\Delta < -1$. For intermediate anisotropy, $|\Delta| < 1$ and below a critical field $B_x^{crit}[\Delta]$, the long range order changes fundamentally. In contrast to the staggered ($\Delta > 1$) or ferromagnetic order ($\Delta < -1$) in the z -direction, it develops a staggered magnetization M_{st}^y along the y -direction. As long as this quantity is finite one can also speak of a spin-flop phase, because the spins are oriented perpendicular to the field. Additionally they are able to tilt continuously towards the field. This phase is the ground state until a critical field $B_x = B_x^{crit}[\Delta]$ is reached at which the perpendicular staggered order vanishes. In this phase the system is gaped except at $B_x = 0$ ^{19,20}.

2 Theoretical considerations

In every case, for fields above the critical value $B_x > B_x^{crit}[\Delta]$, the system is fully polarized. One can speak of a paramagnetic phase, where all spins are aligned along the external field direction.

In the special case of $\Delta = 1$, the model stays integrable, as it is isotropic in the yz -plane. The model stays in the antiferromagnetic phase until the critical field of $B^c = 2J$ is reached. At this critical point the model undergoes a phase transition of the Pokrovsky-Talapov type⁷, where the ground state changes into a fully ferromagnetically ordered state. In the other case where $\Delta = -1$, the model is an isotropic ferromagnetic model in a staggered magnetic field¹⁵. There is no exact solution to it, but it was shown that the system remains gapless up to an critical field B^{crit} , where a phase transition of the Kosterlitz-Thouless type occurs^{20,21}.

Phasediagram

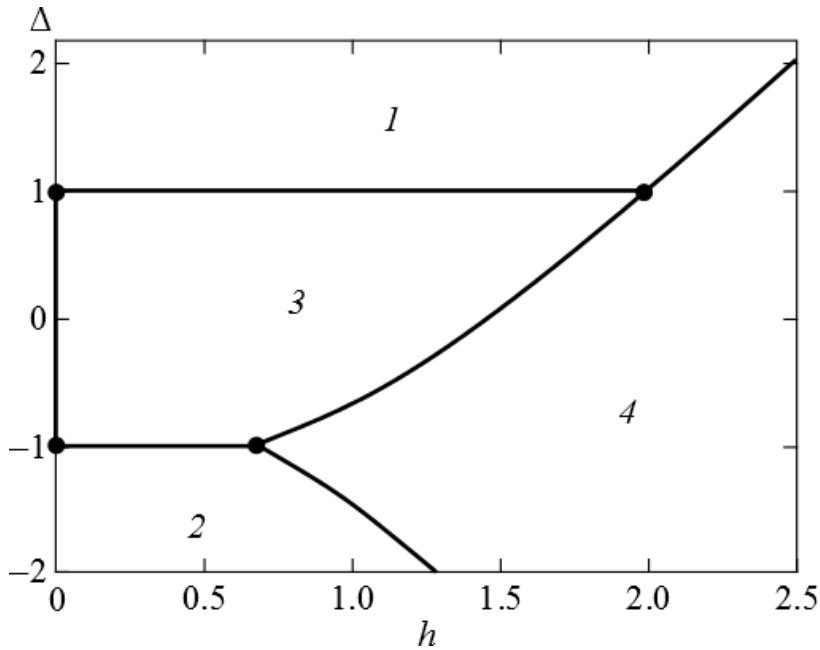


Figure 2.1: Phase diagram¹⁵ of the Heisenberg chain in a transverse field. The solid lines are the critical lines corresponding to $B_c[\Delta]$. The several regions correspond to the following long range orders. 1: Néel_z, 2: Ferro_z, 3: Néel_y and 4: Para_x. Explanation and further details can be found in the text Sec.2.1

All together one can draw the following conclusion. The XXZ chain in a transverse field owns a phase diagram containing four regions corresponding to several distinct long range ordered phases. In Fig.2.1 the region 1 is characterized by a Néel order along the z -axis. The region 2 carries mainly a ferromagnetic order in the z -direction. In the region 3 there is predominantly Néel order along the y -axis. Finally in the region 4 there is no long range order additionally to the magnetization along the external field in x -direction, which is present in every region (1-4).

3 Mean Field Concept

3.1 Physical input and geometry of Cs_2CoCl_4

There are several aspects to describe concerning Cs_2CoCl_4 . The basic aspect certainly is the crystal structure. Another aspect is how this system can be described in terms of spin chains and how it orders. The second point strongly depends on how the system and its constituent interact. Therefore a picture of how interactions are mediated is needed.

The real space, unit cell of Cs_2CoCl_4 , is given by the lattice parameters:

$$a = 9.71 \text{ \AA} \quad b = 7.27 \text{ \AA} \quad c = 12.73 \text{ \AA} \quad (3.1)$$

at $T = 0.3\text{K}$ ^{23,24}. The unit cell of Cs_2CoCl_4 is shown in Fig. 3.1. It crystallizes in an orthorhombic (and non symmorphic) space group Pnma ^{12,25}. There are four spin-3/2 Co^{2+} ions per unit cell, occupying the following positions¹² (in units of Eq. (3.1)), where the numbering refers to Fig. 3.1:

$$\mathbf{v}_1 = \left(z_0, \frac{1}{4}, y_0 \right) \quad \mathbf{v}_2 = \left(\frac{1}{2} + z_0, \frac{1}{4}, \frac{1}{2} - y_0 \right) \quad (3.2)$$

$$\mathbf{v}_3 = \left(1 - z_0, \frac{3}{4}, 1 - y_0 \right) \quad \mathbf{v}_4 = \left(\frac{1}{2} - z_0, \frac{3}{4}, \frac{1}{2} + y_0 \right) \quad (3.3)$$

with $y_0 = 0.422$ and $z_0 = 0.235$.

Each Co^{2+} ion is tetrahedrally surrounded by chlorine ions (a sketch of the situation is given in Fig. 3.2). If this tetrahedral environment would not be distorted the ground state of every Co^{2+} ion would be a fourfold degenerated. In Cs_2CoCl_4 two of the four surrounding Cl^- are shifted out of the symmetry position, they are axial distorted⁵. This fact together with spin-orbit coupling lead to a splitting into two Kramer's doublets.

It depends on the sign of the axial distortion D which doublet will be higher in energy, the high-spin $|\pm 3/2\rangle$ or the low-spin doublet $|\pm 1/2\rangle$. For this effect one can write down a crystal field Hamiltonian for the spin-3/2 operators J_i^z :

$$\mathcal{H}[D] = D \sum_i (J_i^z)^2 \quad (3.4)$$

In Materials such as, Cs_3CoCl_5 , Cs_3CoBr_5 and Rb_3CoCl_5 , which have similar tetrahedral cobalt salt surrounding⁵ D is negative and thus the high-spin doublet is lower than the low-spin doublet. They are separated by about $-2D/k_B \sim 10 - 15\text{K}$. Susceptibility measurements done by Figgis *et al.*²² provided that in the case of Cs_2CoCl_4

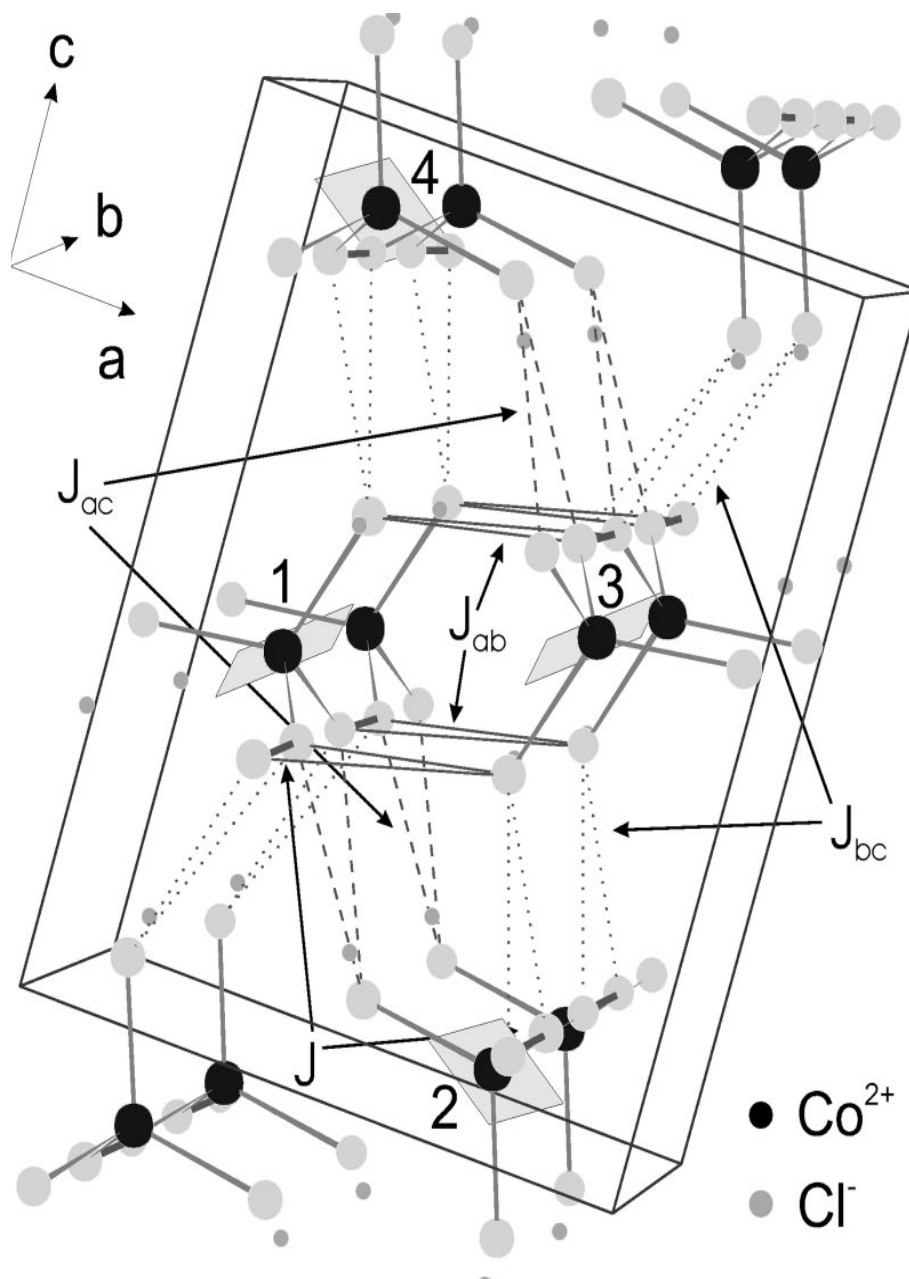


Figure 3.1: This figure shows the crystal structure of Cs_2CoCl_4 (figure taken from Kenzelmann *et al.*¹²). There are twelve Co^{2+} ions shown, each of them is surrounded by four Cl^- ions. The indicated box is the unit cell containing four of the Co^{2+} ions, labeled from 1 to 4. There are several interaction paths visualizing the interaction of the Co^{2+} ions. J denotes an antiferromagnetic super exchange interaction path along the b -axis with interaction energy J . This interaction direction is meant to be the chain direction. Then there are several paths, labeled with J_{ac} , J_{ab} and J_{bc} . The suffix indicates in which plane the path 'lies', or more precise the involved Co^{2+} are lying. The shaded rectangular planes symbolically indicate the orientations of the xy easy-planes (e.g. Figgis *et al.*²²). Further descriptive details can be found in the text.

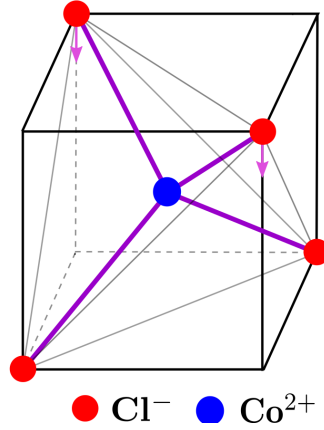


Figure 3.2: In this figure the tetrahedral surrounding of the Co^{2+} ions by Cl^- ions is sketched. One option how the CoCl_4^{2-} tetrahedron can be deformed from a perfect tetrahedron is indicated with arrows. The distortion is reported to be about some degrees²⁶

the sign of D is opposite. With the confirmation by McElearney *et al.*²⁷, it became clear that in the case of Cs_2CoCl_4 the low-spin states are lowest (see Fig.3.3). The separation of those doublets is of the same order and the spin-spin interaction was found to be antiferromagnetic.

The crystalline structure derived by now, is assumed to have magnetic Co^{2+} ions sitting on given sites, surrounded by an distorted tetrahedral crystal field. To each ion an effective spin-3/2 can be assigned, resulting in two energy levels, both doubly degenerated. The question at this stage is, how these spins interact and what are the nearest neighbours. The distances between the Co^{2+} atoms, following the notation of Fig.3.1, are:

$$d_{1,1}^{\text{Co}} = b \quad d_{1,2}^{\text{Co}} = d_{3,4}^{\text{Co}} = 6.56 \text{ \AA} \quad d_{1,3}^{\text{Co}} = 6.61 \text{ \AA} \quad d_{1,4}^{\text{Co}} = d_{2,3}^{\text{Co}} = 7.34 \text{ \AA}, \quad (3.5)$$

where the underscript i, j refers to the several sites introduced in Fig.3.1. Naively judging from these distances one would follow that the sites 1, 2 and 3, 4 are nearest neighbours, as $d_{1,2}^{\text{Co}} < b$. More established analysis considers the interaction of neighbouring spins via super exchange interaction, involving at least two Cl^- atoms. This Cl^- atoms act as mediators and because the super exchange integral decreases rapidly with distance, one has to focus on the Cl^- distances. It turns out that there is one distance about 10 percent shorter than all others, namely $d_{1,1}^{\text{Cl}}$ which is in b -direction¹²:

$$d_{1,1}^{\text{Cl}} = \frac{b}{2} = 3.64 \text{ \AA} \quad d_{1,2}^{\text{Cl}} = 4.05 \text{ \AA} \quad d_{1,3}^{\text{Cl}} = 4.04 \text{ \AA} \quad d_{1,4}^{\text{Cl}} = 4.01 \text{ \AA} \quad (3.6)$$

Considering these distances, there is a specific direction, which provides the most energy gain by super exchange interaction. Moreover the angle between the Co-Cl bond and the Cl-Cl bond is relatively large (145°) with respect to the other bonds. The other paths have distances of about $\sim 4 \text{ \AA}$ and have sharper angles. From these considerations one expect the super exchange interaction in the b -direction to be the strongest. This path is labeled with J, which will be the notation for the interaction

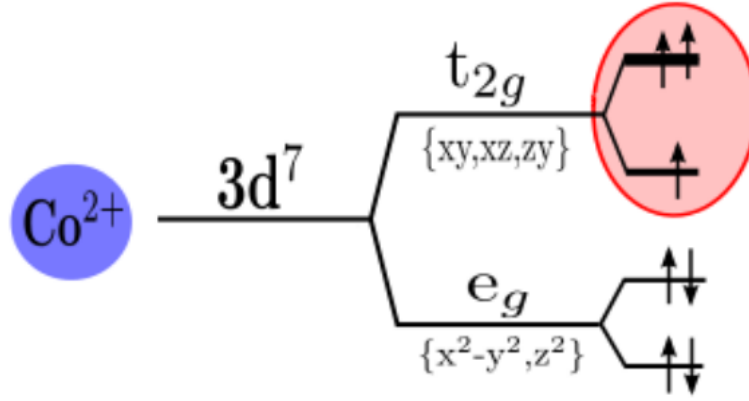


Figure 3.3: Shown is the term diagram of the Co^{2+} ions in the tetrahedral surrounding. The electronic configuration of Cs_2CoCl_4 is such that there are seven of in total $25 e^-$ electrons per ion, in the 3d orbital. This level splits up into the two well known levels: t_{2g} and e_g , containing the orbitals indicated. The reason for this splitting is the presence of the tetrahedral crystal field. This two levels split up further due to the non perfect cubic symmetry. The e_g level is fully occupied, but the t_{2g} is not and the two(!) levels are not fully occupied. To indicate that there are two high energy levels (xz , zy), they are artificially drawn not at the same height. This three spins form the effective spin-3/2 system, which is analyzed (more details can be found in the text).

energy in the formal description. Other paths can be related, as in Fig. 3.1 marked, there is $d_{1,2}^{Cl} \hat{=} J_{ac}$, $d_{1,3}^{Cl} \hat{=} J_{ab}$ and $d_{1,4}^{Cl} \hat{=} J_{bc}$.

For small temperatures, $T \ll D$, one can assume that only the lower lying doublet is occupied. This induces the picture of an effective spin-1/2 chain system in the b -direction. In this temperature regime one can describe the system using an XXZ-Hamiltonian. As long as one is interested in the calculation for one chain, one could start at this point constructing the Hamiltonian (see 3.3).

If 3d effects should be encountered one has to refer to the fact, that rotations of the distorted CoCl_4 tetrahedron lead to different orientations of the xy -easy-planes and thus there is only the b -axis as a common axis left. Even and odd site indices carry the same easy-plane, which lead to two types of chains: A- and B-type (c.f. Fig. 3.4). The angle between those planes is called β . Its numerical values is given contradictory to be: $\beta = -38.8^\circ$ ²² or $\beta = 19.4^\circ$ ¹².

An additional aspect is the lattice formed by these different chains. Concerning the real positions of the different ions, several assumptions are taken to describe the material in a simplified way. It was already argued that there is one predominant interaction direction, so that the system can be regarded as weakly coupled spin chains.

By considering the results of neutron scattering done by Kenzelmann *et al.*¹² presented in Fig. 3.5 one can see that several chains couple frustrated and others not. Especially there is frustrated coupling from sites 1&2 to sites 3&4 and vice versa. Elsewise

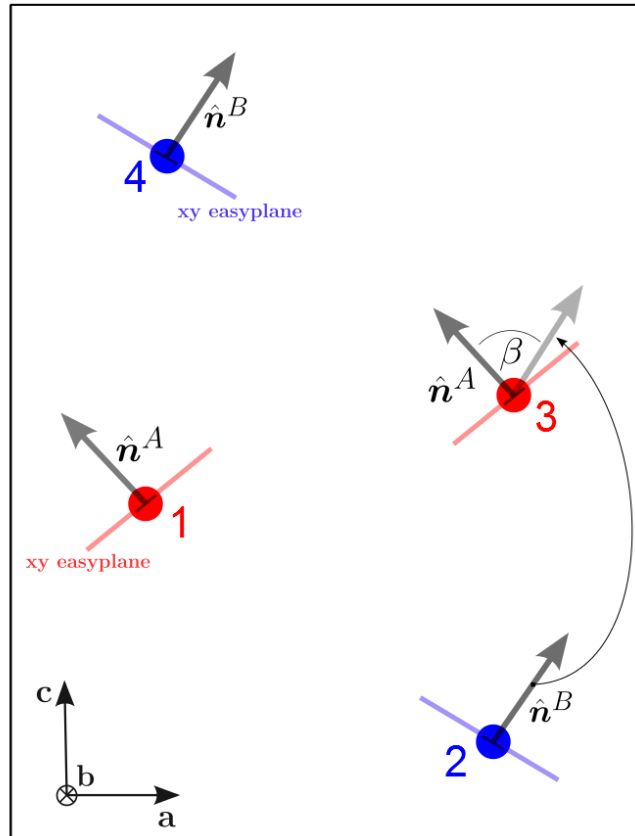


Figure 3.4: In this figure again the unit cell of Cs_2CoCl_4 is shown. But now the focus lies on the relative angle between the denoted local easy-planes according to the four Co^{2+} ions. The numbering is similar to that of Fig. 3.1. As two of them carry the same easy-plane there are two specific directions perpendicular to the b direction: \hat{n}^A and \hat{n}^B . This two directions define the two types of chains: A and B , which is considered in the further calculation.

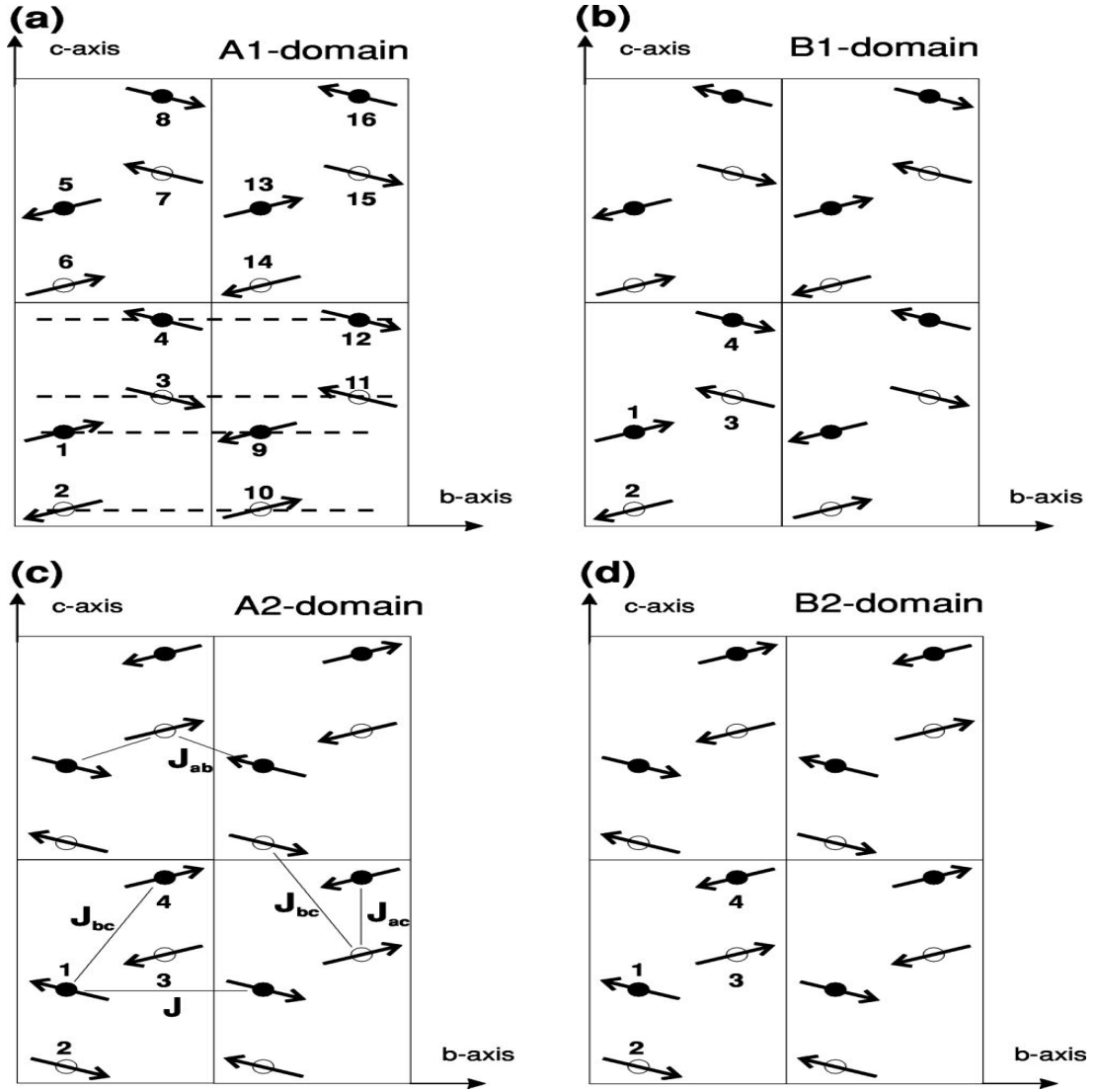


Figure 3.5: This table of figures shows the magnetic structure of Cs_2CoCl_4 obtained using neutron scattering techniques¹². Every sub figure (a)-(d) shows four chemical unit cells, containing the sites 1-4 from Fig. 3.1, which form the magnetic unit cell containing 16 sites (labeled 1-16). Solid and open circles are Co^{2+} ions with different height above the bc plane, around 0.25 and 0.75 respectively (see Eq. (3.2) and Eq. (3.3)). In (a) the chains are indicated with dashed lines and the spins (depict by arrows) order antiferromagnetically. The local ordered moments m are lying in the bc plane having a small angle with the b axis. A certain relative ordering of the chains to each other lead to different sub figures (a)-(d). Taking the structure in (a) as a basic structure, following operations on the b - and/or c -component $\{m_b, m_c\}_i$ lead to the figures (b)-(d):

$$(b): \rightarrow \begin{cases} \{m_b, m_c\}_i & i=1,2 \\ -\{m_b, m_c\}_i & i=3,4 \end{cases}; \quad (c): \rightarrow \{-m_b, m_c\}_i; \quad (d): \rightarrow \begin{cases} \{-m_b, m_c\}_i & i=1,2 \\ \{m_b, -m_c\}_i & i=3,4 \end{cases}.$$

there is non frustrated coupling between site 1 and 2 as well as between site 3 and 4. Additionally there are two planes, parallel to the bc -plane, corresponding to solid and open circles. Each plane contains only sites which couple frustratedly (J_{bc}) in the bc -plane (see Fig. 3.7b). Thus one can identify two kinds of planes, one plane contains chains with sites 1&4 respectively 2&3. An other plane is defined by the ions labeled with 1&2 and in parallel 3&4, which contains non frustrated chains (J_{ac}). The last interaction direction J_{ab} is between sites of even or odd label.

This lattice is represented in the space group Pnma. As a remark, there is an other material Cs_2CuCl_4 which has the same symmetry group as Cs_2CoCl_4 mentioned by Carlin *et al.*²⁸. This symmetry group contains eight operations on the spatial components and on the magnetic moments. There are eight additional operations related to time reversal and combinations with it. This operations can be found in the paper of Starykh *et al.*²⁹. They can be represented in two irreducible representation using 2x2 matrices. With the application of these operations to the several moments, positioned at the given sites, one can specify which representation applies to the following condition. The application of symmetry operations should map the unit cell back on itself. Surely a cell shifted by a unit vector applies as well. By this one can specify the irreducible representation of the symmetry group.

One can diagonalize this representation and use the eigenvectors to test several configurations. To do so one defines a projector into trial states $|\nu\rangle$ using the usual definition $P \equiv |\nu\rangle\langle\nu|$. The interesting components are the staggered magnetizations. Given the eigenvectors $|\lambda\rangle$, one can check if the chosen configuration of staggered moments is allowed by symmetry. This is done by the evaluation of $\langle\lambda|P|\lambda\rangle$. If it evaluates to a finite scalar, the trial state is allowed. This analysis can be used to show which terms can be added to the interaction fulfilling the symmetry conditions.

With these considerations one can construct a three dimensional model of coupled spin chains of two different types, A(site 1&3)- and B(site 2&4)-type. Deforming the real unit cell in the following way: $y_0 \equiv 1/4 \equiv z_0$ (see Eq. (3.2) and Eq. (3.3)) (motivated by the analysis of the Cs_2CuCl_4 ²⁹), one can think of a model of chains in planes, where these chains are coupled differently. The intra chain coupling is labeled with J . Basically there are two basic planes parallel to the ab -plane, containing the same structure, but different constituents. This planes are shown in Fig. 3.6, where one plane contains the sites 3&4 and the other plane the sites 1&2. In these planes the moments couple non frustratedly, labeled with J'' , as they form a square lattice (see Fig. 3.7a). Beside the relative orientation of these two planes, they are continued exactly on top each other in the c -direction. This means every second plane is a copy of its after next neighbouring plane. The relative orientation of the planes is such, that a corresponding site of one plane couple frustratedly to a site of the neighbouring plane labeled with J' (see Fig. 3.7b). The figures Fig. 3.7a and Fig. 3.7b can be understood as two similar copies of the same situation indicated with the site indices in brackets. This situation forbids the interaction of staggered moments between the considered basic planes, especially terms like $\phi_1^{st}\phi_4^{st}$. Using symmetry considerations one can construct the following map: $\phi_1^{st}\phi_4^{st} \rightarrow -\phi_1^{st}\phi_4^{st}$. This shows that the mentioned term has to vanish (see Starykh *et al.*²⁹).

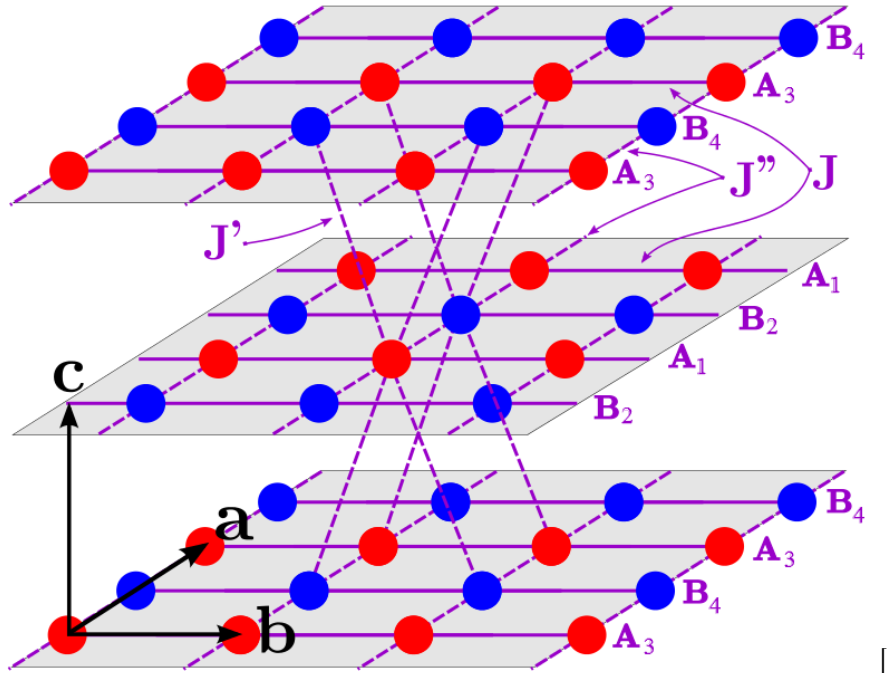


Figure 3.6: Shown is a sketch of the geometrical setup for the numerical calculation in 3d. Three non frustrated basic planes are drawn. They are parallel to the ab -plane and contain spins of two types. The spins correspond to the types A (●) and B (●), which are indicated by their colour. Each type contains two individual sites, so that in total four different types appear (underscript 1-4). They form chains in the b -direction, which is indicated with solid lines. The dashed lines stand for different interchain couplings. The corresponding lines in the mentioned plane represent the non frustrated couplings J'' in a -direction. The diagonal dashed lines in the bc -plane are standing for the frustrated coupling J' . The specific indices numbering each spin and the unit vectors translating the unit cell is specified in Fig.??.

The numerical calculations are done on a reduced lattice. The four individual sites are restricted to two kinds of sites, A and B-type. By these considerations, the interplanar coupling of staggered moments is suppressed. In the figures Fig. 3.6 - Fig. 3.7b the setup for the calculation is sketched. Referring to the restricted setup, each set of indices (ijk) , counting the continuation of the unit cell, contains two sites, one site of each chain type. This is labeled with the capital letters A and B. In reference to the initial system described above, the unit cell would contain four sites, labeled partially in brackets with 1, 2, 3 and 4. In the following only the restricted version will be considered.

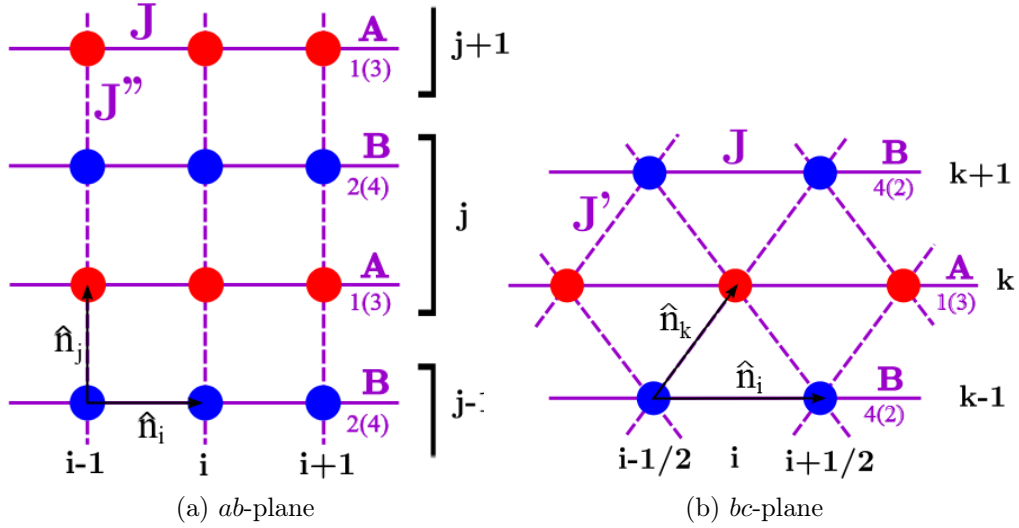


Figure 3.7: In figure (a) the planes of Fig. 3.6 are drawn. Every site is definitely defined by the specific indices $\{ij\}$ and the type A or B-type. The unit vectors $\hat{n}_i(\hat{n}_j)$ in $b(a)$ -direction are added to illustrate the counting direction of the indices. Because the unit cell contains two spins the index j corresponds to two chains. Moreover the corresponding coupling constants, the chain coupling J and the non frustrated coupling J'' , is shown. The third unit vector, $\hat{n}_k = (1, 1/2, 1)$, is not only in the c -direction. With figure (b) one can imagine the direction of this unit vector. In this figure one of the planes perpendicular to the a -direction is shown. The index j refers to two planes, one with A and B interchanged. Additionally the index k for the counting in the c -direction is put into place. In the case of four individual sites, both sub figures of this figure has to be thought of two copies of the same geometric structure, but this structure is occupied by different constituent spins, labeled with 1-4.

3.2 Concept of Mean Field Theory

The usual Mf theory is a concept to deal with many-body-systems on the level of one body problems. The influence of all particles on one specific particle is approximated via a well chosen Mean field. In the case of spins, one has to think about an additional

magnetic field. In total the many-body interaction is described by an effective Mf field (Mffs)¹⁶ on one particle.

The concept used to describe the situation is an advanced Mf approach. Basically there are two additional ideas which were used: the notion of spin chains and their self-consistent interaction. The whole cloud of spins is divided into spin chains of finite length. Every chain and its constituent spins will order according to occurring external magnetic fields. These fields are first of all, the external magnetic field B_x and besides this, there are additional fields created by the neighbouring chains. As chains can have either a uniform magnetization or a staggered magnetization, one can think of two additional fields to the external one. In turn these magnetizations will influence the local configuration of every single spin. But on the other side these spins give rise to additional fields. This leads to the idea of self-consistent solutions to equations connecting fields and magnetizations.

Up to this stage the interaction of spins in several chains with one specific spin is described via two additional fields. As long as one uses usual Mf theory one can speak of a one-site approximation. The method used in this work is an extended version of this approach. In contrast to usual Mf, the problem is formulated such that every chain forms additional Mffs. This approach leads in principle to independent additional fields occurring from each chain separately.

To do this technically first of all one has to define a reference Hamiltonian \mathcal{H}_{Mf} representing one spin chain in external fields. Basically one can choose an arbitrary reference Hamiltonian, but as it is used to do the calculation of the partition sum \mathcal{Z}_{Mf} and the expectation values $\langle \mathbf{S} \rangle_{\text{Mf}}$, one chooses an exact solvable reference Hamiltonian. As mentioned in section 2.1 the anisotropic 1d chain in a transversal field cannot be solved exactly. This means that one has either to use approximations (like a Mf approach) or use numerical exact diagonalization schemes to obtain information about the system. By doing so one can calculate the uniform and staggered magnetization of a 1d chain in specific fields. These magnetizations cause fields, which have to be adjusted such that the arising self-consistent equations are solved. To find these equations one can use a minimum condition for the free energy. In general it will be shown that the minimization of this free energy is equivalent to solving the Mf equations self-consistently.

Theorem

This minimum condition is provided by the Bogoliubov inequality:

$$\mathcal{F} \leq \tilde{\mathcal{F}} \equiv \mathcal{F}_{\text{Mf}} + \langle \mathcal{H} - \mathcal{H}_{\text{Mf}} \rangle_{\text{Mf}}. \quad (3.7)$$

Here \mathcal{H} denotes the full Hamiltonian and \mathcal{H}_{Mf} the approximative Mf Hamiltonian.

To prove (c.f. Sachdev¹⁶) this inequality one needs a concept of the trace and to build expectation values. With $\text{tr}[\hat{O}]$, the sum over all eigenstates of the operator \hat{O} will be denoted:

$$\text{tr}[\hat{O}] \equiv \sum_{n=1}^{2^L} \langle n | \hat{O} | n \rangle \quad (3.8)$$

with $|n\rangle$ the eigenstate of \hat{O} . A definition of an expectation value can be given in the following way:

$$\langle \hat{O} \rangle \equiv \frac{\text{tr}[e^{-\beta\mathcal{H}}\hat{O}]}{Z} = \frac{\sum_n \langle n|e^{-\beta\mathcal{H}}\hat{O}|n\rangle}{\sum_n \langle n|e^{-\beta\mathcal{H}}|n\rangle} \quad (3.9)$$

with $\beta \equiv 1/T$ and the partition sum $Z \equiv \text{tr}[e^{-\beta\mathcal{H}}]$. The partition sum is the starting point for the following computation.

$$\mathcal{Z} = \text{tr}[e^{-\beta(\mathcal{H}-\mathcal{H}_{\text{Mf}})-\beta\mathcal{H}_{\text{Mf}}}] \quad (3.10)$$

$$= \mathcal{Z}_{\text{Mf}} \langle e^{-\beta(\mathcal{H}-\mathcal{H}_{\text{Mf}})} \rangle_{\text{Mf}} \quad (3.11)$$

where the basic properties of the $\text{tr}[\cdot]$ operation and Eq. (3.8) was used. Because the exponential function is convex the following inequality is valid:

$$\langle e^{-\hat{O}} \rangle \geq e^{-\langle \hat{O} \rangle}. \quad (3.12)$$

This provides with the free energy $\mathcal{F} = -\beta^{-1} \ln \mathcal{Z}$ and therefore $\mathcal{Z} = e^{-\beta\mathcal{F}}$ the following statement about Eq. (3.11):

$$\mathcal{Z} \geq \mathcal{Z}_{\text{Mf}} e^{-\beta\langle \mathcal{H}-\mathcal{H}_{\text{Mf}} \rangle_{\text{Mf}}} \quad (3.13)$$

Taking the logarithms of both sides of Eq. (3.13) and the multiplication by $-\beta^{-1}$ proofs Eq. (3.7) \square

The minimization condition with respect to an arbitrary Mf parameter \tilde{H} is:

$$\frac{d\tilde{\mathcal{F}}}{d\tilde{H}} = \frac{d\mathcal{F}_{\text{Mf}}}{d\tilde{H}} + \frac{d\langle \mathcal{H}-\mathcal{H}_{\text{Mf}} \rangle_{\text{Mf}}}{d\tilde{H}} = 0 \quad (3.14)$$

with the definition $\tilde{\mathcal{F}} \equiv \mathcal{F}_{\text{Mf}} + \langle \mathcal{H}-\mathcal{H}_{\text{Mf}} \rangle_{\text{Mf}}$. This variational principle applied to the Mf free energy leads to self consistent equations for the fields or chosen Mf parameters. To solve this equation one has two options. The first option is to solve the occurring equations self consistently. This is one reason why this Mf theory sometimes is called self consistent field theory. But there is an additional way of solving this problem. Namely minimizing the Mf free energy⁴. In the numerical part of this work the occurring equations are solved iteratively as well as by the minimization of the free energy.

Lemma

Given a reference Hamiltonian \mathcal{H}_{Mf} which contains the bare Hamiltonian \mathcal{H}_0 and an additional general force times coordinate term fx . The exact free energy of \mathcal{H}_{Mf} is given by:

$$\mathcal{F}_{\text{Mf}} = -\beta^{-1} \log \sum_n \langle n|e^{-\beta(\mathcal{H}_1+fx)}|n\rangle = -\beta^{-1} \log \mathcal{Z}_{\text{Mf}} \quad (3.15)$$

The derivative of \mathcal{F}_{Mf} with respect to f gives:

$$\frac{d\mathcal{F}_{\text{Mf}}}{df} = -\beta^{-1} \frac{1}{\mathcal{Z}_{\text{Mf}}} \sum_n \langle n|(-\beta x)e^{-\beta(\mathcal{H}_1+fx)}|n\rangle = \langle x \rangle_{\text{Mf}} \quad (3.16)$$

This relation will be used in the following part, where the Mf equations will be derived.

3.3 Mean field approach in one dimension

In this section the anisotropic Heisenberg chain in a transverse field (see 2.1) is considered. This model is treated, using a self consistent ansatz to solve the occurring equations¹². In this section the problem is formulated in the language of 2nd quantization. This means that the usual spin operators are mapped onto fermionic creation and annihilation operators. Additionally a Bogoliubov transformation is used to map the problem onto a theory, where the particle number is conserved. The main goal of this section is to find an expression for the specific heat which was measured on the Cs₂CoCl₄ system by Breuning³⁰. The specific heat is calculated via an expression for the free energy which is used to find the Mf equations, as motivated in Eq. (3.14).

3.3.1 Operator Identities

To start with, the usual spin-1/2 operators are considered:

$$S_i^\pm = S_i^x \pm iS_i^y \quad (3.17)$$

$$S_i^x = \frac{1}{2}(S_i^- + S_i^+) \quad (3.18)$$

$$S_i^y = \frac{i}{2}(S_i^- - S_i^+) \quad (3.19)$$

The following equivalence,

$$|\uparrow\rangle \triangleq |0\rangle \quad |\downarrow\rangle \triangleq |1\rangle \quad (3.20)$$

states that a spin up state is described by an empty state and spin down state refers to an occupied fermionic state. This equivalence only holds for one site. Concerning the commutation relations, there is a fundamental difference between the fermion operators and the spin operators, while fermionic operators anticommute,

$$\{c_i, c_j^\dagger\} = \delta_{ij} \quad \{c_i, c_j\} = 0 = \{c_i^\dagger, c_j^\dagger\} \quad (3.21)$$

where spin operators commute¹⁶. The solution to this problem was found by Jordan and Wigner, namely by the introduction of the so called string operators:

$$S_i^+ \equiv \prod_{j<i} (1 - 2c_j^\dagger c_j) c_i \quad (3.22)$$

$$S_i^- \equiv \prod_{j<i} (1 - 2c_j^\dagger c_j) c_i^\dagger \quad (3.23)$$

$$S_i^z = c_i^\dagger c_i - \frac{1}{2} \quad (3.24)$$

With the commutation relation as follows:

$$[S_i^+, S_j^-] = 2\delta_{ij} S_i^z \quad [S_i^-, S_j^-] = 0 = [S_i^+, S_j^+] \quad [S_i^z, S_j^\pm] = \pm\delta_{ij} S_i^\pm \quad (3.25)$$

The notation Eq. (3.22) - Eq. (3.28) is the conventional Jordan Wigner mapping, but in the specific case, where S_x couples to the external field a $\pi/2$ rotated version, $S^z \rightarrow S^x$ and $S^x \rightarrow -S^z$ is useful. This induces the following identities:

$$S_i^x = c_i^\dagger c_i - \frac{1}{2} \quad (3.26)$$

$$S_i^y = \frac{i}{2}(S_i^- - S_i^+) \quad (3.27)$$

$$S_i^z = -\frac{1}{2}(S_i^- + S_i^+). \quad (3.28)$$

3.3.2 Mean-field approach

A first step is to insert the Spin creation and annihilation operators Eq. (3.26) - Eq. (3.28) into Eq. (2.5).

$$\mathcal{H} = \sum_i \left(\frac{J_+}{2}(S_i^- S_{i+1}^+ + hc) + \frac{J_-}{2}(S_i^- S_{i+1}^- + hc) + S_i^x S_{i+1}^x + B S_i^z \right) \quad (3.29)$$

with $J_\pm \equiv \frac{J(\Delta \pm 1)}{2}$ and $J = 1$ for instance.

Now substitution of Eq. (3.22) and Eq. (3.23) in Eq. (3.29) yields

$$\mathcal{H} = \sum_i \left(\frac{J_+}{2}(c_i^\dagger c_{i+1} + hc) + \frac{J_-}{2}(c_i^\dagger c_{i+1}^\dagger + hc) + (n_i - \frac{1}{2})(n_{i+1} - \frac{1}{2}) + B(n_i - \frac{1}{2}) \right) \quad (3.30)$$

with $(c_i^\dagger)^2 = 0 = c_i^2$ (from Eq. (3.21)) and $n_i = c_i^\dagger c_i$. The problematic term is the term quartic in c . From here Eq. (3.30) isn't exact solvable. The key to proceed analytically is to approximate the original Hamiltonian with an one particle Mf Hamiltonian. This Mf Hamiltonian will depend on new Mf parameters, that could be identified with the Mffs.

The used choice for a Mf reference Hamiltonian is:

$$\mathcal{H}_{\text{Mf}} = \mathcal{H}_{\text{Mf}}[\tilde{H}, \tilde{J}_+, \tilde{J}_-] = \sum_i \left(\frac{\tilde{J}_+}{2}(c_i^\dagger c_{i+1} + hc) + \frac{\tilde{J}_-}{2}(c_i^\dagger c_{i+1}^\dagger + hc) + \tilde{H}(n_i - \frac{1}{2}) \right) \quad (3.31)$$

with the Mf parameters $\{\tilde{H}, \tilde{J}_+, \tilde{J}_-\}$.

The central aspect is how to find the right parameters. For this purpose the minimum condition Eq. (3.14) for the Mf free energy Eq. (3.7) with respect to the Mf parameters is used. The difference term in the free energy reads:

$$\begin{aligned} \langle \mathcal{H} - \mathcal{H}_{\text{Mf}} \rangle_{\text{Mf}} &= \sum_i \frac{J_+ - \tilde{J}_+}{2} \langle c_i^\dagger c_{i+1} + hc \rangle_{\text{Mf}} \\ &\quad + \frac{J_- - \tilde{J}_-}{2} \langle c_i^\dagger c_{i+1}^\dagger + hc \rangle_{\text{Mf}} \\ &\quad + \langle (n_i - \frac{1}{2})(n_{i+1} - \frac{1}{2}) \rangle_{\text{Mf}} \\ &\quad + (H - \tilde{H}) \langle c_i^\dagger c_i - \frac{1}{2} \rangle_{\text{Mf}}. \end{aligned} \quad (3.32)$$

3 Mean Field Concept

One can define several expectation values, following the notation of the paper by Löw³¹. There is the on-site magnetization, a kinetic and a superconducting expectation value term denoted in the following way:

$$M = \langle c_i^\dagger c_i \rangle_{\text{Mf}} - \frac{1}{2} \quad K = \langle c_{i+1}^\dagger c_i \rangle_{\text{Mf}} \quad P = \langle c_{i+1} c_i \rangle_{\text{Mf}} \quad (3.33)$$

These terms are real per definition, which induce $\langle AB \rangle = \langle B^+ A^+ \rangle$. By Wicks theorem (c.f. Altland and Simons³²) one can massage the second last term in Eq. (3.32) using discrete translational invariance:

$$\begin{aligned} \langle n_i n_{i+1} \rangle_{\text{Mf}} &= \langle c_i^\dagger c_i c_{i+1}^\dagger c_{i+1} \rangle_{\text{Mf}} \\ &= \langle c_i^\dagger c_{i+1} \rangle_{\text{Mf}} \langle c_i c_{i+1}^\dagger \rangle_{\text{Mf}} - \langle c_i^\dagger c_{i+1}^\dagger \rangle_{\text{Mf}} \langle c_i c_{i+1} \rangle_{\text{Mf}} + \langle c_i^\dagger c_i \rangle_{\text{Mf}} \langle c_{i+1}^\dagger c_{i+1} \rangle_{\text{Mf}} \end{aligned} \quad (3.34)$$

Thus

$$\langle (n_i - \frac{1}{2})(n_{i+1} - \frac{1}{2}) \rangle_{\text{Mf}} = K^2 - P^2 + M^2 \quad (3.35)$$

and the difference in the free energy becomes

$$(\mathcal{H} - \mathcal{H}_{\text{Mf}})_{\text{Mf}} = (J_+ - \tilde{J}_+)K + (J_- - \tilde{J}_-)P + (H - \tilde{H})M + K^2 - P^2 + M^2. \quad (3.36)$$

With this expression it is possible to find the MF parameters as functions of the old parameters and the expectation values. This is done by the minimization of the Mf free energy. In general the derivative reads as:

$$\frac{d\mathcal{F}_{\text{Mf}}}{d\tilde{H}_i} = (J_+ - \tilde{J}_+) \frac{dK}{d\tilde{H}_i} + (J_- - \tilde{J}_-) \frac{dP}{d\tilde{H}_i} + (H - \tilde{H}) \frac{dM}{d\tilde{H}_i} + 2K \frac{dK}{d\tilde{H}_i} - 2P \frac{dP}{d\tilde{H}_i} + 2M \frac{dM}{d\tilde{H}_i} \quad (3.37)$$

where $\tilde{H}_i \in \{\tilde{H}, \tilde{J}_+, \tilde{J}_-\}$. By construction the expectation values referring to the first term in the free energy (see 3.16) will be cancelled by the specific derivative for each parameter \tilde{H}_i :

$$M_i + \frac{d(J_+ - \tilde{J}_+)}{d\tilde{H}_i} K + \frac{d(J_- - \tilde{J}_-)}{d\tilde{H}_i} P + \frac{d(H - \tilde{H})}{d\tilde{H}_i} M = 0 \quad (3.38)$$

With 3.14 one obtains the following system of equations in matrix notation:

$$\begin{bmatrix} \frac{dM}{d\tilde{H}} & \frac{dK}{d\tilde{H}} & \frac{dP}{d\tilde{H}} \\ \frac{dM}{d\tilde{J}_+} & \frac{dK}{d\tilde{J}_+} & \frac{dP}{d\tilde{J}_+} \\ \frac{dM}{d\tilde{J}_-} & \frac{dK}{d\tilde{J}_-} & \frac{dP}{d\tilde{J}_-} \end{bmatrix} \begin{bmatrix} H - \tilde{H} \\ J_+ - \tilde{J}_+ \\ J_- - \tilde{J}_- \end{bmatrix} = \begin{bmatrix} \frac{dM}{d\tilde{H}} & \frac{dK}{d\tilde{H}} & \frac{dP}{d\tilde{H}} \\ \frac{dM}{d\tilde{J}_+} & \frac{dK}{d\tilde{J}_+} & \frac{dP}{d\tilde{J}_+} \\ \frac{dM}{d\tilde{J}_-} & \frac{dK}{d\tilde{J}_-} & \frac{dP}{d\tilde{J}_-} \end{bmatrix} \begin{bmatrix} -2M \\ -2K \\ 2P \end{bmatrix} \quad (3.39)$$

From these equations one can read of the new parameters:

$$\tilde{H} = H + 2M \quad \tilde{J}_+ = J_+ + 2K \quad \tilde{J}_- = J_- - 2P \quad (3.40)$$

Thus the Hamiltonian Eq. (3.30) describing the system, will be replaced by an approximative Mf Hamiltonian:

$$\mathcal{H}_{\text{Mf}} = \sum_i \frac{\tilde{J}_+}{2} (c_i^\dagger c_{i+1} + hc) + \frac{\tilde{J}_-}{2} (c_i^\dagger c_{i+1}^\dagger + hc) + \tilde{H} (c_i^\dagger c_i - \frac{1}{2}) \quad (3.41)$$

3.3.3 Exact solution of the effective 1d model

With the usual Fourier transformation $c_j = \frac{1}{\sqrt{N}} \sum_k c_k e^{ikj}$ and $c_k = \frac{1}{\sqrt{N}} \sum_j c_j e^{-ikj}$ Eq. (3.41) becomes:

$$\mathcal{H}_{\text{MF}} = \sum_k (\tilde{J}_+ \cos k + \tilde{H}) c_k^\dagger c_k + \frac{\tilde{J}_-}{2} (i \sin k c_k^\dagger c_{-k}^\dagger + hc) \quad (3.42)$$

with the fact that $\sum_k \cos k c_k^\pm c_{-k}^\pm = \sum_k \cos[-k] c_{-k}^\pm c_k^\pm = 0$. This expression can be rewritten to the following form:

$$\mathcal{H} = \sum_k \omega_k (\cos \vartheta_k c_k^\dagger c_k + \frac{i \sin \vartheta_k}{2} (c_{-k} c_k - c_k^\dagger c_{-k}^\dagger)) \quad (3.43)$$

The next step is to use the Bogoliubov transformation restricted to a particle conserving theory.

$$\gamma_k = \cos \frac{\vartheta_k}{2} c_k - i \sin \frac{\vartheta_k}{2} c_{-k}^\dagger \quad \gamma_{-k}^\dagger = -i \sin \frac{\vartheta_k}{2} c_k + \cos \frac{\vartheta_k}{2} c_{-k}^\dagger \quad (3.44)$$

$$c_k = \cos \frac{\vartheta_k}{2} \gamma_k + i \sin \frac{\vartheta_k}{2} \gamma_{-k}^\dagger \quad c_{-k}^\dagger = i \sin \frac{\vartheta_k}{2} \gamma_k + \cos \frac{\vartheta_k}{2} \gamma_{-k}^\dagger \quad (3.45)$$

In matrix formulation:

$$\begin{aligned} \begin{bmatrix} \gamma_k \\ \gamma_{-k}^\dagger \end{bmatrix} &= \begin{bmatrix} \cos \frac{\vartheta_k}{2} & -i \sin \frac{\vartheta_k}{2} \\ -i \sin \frac{\vartheta_k}{2} & \cos \frac{\vartheta_k}{2} \end{bmatrix} \begin{bmatrix} c_k \\ c_{-k}^\dagger \end{bmatrix} \\ \begin{bmatrix} c_k \\ c_{-k}^\dagger \end{bmatrix} &= \begin{bmatrix} \cos \frac{\vartheta_k}{2} & i \sin \frac{\vartheta_k}{2} \\ i \sin \frac{\vartheta_k}{2} & \cos \frac{\vartheta_k}{2} \end{bmatrix} \begin{bmatrix} \gamma_k \\ \gamma_{-k}^\dagger \end{bmatrix} \end{aligned} \quad (3.46)$$

From that point on, one can write the Hamiltonian in a matrix expression:

$$\mathcal{H} = \sum_k \frac{\omega_k}{2} \begin{bmatrix} c_k^\dagger & c_{-k} \end{bmatrix} \begin{bmatrix} \cos \vartheta_k & -i \sin \vartheta_k \\ i \sin \vartheta_k & -\cos \vartheta_k \end{bmatrix} \begin{bmatrix} c_k \\ c_{-k}^\dagger \end{bmatrix}. \quad (3.47)$$

where the initial fermionic operators are written in terms of the Bogoliubov particles. With the Eq. (3.46) the Hamiltonian Eq. (3.47) can be rewritten such that:

$$\mathcal{H} = \sum_k \frac{\omega_k}{2} \begin{bmatrix} \gamma_k^\dagger & \gamma_{-k} \end{bmatrix} \mathcal{H}_1 \begin{bmatrix} \gamma_k \\ \gamma_{-k}^\dagger \end{bmatrix} \quad (3.48)$$

where

$$\mathcal{H}_1 \equiv \begin{bmatrix} \cos \frac{\vartheta_k}{2} & -i \sin \frac{\vartheta_k}{2} \\ -i \sin \frac{\vartheta_k}{2} & \cos \frac{\vartheta_k}{2} \end{bmatrix} \begin{bmatrix} \cos \vartheta_k & -i \sin \vartheta_k \\ i \sin \vartheta_k & -\cos \vartheta_k \end{bmatrix} \begin{bmatrix} \cos \frac{\vartheta_k}{2} & i \sin \frac{\vartheta_k}{2} \\ i \sin \frac{\vartheta_k}{2} & \cos \frac{\vartheta_k}{2} \end{bmatrix} = \begin{bmatrix} 1 & 0 \\ 0 & -1 \end{bmatrix}.$$

Thus Eq. (3.48) becomes

$$\mathcal{H} = \sum_k \frac{\omega_k}{2} (\gamma_k^\dagger \gamma_k - \gamma_{-k} \gamma_{-k}^\dagger) = \sum_k \omega_k \left(\gamma_k^\dagger \gamma_k - \frac{1}{2} \right) \quad (3.49)$$

3 Mean Field Concept

This shows, that the γ particles diagonalize the Hamiltonian. One can go further and specify the parameter ϑ_k . This is done by the comparison of 3.42 with 3.43 yielding to:

$$\omega_k \cos \vartheta_k = \tilde{J}_+ \cos k + \tilde{H} \quad \omega_k \sin \vartheta_k = -\tilde{J}_- \sin k. \quad (3.50)$$

From that it follows directly with $\cos x = 1/\sqrt{1 + \tan^2 x}$, that

$$\cos \vartheta_k = \frac{1}{\sqrt{1 + \left[\frac{\tilde{J}_- \sin k}{\tilde{J}_+ \cos k + \tilde{H}} \right]^2}}. \quad (3.51)$$

Again with Eq. (3.50) there is a closed form for the dispersion relation:

$$\begin{aligned} \omega_k^\pm &= \pm [\tilde{J}_+ \cos k + \tilde{H}] \sqrt{1 + \left[\frac{\tilde{J}_- \sin k}{\tilde{J}_+ \cos k + \tilde{H}} \right]^2} \\ &= \sqrt{[\tilde{J}_+ \cos k + \tilde{H}]^2 + \tilde{J}_-^2 \sin^2 k} \end{aligned} \quad (3.52)$$

This result is plotted in the section of the results of the numerical calculation (see 4.3.1). It enables to rewrite $\cos \vartheta_k$ and $\sin \vartheta_k$ as:

$$\cos \vartheta_k = \frac{1}{\sqrt{2}} \sqrt{1 + \frac{\tilde{J}_+ \cos k + \tilde{H}}{\omega_k}} \quad \sin \vartheta_k = \frac{\text{sgn } k}{\sqrt{2}} \sqrt{1 - \frac{\tilde{J}_+ \cos k + \tilde{H}}{\omega_k}}. \quad (3.53)$$

The $\text{sgn } k$ is introduced, to make Eq. (3.44) and Eq. (3.45) valid for all values of k . Moreover the derivatives with respect to the three parameters become:

$$\frac{\partial \omega_k^-}{\partial \tilde{H}} = -\frac{\tilde{J}_+ \cos k + \tilde{H}}{\sqrt{[\tilde{J}_+ \cos k + \tilde{H}]^2 + \tilde{J}_-^2 \sin^2 k}} = -\cos \vartheta_k \quad (3.54)$$

$$\frac{\partial \omega_k^-}{\partial \tilde{J}_+} = -\cos k \cos \vartheta_k \quad (3.55)$$

$$\frac{\partial \omega_k^-}{\partial \tilde{J}_-} = -\frac{\tilde{J}_- \sin k}{\sqrt{[\tilde{J}_+ \cos k + \tilde{H}]^2 + \tilde{J}_-^2 \sin^2 k}} = \sin k \sin \vartheta_k \quad (3.56)$$

Now one can introduce temperature. For that, one needs the notion of temperature dependent expectation values defined in Eq. (3.9). From this one can see, that with the Fermi Dirac distribution $f(\omega_k) = \frac{1}{1 + e^{\beta \omega_k}}$, following identities appear:

$$\langle \gamma_k^\dagger \gamma_k \rangle = \langle \hat{n}_k \rangle = f(\omega_k) \quad (3.57)$$

$$\langle \gamma_k \gamma_k^\dagger \rangle = 1 - f(\omega_k) \quad (3.58)$$

$$\langle \gamma_k^\dagger \gamma_k^\dagger \rangle = 0 = \langle \gamma_k \gamma_k \rangle. \quad (3.59)$$

Now one can show that the Mean-Field expectation values Eq. (3.33) can be expressed using the dispersion relation. For this purpose the following notation is used:

$$M_i \in \{M, K, P\} \quad \tilde{H}_i \in \{\tilde{H}, \tilde{J}_+, \tilde{J}_-\} \quad (3.60)$$

where the expectation values M_i are given in Eq. (3.40). Using this notation the expectation values can be written like:

$$M_i = \int_0^\pi \frac{dk}{2\pi} \frac{\partial \omega_k^- [\tilde{H}, \tilde{J}_+, \tilde{J}_-]}{\partial \tilde{H}_i} (1 - 2f[\omega_k^- [\tilde{H}, \tilde{J}_+, \tilde{J}_-], T]). \quad (3.61)$$

where the parameters \tilde{H}_i depend on the corresponding initial parameters and expectation values, e.g. $\tilde{H} = \tilde{H}[H, M]$. As a partial proof, the calculation of the magnetization term is exemplarily shown:

$$\begin{aligned} M &= \frac{1}{N} \sum_k \langle c_k^\dagger c_k \rangle - \frac{1}{2} = \frac{1}{2N} \sum_k \langle c_k^\dagger c_k - c_k c_k^\dagger \rangle \\ &= \frac{1}{2N} \sum_k \langle \begin{bmatrix} c_k^\dagger & c_{-k} \end{bmatrix} \begin{bmatrix} 1 & 0 \\ 0 & -1 \end{bmatrix} \begin{bmatrix} c_k \\ c_{-k}^\dagger \end{bmatrix} \rangle \\ &= \frac{1}{2N} \sum_k \langle \begin{bmatrix} \gamma_k^\dagger & \gamma_{-k} \end{bmatrix} \begin{bmatrix} \cos \vartheta_k & i \sin \vartheta_k \\ -i \sin \vartheta_k & -\cos \vartheta_k \end{bmatrix} \begin{bmatrix} \gamma_k \\ \gamma_{-k}^\dagger \end{bmatrix} \rangle \\ &= \frac{1}{2N} \sum_k \langle \begin{bmatrix} \gamma_k^\dagger & \gamma_{-k} \end{bmatrix} [\cos \vartheta_k \sigma^z - \sin \vartheta_k \sigma^y] \begin{bmatrix} \gamma_k \\ \gamma_{-k}^\dagger \end{bmatrix} \rangle \end{aligned} \quad (3.62)$$

With Eq. (3.57) - Eq. (3.59) one can easily calculate the following expressions:

$$\langle \begin{bmatrix} \gamma_k^\dagger & \gamma_{-k} \end{bmatrix} [\mathbb{1}] \begin{bmatrix} \gamma_k \\ \gamma_{-k}^\dagger \end{bmatrix} \rangle = 1 \quad (3.64)$$

$$\langle \begin{bmatrix} \gamma_k^\dagger & \gamma_{-k} \end{bmatrix} [\sigma^z] \begin{bmatrix} \gamma_k \\ \gamma_{-k}^\dagger \end{bmatrix} \rangle = 2f[\omega_k] - 1 \quad (3.65)$$

$$\langle \begin{bmatrix} \gamma_k^\dagger & \gamma_{-k} \end{bmatrix} [\sigma^{x,y}] \begin{bmatrix} \gamma_k \\ \gamma_{-k}^\dagger \end{bmatrix} \rangle = 0 \quad (3.66)$$

Now Eq. (3.63) becomes using $1/N \sum_k \rightarrow 1/2\pi \int_{-\pi}^\pi$ and Eq. (3.54):

$$M = \frac{1}{2N\pi} \sum_k \cos \vartheta_k (2f[\omega_k] - 1) = \int_{-\pi}^\pi \frac{dk}{2\pi} \cos \vartheta_k \left(f[\omega_k] - \frac{1}{2} \right) \quad (3.67)$$

$$= \int_0^\pi \frac{dk}{2\pi} (-\cos \vartheta_k) (1 - 2f[\omega_k]) = \int_0^\pi \frac{dk}{2\pi} \frac{\partial \omega_k^-}{\partial \tilde{H}} (1 - 2f[\omega_k]) \quad (3.68)$$

The calculation of the kinetic and the pairing term goes totally analogous.

3.3.4 Self consistent equations

The calculation above showed that one can write the expectation values in a closed form, namely:

$$M_i = \int_0^\pi \frac{dk}{2\pi} \frac{\partial \omega_k^- [\tilde{H}, \tilde{J}_+, \tilde{J}_-]}{\partial \tilde{H}_i} (1 - 2f[\omega_k, T]). \quad (3.69)$$

This self consistent equations can be solved at least in two equivalent ways, which is discussed in Sec. 3.2. The goal is to find the set of parameters solving Eq. (3.40).

One way would be to solve the equations iteratively to find the Mf parameters \tilde{H}_i . Using this method one has to fix temperature and external field and take an initial set of expectation values \tilde{M}_i . With those, one calculates the first set of \tilde{H}_i and starts an iteration, in which alternately the M_i and \tilde{H}_i will be calculated until the Eq. (3.40) are solved inside an given error. Alternatively one can minimize the free energy which is given by Eq. (3.36):

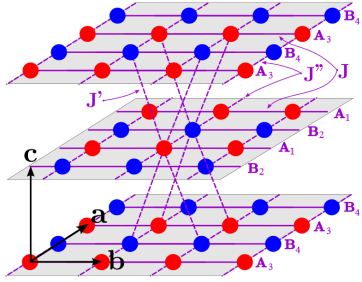
$$\tilde{\mathcal{F}} = \mathcal{F}_{\text{Mf}} + (J_+ - \tilde{J}_+)K + (J_- - \tilde{J}_-)P + (H - \tilde{H})M + K^2 - P^2 + M^2. \quad (3.70)$$

It was checked that the minimized free energy is indeed minimal at the set \tilde{H}_i obtained from the iteration. As this work was initialized by specific heat measurements, the theoretic results will be compared to it in the next chapter:

$$C_V = -T \frac{d^2 \tilde{\mathcal{F}}}{dT^2} \quad (3.71)$$

3.4 Mean field approach for coupled chains

3.4.1 Introduction to the 3d Problem



In this chapter coupling between chains is considered. The difference is that now the spins interact antiferromagnetically with spins on different chains. In addition to the intrachain coupling J there are interchain couplings J' and J'' . In these interactions the same anisotropy is assumed as in the spin-spin interaction inside of chains. The construction of the Hamiltonian representing interacting spin chains in the Cs_2CoCl_4 material refers to the geometrical situation described in 3.1 and especially to Fig. 3.6. The calculation presented in

the following is restricted to only two inequivalent chains, A- and B-type. This is in contrast to the real situation, where four different chains are present. The goal of this section is to calculate the phase diagram of this model, involving coupled anisotropic Heisenberg chains. One has to set up different tools to detect the specific transitions, as transitions of first and second order will be expected. One quantity providing a good definition of a transition is the Mf free energy (Eq. (3.14)) as a function of external field. With the aid of differing initial values for the staggered magnetization (mainly in x - or in y -direction), it is possible to track a level crossing. This crossing labels a first order phase transition between two ordered phases, at which the system changes its ground state. There will be a second order phase transition from order to non order. A good definition for an order parameter is the staggered magnetization. With the calculation of the corresponding staggered susceptibility one is able to define this transition as well. It turns out that the system will have two ordered phases corresponding to predominantly staggered magnetization in either x - or in y -direction.

3.4.2 Construction of the Effective Hamiltonian

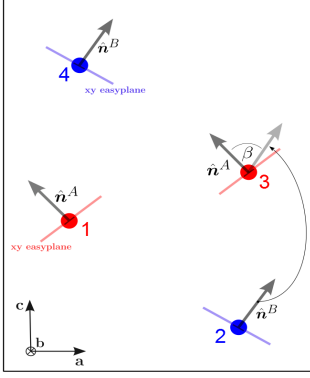


Figure 3.8: see Fig. 3.4

in detail:

As already mentioned the calculation is restricted to two types of chains, $A \hat{=} \{1, 3\}$ and $B \hat{=} \{2, 4\}$. Every chain ($\alpha = A, B$) has its own easy-plane and local unit vector \hat{n}^α standing perpendicular on this plane (see Fig. 3.4). Following the description in section 3.1 one has several contributions to the spin-3/2 Hamiltonian,

$$\mathcal{H} = \mathcal{H}_{chain} + \mathcal{H}_{3d} + \mathcal{H}_D + \mathcal{H}_{ext} \quad (3.72)$$

where \mathcal{H}_{chain} contains the intrachain couplings, \mathcal{H}_{3d} refers to the interchain coupling, \mathcal{H}_D is related to the crystal field energy and \mathcal{H}_{ext} couples the spins to the external magnetic field. The several terms in the Hamiltonian read

$$\mathcal{H}_{chain} = J \sum_r (\mathbf{J}_r^A \mathbf{J}_{i+1,jk}^A + \mathbf{J}_r^B \mathbf{J}_{i+1,jk}^B) \quad (3.73)$$

$$\begin{aligned} \mathcal{H}_{3d} = J' \sum_r & (\mathbf{J}_r^A (\mathbf{J}_{i-1/2,j,k+1}^B + \mathbf{J}_{i+1/2,j,k+1}^B) \\ & + \mathbf{J}_{i-1/2,j,k-1}^B (\mathbf{J}_{i-1,j,k}^A + \mathbf{J}_r^A)) \\ & + J'' \sum_r (\mathbf{J}_r^A \mathbf{J}_r^B + \mathbf{J}_r^B \mathbf{J}_{i,j,k+1}^A) \end{aligned} \quad (3.74)$$

$$\mathcal{H}_D = D \sum_r ((\hat{n}^A \mathbf{J}_r^A)^2 + (\hat{n}^B \mathbf{J}_r^B)^2) \quad (3.75)$$

$$\mathcal{H}_{ext} = -B \sum_r (J_{r,x}^A + J_{r,x}^B) \quad (3.76)$$

where r is a multi-index $r = \{ijk\}$ and thus \mathbf{J}_r^α is a spin-3/2 operator at site $\{ijk\}$. The indices have the following orientation: $i \parallel a$, $j \parallel b$ and $k \parallel c$. Additionally applies in the J'' term for even k : $i \in \{0, 1, 2, \dots\}$ and for odd k : $i \in \{1/2, 3/2, 5/2, \dots\}$. The chains labeled with A have the same easy-plane, they are equivalent, in contrast to the chains labeled with B ($\hat{n}^A \not\parallel \hat{n}^B$). One chooses the unit vector such that $\hat{n}^A \parallel \hat{z}$. This induces $\hat{n}_B = \cos \beta \hat{z} + \sin \beta \hat{y}$ with β the relative angle between the easy-planes (see Fig. 3.9). There is a common axes of the inequivalent planes, which is in this choice the \hat{x} axis. One would like to describe the spins in local coordinates to have them quantized to a local \hat{z} axes.

Rotation

The rotation of one kind of the chains, can be realized by the introduction of new rotated spin variables for the B -chain

$$\mathbf{J}' = R[\beta] \mathbf{J} \quad (3.77)$$

with $R[\beta] = \begin{bmatrix} 1 & & \\ & \cos \beta & -\sin \beta \\ & \sin \beta & \cos \beta \end{bmatrix}$ the usual rotation matrix around the \hat{x} -axis. It has the property that: $R[\beta]^{-1} = R(-\beta)$. Thus one can replace all spin operators in the B-chain

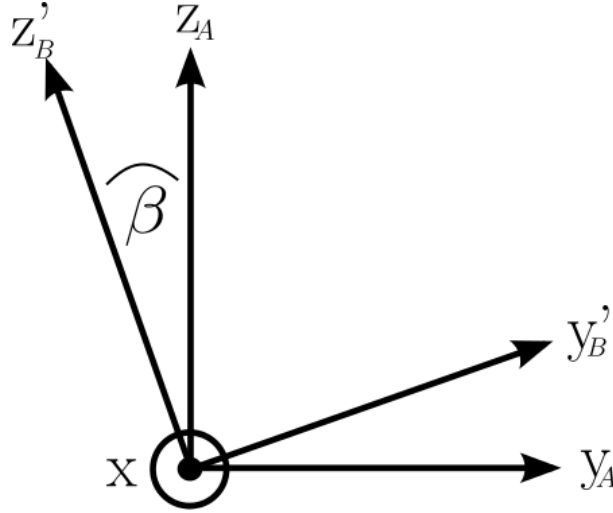


Figure 3.9: In this sketch the relative angle β is introduced. The \hat{x} axis is unchanged in both types of chains (A or B), but the y_B - and the z_B -coordinate are rotated along the common x -direction and thus they contain contributions of both components. A more strict definition of this facts can be found in the text.

to maintain quantization to a local axis:

$$\begin{aligned} \mathbf{J}_i^{B'} &= R^{-1}(\beta)\mathbf{J}_i^B \\ &= \begin{bmatrix} J_x^B \\ \cos \beta J_y^B + \sin \beta J_z^B \\ -\sin \beta J_y^B + \cos \beta J_z^B \end{bmatrix}_i. \end{aligned} \quad (3.78)$$

One can check that $\mathbf{J}_i^{B'}\mathbf{J}_{i+1}^{B'} = \mathbf{J}_i^B\mathbf{J}_{i+1}^B$ and $(\hat{n}_B\mathbf{J}_i^B)^2 = J_i^{zB^2}$. Until now all Spin operators are spin-3/2 operators. One is interested in the limit of large crystall field $D \rightarrow \infty$, as experimentally $D \ll J$ applies. This is equivalent to take only the lower lying total spin $S_z = \pm 1/2$ doublet. To make this point more clear one considers the spin-3/2 operators $\mathbf{J} = \{J_x, J_y, J_z\}^T$:

$$J_x = \frac{1}{2} \begin{bmatrix} & \sqrt{3} & & \\ \sqrt{3} & & 2 & \\ & 2 & & \sqrt{3} \\ & & \sqrt{3} & \end{bmatrix}; \quad J_y = \frac{i}{2} \begin{bmatrix} & -\sqrt{3} & & \\ \sqrt{3} & & -2 & \\ & 2 & & -\sqrt{3} \\ & & \sqrt{3} & \end{bmatrix}; \quad J_z = \frac{1}{2} \begin{bmatrix} 3 & & & \\ & 1 & & \\ & & -1 & \\ & & & -3 \end{bmatrix}$$

Projection

The limit mentioned above is obtained by projecting out the $J_z = \pm 3/2$ states. The corresponding Projector is $P = \begin{bmatrix} 0 & & & \\ & 1 & & \\ & & 1 & \\ & & & 0 \end{bmatrix}$. In the Hamiltonian every Spin operator is

replaced by PJP . This yields:

$$PJ_xP = \begin{bmatrix} 0 & & \\ & 1 & \\ & & 0 \end{bmatrix}; \quad PJ_yP = \begin{bmatrix} 0 & & \\ & i & -i \\ & & 0 \end{bmatrix}; \quad PJ_zP = \frac{1}{2} \begin{bmatrix} 0 & & \\ & 1 & \\ & & -1 \\ & & & 0 \end{bmatrix}.$$

Thus one can write the Hamiltonian in terms of the usual spin-1/2 operators \mathbf{S}_r^α (see definition in Sec. 2.2). The relative factor of 1/2 in the z -component is incorporated in the diagonal matrix $\delta = \begin{bmatrix} 1 & & \\ & 1 & \\ & & 1/2 \end{bmatrix}$:

$$PJ_r^\alpha P = 2\delta \mathbf{S}_r^\alpha \quad (3.79)$$

In Eq. (3.72) one replaces additionally to the mapping $\mathbf{J}^{B'} \rightarrow R^{-1}(\beta)\mathbf{J}^B$, every $\mathbf{J}_r^\alpha \rightarrow 2\delta \mathbf{S}_r^\alpha$. As $S^2 \sim \mathbb{1}$ the D-term in Eq. (3.72) is constant and can be neglected. By now the notation suppressed, that formally the dot product $\mathbf{J} \cdot \mathbf{J}$ should be written $\mathbf{J}^\top \mathbf{J}$. Introducing the matrix

$$\hat{J}[\beta] \equiv \delta R^{-1}[\beta] \delta, \quad (3.80)$$

one can rewrite the dot product concerning the projection mentioned above. This means that

$$\mathbf{J}^\top \mathbf{J} \rightarrow \mathbf{S}^\top \hat{J}[0] \mathbf{S} \quad (3.81)$$

and thus the shape of the terms in Eq. (3.72) become:

$$\mathcal{H}_{chain} = JL_j L_k \sum_i (\mathbf{S}_i^{\top A} \hat{J}[0] \mathbf{S}_{i+1}^A + \mathbf{S}_i^{\top B} \hat{J}[0] \mathbf{S}_{i+1}^B) \quad (3.82)$$

$$\mathcal{H}_{3d} = L_j \sum_{ik} \left(J'' \mathbf{S}_{ik}^{\top A} \hat{J}[\beta] \mathbf{S}_{ik}^B + J' \mathbf{S}_{ik}^{\top A} \hat{J}[\beta] (\mathbf{S}_{i-1/2, k+1}^B + \mathbf{S}_{i+1/2, k+1}^B) + \overset{A \leftrightarrow B}{\hat{j} \rightarrow \hat{j}^\top} \right) \quad (3.83)$$

$$\mathcal{H}_{ext} = -B \sum_i (S_{ij,x}^A + S_{ij,x}^B) \quad (3.84)$$

with redefined couplings J' , J'' and B the mapping $\mathbf{J}^{B'} \rightarrow \mathbf{J}^B$ and $L_j = \sum_j$ respectively. Focusing on the first term in \mathcal{H}_{3d} , because of its special character, one can write

$$\begin{aligned} & J'' L_j L_k \sum_i \mathbf{S}_i^{\top A} \hat{J}[\beta] \mathbf{S}_i^B \\ &= J'' L_j L_k \sum_i \left(S_{i,x}^A S_{i,x}^B + \cos \beta S_{i,y}^A S_{i,y}^B + \frac{\cos \beta}{4} S_{i,z}^A S_{i,z}^B + \frac{\sin \beta}{2} (S_{i,y}^A S_{i,z}^B - S_{i,z}^A S_{i,y}^B) \right) \end{aligned} \quad (3.85)$$

where in contrast to the other terms, the cross product like last term is responsible for additional features of this model. It causes one main aspect of the 3d model, the spins can form staggered magnetization along the x -axis until a finite critical field B_{c1} is reached. This fact will be analyzed further when the phase diagram will be considered. The full form of the Hamiltonian Eq. (3.82) - Eq. (3.84) in the considered limit of large crystal field is considered to be:

$$\mathcal{H}_{eff} = \mathcal{H}_{chain} + \mathcal{H}_{3d} + \mathcal{H}_{ext}. \quad (3.86)$$

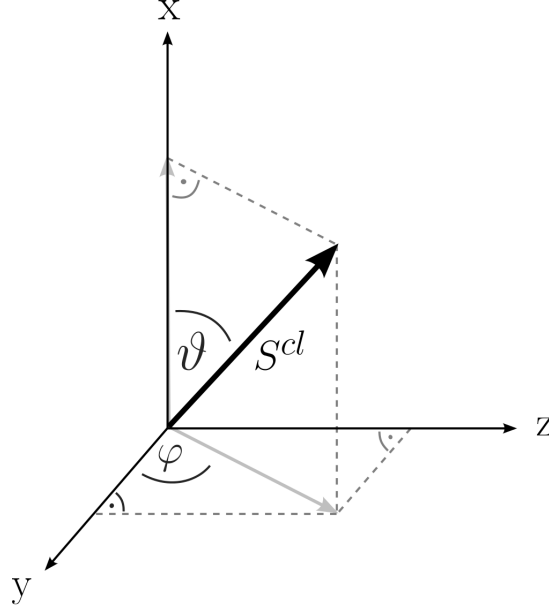
3.4.3 Classical analysis of the effective Hamiltonian \mathcal{H}_{eff}


Figure 3.10: A classical spin parametrized in polar coordinates ϑ and φ

In this section the characteristics of \mathcal{H}_{eff} are analyzed using a classical spin ansatz (c.f. Fig. 3.10). With this ansatz the transition field B_{c1} is derived, at which the phase transition from staggered magnetization in x -direction into staggered order in y -direction occurs. One main issue is the effect according to the angle between the easy-planes β , so that the two terms in Eq. (3.83) containing J'' are neglected. Putting the length of the spin to 1/2, one has the usual expression for the same vector in the two coordinate systems A and B:

$$S_i^A = \frac{1}{2} \begin{bmatrix} \cos \vartheta \\ \sin \vartheta \cos \varphi \\ \sin \vartheta \sin \varphi \end{bmatrix}_i \quad S_i^B = \frac{1}{2} \begin{bmatrix} \cos \vartheta \\ \sin \vartheta \cos \varphi + \beta \\ \sin \vartheta \sin \varphi + \beta \end{bmatrix}_i.$$

Referring to Fig. 3.11, the two phases aside B_{c1} should be considered. By the analysis Eq. (3.85), one can see that the exchange couplings are such that antiferromagnetic order is preferably in the x -direction. Moreover it is obvious that the z -component is always suppressed ($\varphi = 0$), due to the smallest prefactor. This induces the conclusion that in the absence of external fields the system is in the phase called Néel _{x} or AF _{x} . The last term in Eq. (3.86) implies that there is a finite field upon which the system will undergo a first order phase transition into the so called spin flop (SF) or Néel _{y} phase, where the staggered magnetization is predominantly in the y direction. This two cases are sketched in Fig. 3.11. To come back to the classical analysis, this structure is modeled for $B = 0$ via the following attributions:

$$\text{AF}_x : \quad S_i^A = (-1)^i \begin{bmatrix} S_x^A \\ S_y^A \\ 0 \end{bmatrix} \quad S_i^B = - \begin{bmatrix} S_{i,x}^A \\ S_{i,y}^A \\ 0 \end{bmatrix} \quad (3.87)$$

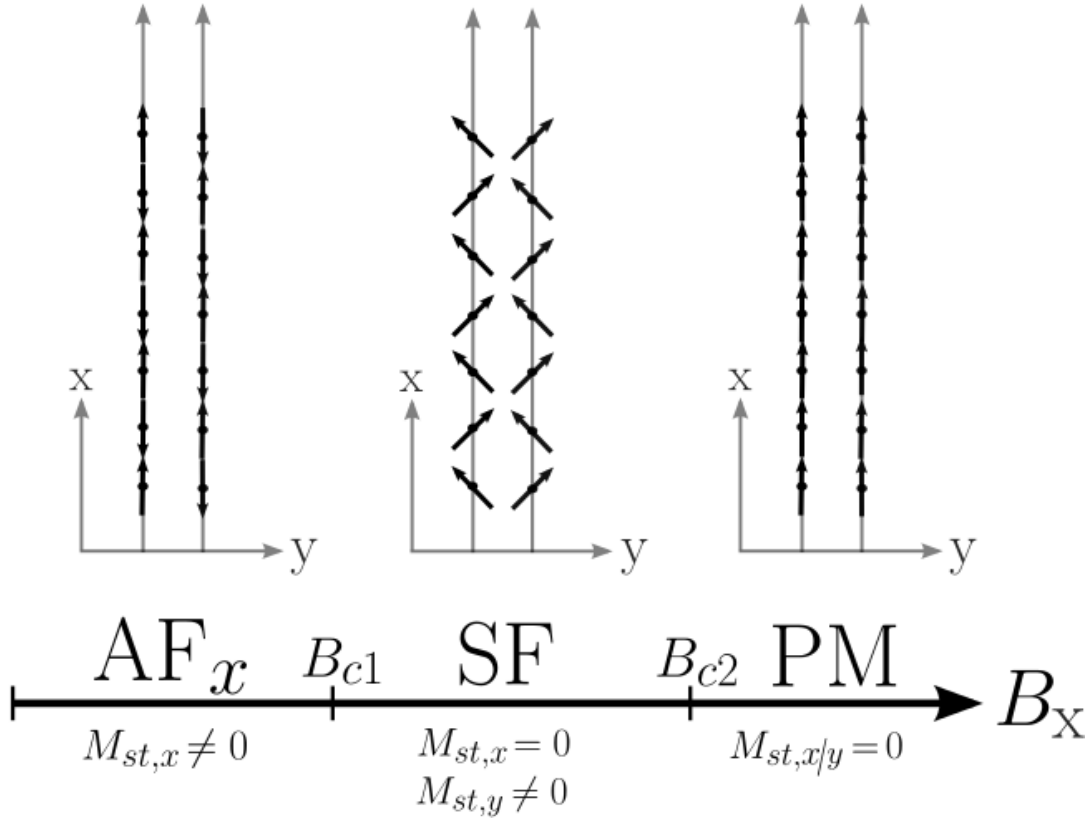


Figure 3.11: Drawn is a sketch of the several phases including a $T = 0$ phase diagram for the coupled chain model. In a one dimensional model the critical field B_{c1} would be zero. In the 3d model several chains are coupled and the main consequence is that this field is finite. Additionally the easy-planes of the constituent chains have a finite angle β and have only one common axis, the x -axis. There are three distinct cases to consider: 1. For $B_x = 0$, the spins (indicated with arrows), are free to order antiferromagnetically (AF_x) in the xy -plane. As long as $0 < B_x \leq B_{c1}$ it is still favorable to form a antiferromagnetic order in the x -direction, which is the common axis of both plane types (A and B). In this phase the spins have finite distribution in the z -component, which is suppressed in the figure. The staggered magnetization in the x -direction ($M_{st,x}$) is an order parameter, being nonzero for $B_x < B_{c1}$. 2. In the case of $B_{c1} < B_x < B_{c2}$ a finite uniform magnetization in the x -direction is created determining the staggered magnetization in this direction to be zero. Additionally staggered magnetization in the y -direction is created ($M_{st,y}$). This phase is called spin flop phase (SF) as the spins form a mixture of uniform and staggered magnetization, with the staggered magnetization mainly perpendicular to the field. 3. In the last case where $B_x > B_{c2}$ the spins are aligned along the field direction and thus the material responses paramagnetically (PM).

3 Mean Field Concept

Where in the Néel_y case following attribution is used:

$$\text{SF:} \quad S_i^A = \begin{bmatrix} S_x^A \\ (-1)^i S_y^A \\ 0 \end{bmatrix} \quad S_i^B = \begin{bmatrix} S_{i,x}^A \\ -S_{i,y}^A \\ 0 \end{bmatrix} \quad (3.88)$$

In the first case the terms \mathcal{H}_{chain} , \mathcal{H}_{3d} and \mathcal{H}_{ext} contribute as follows to the energy per spin:

$$\mathcal{H}_{chain} = -J(\cos^2 \vartheta + \sin^2 \vartheta) \quad (3.89)$$

$$\mathcal{H}_{3d} = -\frac{zJ'}{2}(\cos^2 \vartheta + \cos \beta \sin^2 \vartheta) \quad (3.90)$$

$$\mathcal{H}_{ext} = 0 \quad (3.91)$$

This is minimized for $\vartheta = n\pi$, what implies that in the absence of field, spins are perfectly antiparallel aligned along \hat{x} ($\vartheta = 0$) and the energy per spin is:

$$E_x = -J - \frac{zJ'}{2}$$

, with z the coordination number. In the other case there is β occurring, the terms are:

$$\mathcal{H}_{chain} = J(\cos^2 \vartheta - \sin^2 \vartheta) \quad (3.92)$$

$$\mathcal{H}_{3d} = \frac{zJ'}{2}(\cos^2 \vartheta - \cos \beta \sin^2 \vartheta) \quad (3.93)$$

$$\mathcal{H}_{ext} = -B \cos \vartheta. \quad (3.94)$$

So here the energy is

$$E_y = J(\cos^2 \vartheta - \sin^2 \vartheta) + \frac{zJ'}{2}(\cos^2 \vartheta - \cos \beta \sin^2 \vartheta) - B \cos \vartheta$$

and by minimization of this energy and solving for $\cos \vartheta$ one obtains:

$$\cos \vartheta = \frac{B}{4J + zJ'(1 + \cos \beta)}. \quad (3.95)$$

With this result the minimal energy in the Néel_y-phase is

$$E_y^{min} = -J - \frac{zJ'}{2} \cos \beta - \frac{B^2/2}{4J + zJ'(1 + \cos \beta)}. \quad (3.96)$$

But more importantly, one can solve now by setting $E_x \stackrel{!}{=} E_y^{min}$ for the critical field

$$B_{c1} = \sqrt{zJ'(1 - \cos \beta)(4J + zJ'(1 + \cos \beta))}. \quad (3.97)$$

For small angles β it scales linearly in β : $B_{c1} \sim \sqrt{zJ'}\sqrt{2J + zJ'}\beta + \mathcal{O}(\beta^3)$ but surprisingly it scales as a square root of J' for $J' < 1$: $B_{c1} \sim \sqrt{zJ}\sqrt{1 - \cos \beta}\sqrt{J'} + \mathcal{O}(\sqrt{J'}^3)$.

The main result of this section about the coupling of spin chains of different type is, that the critical field B_{c1} is found to become finite with finite angle β .

3.4.4 Explicit derivation of the Mean field equations

In the conceptual description in Sec. 3.2 the free energy was mentioned as the central expression to derive the Mf fields (Mffs). One has to define a reference Hamiltonian \mathcal{H}_{Mf} , which will contain the several chains, the Mffs and the external fields. The full effective Hamiltonian \mathcal{H}_{eff} (Eq. (3.86)) is given by the sum of 1d chains $\mathcal{H}_{\text{chain}}$ (Eq. (3.82)), a term coupling the spins of several chains $\mathcal{H}_{3d} \sim J' \mathbf{S}^A \mathbf{S}^B$ (Eq. (3.83)) and a term coupling the spins to external fields \mathcal{H}_{ext} (Eq. (3.84)).

$$\mathcal{H}_{\text{eff}} = \mathcal{H}_{\text{chain}} + \mathcal{H}_{3d} + \mathcal{H}_{\text{ext}} \quad (3.98)$$

One can choose a 1d reference Hamiltonian containing the uniform and staggered Mffs $\mathbf{H}_{\text{un}}, \mathbf{H}_{\text{st}}$ to be:

$$\mathcal{H}_{\text{Mf}} = \mathcal{H}_{\text{chain}} + \mathcal{H}_{\text{ext}} - V \sum_{\alpha=A}^B (\mathbf{H}_{\text{un}}^{\alpha} \mathbf{S}_{\text{un}}^{\alpha} + \mathbf{H}_{\text{st}}^{\alpha} \mathbf{S}_{\text{st}}^{\alpha}) \quad (3.99)$$

with $V = L_i L_j L_k$ and obviously the term \mathcal{H}_{3d} will be approximated by the Mffs. Here the self consistent equations are written implicitly, as the Mffs are coupled to spin expectation values contained in the Mffs. As already mentioned above, the $\mathcal{H}_{\text{chain}}$ can be solved exactly but the question is to determine the Mffs. For this one minimizes the free energy with respect to \mathcal{H}_{Mf} (motivated in Eq. (3.14)). The decisive expression is the difference (c.f. Eq. (3.83)):

$$\begin{aligned} \mathcal{H}_{\text{eff}} - \mathcal{H}_{\text{Mf}} &= L_j L_k J'' \sum_i^{L_i} (\mathbf{S}_i^{\top A} \hat{J}(\beta) \mathbf{S}_i^B + \mathbf{S}_i^{\top B} \hat{J}^{\top}[\beta] \mathbf{S}_i^A) \\ &+ L_j J' \sum_{ik}^{L_i L_k} \mathbf{S}_{ik}^{\top A} \hat{J}[\beta] (\mathbf{S}_{i-1/2, k+1}^B + \mathbf{S}_{i+1/2, k+1}^B) + \mathbf{S}_{ik}^{\top B} \hat{J}^{\top}[\beta] (\mathbf{S}_{i-1/2, k+1}^A + \mathbf{S}_{i+1/2, k+1}^A) \\ &+ V \sum_{\alpha=A}^B (\mathbf{H}_{\text{un}}^{\alpha} \mathbf{S}_{\text{un}}^{\alpha} + \mathbf{H}_{\text{st}}^{\alpha} \mathbf{S}_{\text{st}}^{\alpha}). \end{aligned} \quad (3.100)$$

Mean field approximate free energy

The central principle is to take the expectationvalue of the expression Eq. (3.100). In there expectationvalues of spin operators occur. This expectation values itself are evaluated with respect to the chosen reference Hamiltonian:

$$\langle \mathbf{S} \rangle_{\text{Mf}} \equiv \mathbf{M} = \frac{\sum_{n_{\text{Mf}}=1}^{2^L} \langle n_{\text{Mf}} | \mathbf{S} | n_{\text{Mf}} \rangle}{Z_{\text{Mf}}} \quad (3.101)$$

with $\mathbf{S} = \frac{1}{L_i} \sum_{i=1}^{L_i} \mathbf{S}_i$ and $|n_{\text{Mf}}\rangle$ the 2^L eigenfunctions of \mathcal{H}_{Mf} . Every spin expectation value is a superposition of uniform and staggered magnetization, which can be formally written like:

$$\langle \mathbf{S}_i \rangle_{\text{Mf}} \equiv \langle \mathbf{S}_{\text{un}} \rangle_{\text{Mf}} + (-1)^i \langle \mathbf{S}_{\text{st}} \rangle_{\text{Mf}} = \mathbf{M}_{\text{un}} + (-1)^i \mathbf{M}_{\text{st}} \quad (3.102)$$

3 Mean Field Concept

where the indices $\{jk\}$ are suppressed with the specific choice of $S_{k\pm 1}^\alpha = S_k^\alpha$. This particular choice is justified with the fact, that between planes with even and odd k index there is no fixed relation of the spins.

Because the reference Hamiltonian is an one chain object, which induces $\langle \mathbf{S}^A \mathbf{S}^B \rangle_{\text{Mf}} = \langle \mathbf{S}^A \rangle_{\text{Mf}} \langle \mathbf{S}^B \rangle_{\text{Mf}}$, Eq. (3.100) deforms under the application of expectation value into:

$$\begin{aligned} \frac{\langle \mathcal{H}_{eff} - \mathcal{H}_{\text{Mf}} \rangle_{\text{Mf}}}{V} = & 2J'' (\mathbf{M}_{un}^{\top A} \hat{J}[\beta] \mathbf{M}_{un}^B + \mathbf{M}_{st}^{\top A} \hat{J}[\beta] \mathbf{M}_{st}^B) \\ & + 4J' \mathbf{M}_{un}^{\top A} \hat{J}[\beta] \mathbf{M}_{un}^B + \sum_{\alpha=A}^B (\mathbf{H}_{un}^{\top \alpha} \mathbf{M}_{un}^\alpha + \mathbf{H}_{st}^{\top \alpha} \mathbf{M}_{st}^\alpha). \end{aligned} \quad (3.103)$$

The calculation of the first J' -term in Eq. (3.100) will be shown explicitly:

$$\begin{aligned} & \langle \sum_i^{L_j} \mathbf{s}_i^{\top A} \hat{J}[\beta] (\mathbf{s}_{i-1/2}^B + \mathbf{s}_{i+1/2}^B) \rangle_{\text{Mf}} \\ & = \sum_i^{L_j} (\mathbf{M}_{un}^{\top A} + (-1)^i \mathbf{M}_{st}^{\top A}) \hat{J}[\beta] (\mathbf{M}_{un}^B + (-1)^{i-1/2} \mathbf{M}_{st}^B + \mathbf{M}_{un}^B + (-1)^{i+1/2} \mathbf{M}_{st}^B) \\ & = \sum_i^{L_j} (\mathbf{M}_{un}^A + (-1)^i \mathbf{M}_{st}^A) \hat{J}[\beta] 2\mathbf{M}_{un}^B \\ & = 2L_i \mathbf{M}_{un}^{\top A} \hat{J}[\beta] \mathbf{M}_{un}^B. \end{aligned} \quad (3.104)$$

It is obvious that the second part is totally analogous with $A \leftrightarrow B$ and $\hat{J}[\beta] \rightarrow \hat{J}^\top[\beta]$ exchanged. With this derivation, an expression for the Mf free energy per spin (division by $1/(2V)$) is found. This is an important result as it will firstly be used to derive the Mffs.

$$\begin{aligned} \tilde{\mathcal{F}} = & \mathcal{F}_{\text{Mf}} + \langle \mathcal{H}_{eff} - \sum_{\alpha} \mathcal{H}_{\text{Mf}}^\alpha \rangle_{\text{Mf}} \\ = & \mathcal{F}_{\text{Mf}} + J'' (\mathbf{M}_{un}^{\top A} \hat{J}[\beta] \mathbf{M}_{un}^B + \mathbf{M}_{st}^{\top A} \hat{J}[\beta] \mathbf{M}_{st}^B) + 2J' \mathbf{M}_{un}^{\top A} \hat{J}[\beta] \mathbf{M}_{un}^B \\ & + \sum_{\alpha=A}^B (\mathbf{H}_{un}^{\top \alpha} \mathbf{M}_{un}^\alpha + \mathbf{H}_{st}^{\top \alpha} \mathbf{M}_{st}^\alpha) \end{aligned} \quad (3.105)$$

Mean field fields \mathbf{H}_{un} , \mathbf{H}_{st}

Having the free energy in the considered approximation one can find the Mffs by the evaluation of the derivatives of the Mf free energy with respect to the specific field components (c.f. Eq. (3.14)). From Eq. (3.16) it is known that:

$$\frac{d\mathcal{F}_{\text{Mf}}}{d\mathbf{H}_{un(st)}^\alpha} = -\mathbf{M}_{un(st)}^\alpha. \quad (3.106)$$

The central part is the derivative of \mathcal{F}_{Mf} . Exemplarily the derivative concerning \mathbf{H}_{un}^A is shown:

$$\frac{\partial \mathcal{F}_{\text{Mf}}}{\partial \mathbf{H}_{un}^A} = J'' \frac{\partial \mathbf{M}_{un}^{\top A}}{\partial \mathbf{H}_{un}^A} \hat{J}[\beta] \mathbf{M}_{un}^B + 2J' \frac{\partial \mathbf{M}_{un}^{\top A}}{\partial \mathbf{H}_{un}^A} \hat{J}[\beta] \mathbf{M}_{un}^B + \mathbf{H}_{un}^{\top A} \frac{\partial \mathbf{M}_{un}^A}{\partial \mathbf{H}_{un}^A} \quad (3.107)$$

where the uniform magnetization \mathbf{M}_{un}^A from Eq. (3.106) is cancelled by a similar term in $\frac{\partial \langle \mathcal{H}_{eff} - \sum_{\alpha} \mathcal{H}_{Mf}^{\alpha} \rangle_{Mf}}{\partial \mathbf{H}_{un}^A}$. As all terms are scalar quantities they can be transposed independently. The application of transposition to the last term in Eq. (3.107) in combination with $\frac{\partial \mathcal{F}_{Mf}}{\partial \mathbf{H}_{un}^A} = 0$ gives:

$$\frac{\partial \mathbf{M}_{un}^{A\top}}{\partial \mathbf{H}_{un}^A} \mathbf{H}_{un}^A = -J'' \frac{\partial \mathbf{M}_{un}^{A\top}}{\partial \mathbf{H}_{un}^A} \hat{J}(\beta) \mathbf{M}_{un}^B - 2J' \frac{\partial \mathbf{M}_{un}^{A\top}}{\partial \mathbf{H}_{un}^A} \hat{J}[\beta] \mathbf{M}_{un}^B. \quad (3.108)$$

This equation demonstrates one nice aspect of this approach, namely that one does not have to calculate the quantity $\frac{\partial \mathbf{M}_{un}^{A\top}}{\partial \mathbf{H}_{un}^A}$ due to cancellation. So finally the uniform field in the A-chain created from its neighbouring chains read:

$$\mathbf{H}_{un}^A = -\hat{J}[\beta] (J'' \mathbf{M}_{un}^B + 2J' \mathbf{M}_{un}^B) \quad (3.109)$$

In analogous way the staggered field on the A-chain can be calculated to be:

$$\mathbf{H}_{st}^A = -J'' \hat{J}(\beta) \mathbf{M}_{st}^B \quad (3.110)$$

The fields acting on the B-chain are related to the fields of the A-chain by the exchange of $A \leftrightarrow B$ and $\hat{J}[\beta] \rightarrow \hat{J}^{\top}[\beta]$. They are for completeness:

$$\mathbf{H}_{un}^B = -\hat{J}^{\top}[\beta] (J'' \mathbf{M}_{un}^A + 2J' \mathbf{M}_{un}^A) \quad (3.111)$$

$$\mathbf{H}_{st}^B = -J'' \hat{J}^{\top}[\beta] \mathbf{M}_{st}^A. \quad (3.112)$$

Staggered susceptibility

One main goal is to calculate the phase diagram. This means having the Mffs and the free energy it is possible to track the transition between the ordered phases. The question is how to find the transition from the ordered phase into the paramagnetic phase. Here the determining quantity is the staggered susceptibility, as in general it describes the magnetizability of a material. In the paramagnetic phase the system its ability to form staggered magnetization goes to zero. Calculating this susceptibility gives the possibility to solve the coupled self consistent equations Eq. (3.109) - Eq. (3.112). In general the susceptibility is defined as

$$\mathbf{M}^{\alpha} = -\chi^{\alpha} \mathbf{H}^{\alpha}. \quad (3.113)$$

This means for the staggered part of the Mf equations (Eq. (3.110) and Eq. (3.112)) that the magnetizations can be replaced:

$$\mathbf{H}_{st}^A = J'' \hat{J}(\beta) \chi_{st}^B \mathbf{H}_{st}^B \quad (3.114)$$

$$\mathbf{H}_{st}^B = J'' \hat{J}^{\top}(\beta) \chi_{st}^A \mathbf{H}_{st}^A \quad (3.115)$$

and in consequence these equations can be written in matrix form:

$$\begin{bmatrix} \mathbf{H}_{st}^A \\ \mathbf{H}_{st}^B \end{bmatrix} = J'' \begin{bmatrix} 0 & \hat{J}(\beta) \chi_{st}^B \mathbf{H}_{st}^B \\ \hat{J}^{\top}(\beta) \chi_{st}^A \mathbf{H}_{st}^A & 0 \end{bmatrix} \begin{bmatrix} \mathbf{H}_{st}^A \\ \mathbf{H}_{st}^B \end{bmatrix}. \quad (3.116)$$

3 Mean Field Concept

They are solved for eigenvalues of the matrix $\chi^{AB} \equiv J'' \begin{bmatrix} 0 & \hat{J}(\beta)\chi_{st}^B \mathbf{H}_{st}^B \\ \hat{J}^\top(\beta)\chi_{st}^A \mathbf{H}_{st}^A & 0 \end{bmatrix}$ equal to one. As it was mentioned that outside the ordered phase the staggered susceptibility will be smaller than one, it is possible to find the disorder order phase transition, at the point where the largest eigenvalue of the staggered susceptibility becomes one the first time (equivalent with the largest eigenvalue).

4 Numerical solutions

In this chapter the results obtained by doing several Mf based calculations are presented. Basically two different ways are used to solve the Mf equations, Eq. (3.69) respectively Eq. (3.109) - Eq. (3.112). In the first case, where only one chain was considered, the free energy was minimized. In the other case in a first step every chain was solved exactly. Numerical tools were used to calculate the interplay between the chains and to solve for the occurring Mffs.

4.1 Experimental results of measurements on Cs_2CoCl_4

4.1.1 Specific heat measurements

One of the first measurements for the specific heat of Cs_2CoCl_4 were done in the 1980's⁵ and redone by Breunig *et al.*³⁰. To do so a low temperature-calorimeter was built and used in the following. It was constructed to measure the specific heat down to $T = 0.25\text{Kelvin}$ in fields up to 17 Tesla. The measuring technique was the relaxation method. The measured data is shown in the figures Fig. 4.1 to compare to the numerical result. This work is focused on the theoretical description of a model describing the same features than the measurements on the material Cs_2CoCl_4 .

There are several basic features one has to explain. Chiefly, neglecting the low temperature divergences in Fig. 4.1, one can see that for every field the specific heat reaches a maximum. Furthermore one can see that in between, for a specific magnetic field this maximum is minimal compared to the other ones. In Fig. 4.1 one has to distinguish the high and the low temperature part of the figure. The divergences in the low temperature region of the specific heat refer to degrees of freedom related to an inter chain coupling. The energy scale of such excitation is small compared to the scale of the intra chain coupling. This explains, that only for small temperatures these 3d features are visible. Beside this in the high field regime at small temperatures, the left flank of the curves can be described with an two level system having an energy gap ΔE (see Section 4.2.2). The high temperature tail and its T^{-2} power law can be found exactly (see Section 4.2.3).

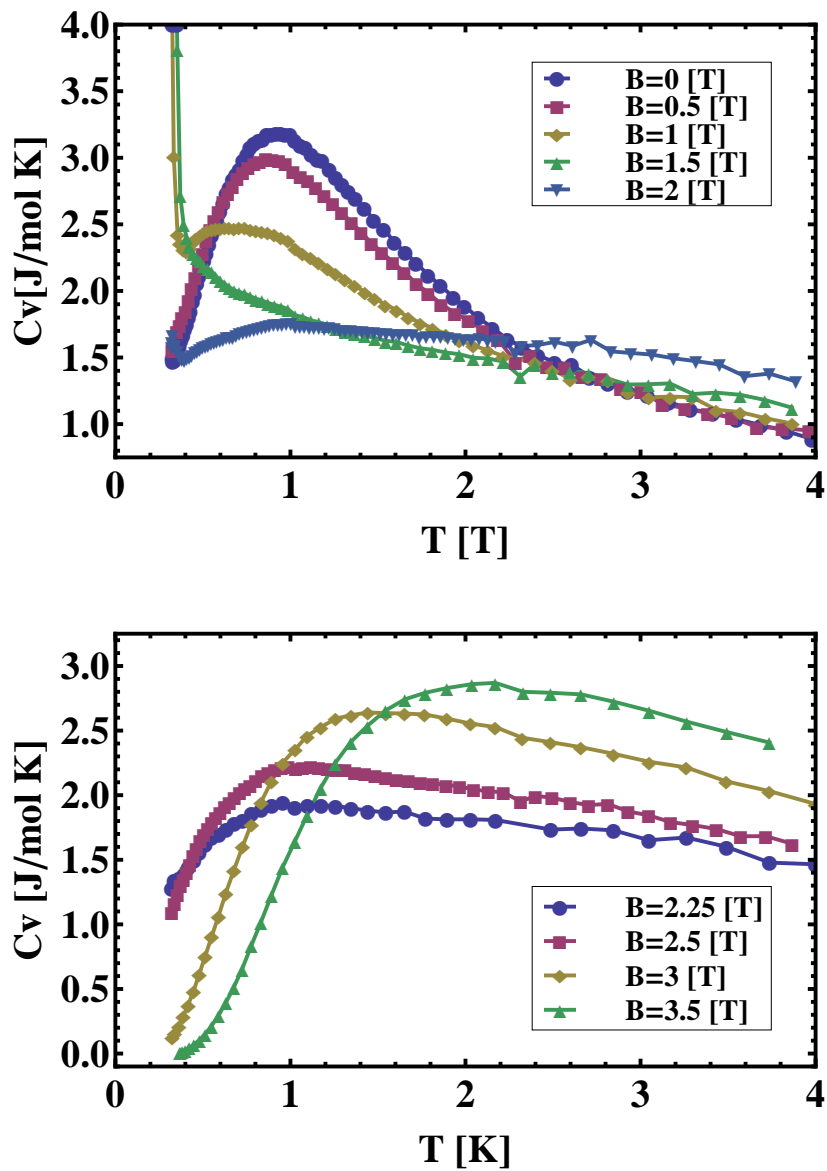


Figure 4.1: Shown are experimental results of the specific heat measurements for the external magnetic fields indicated, done by Breunig *et al.*³⁰. Further explanation can be found in Sec. 4.1.1

4.1.2 Phase diagram of Cs_2CoCl_4

The second experimental result used as an orientation mark is the phase diagram in Fig. 4.2 measured by Breunig *et al.*³⁰ as well. This phase diagram is not yet fully understood, but basic features can be read of. For small fields the system is expected to be in an antiferromagnetic phase (AF, see Sec. 3.4) along the field direction. After crossing a first order phase transition line, the phase labeled with I is reached. It is not clear which phase it is, but a mixture of the AF-phase and the subsequent spin flop (SF) phase can be assumed. The argument for this assumption is based on the frustrated coupling between the ab -planes (see Fig. 3.7b). First of all one has to use the full unit cell, namely all four sites. One can break the frustration with additional spin-orbit coupling. This would induce an intermediate phase, in which one part e.g. all even (index k in Fig. 3.7b) planes are in the SF-phase in contrast to all odd planes remaining in the AF-phase. Above a critical field H_{c1} , the spins fully order antiferromagnetically but perpendicular to the field direction (SF) being mainly in the y -direction (z -direction is suppressed due to the anisotropy Δ). In the performed calculation no spin orbit term is included and thus the two fields H_{c0} and H_{c1} fall together. Above a critical field H_{c2} a second unknown phase II was measured. For this phase again one can construct an explanation proceeding from the inter planar coupling mentioned above. In the derivation of the Mffs in the previous chapter the staggered magnetization only interacts with J'' in the ab -planes (see Fig. 3.7a). There is no contribution coming from the coupling J' .

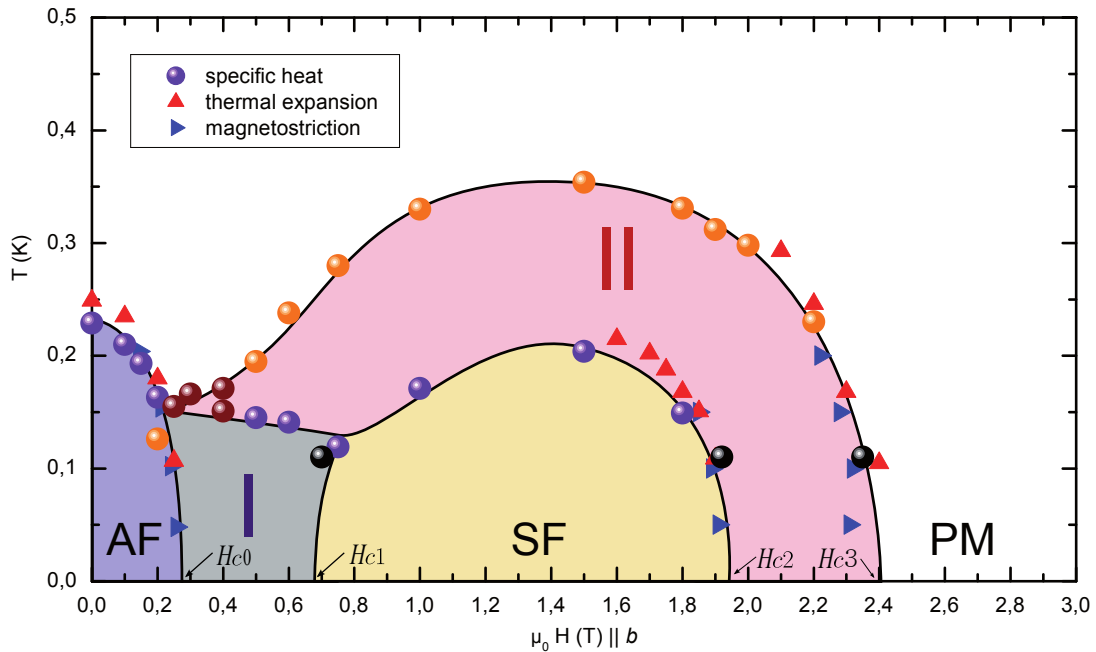


Figure 4.2: Experimental results of combined measurements done by Breunig *et al.*³⁰, to extract the phase diagram of Cs_2CoCl_4 . Besides the labeled phases the two phases I and II are unknown. Several assumptions are presented in the text of Sec. 4.1.2

This means the staggered magnetizations of several ab -planes have no relation between themselves, as it is forbidden by symmetry (see Sec. 3.1). The idea of spontaneously broken symmetry can be realized with a tilted external magnetic field (relative to the b -direction). With this different external field it might be possible that the system favor a unknown but different configuration than the SF-phase. Basically one can think of a deformed lattice such that the perfect frustration is broken. One can assume, that there is a classical transition or crossover line from no order in the phase II, lying in temperature above the calculated phase transition into the SF-phase. Basically the two phases I and II has to be studied further to enable clear statements to them.

4.2 Verification of the one dimensional model

In this section the 1d model under consideration, namely a XXZ model in a transverse field, is checked by several means. One thing is a comparison of the experimental data to an exact diagonalizing scheme. As the model is not analytically solvable, numerical tools³³ are used to check the model on this basis. It will be shown that the XXZ model will mainly reproduce the features one can expect from an 1d theory. The main goal of this section is to verify that the model can describe the physical system. With the verified validity of the numerical exact diagonalization, it will be used to check the theory in further limits. Secondly in sufficiently large fields and small temperatures one can view the model as two level system, involving a gap energy ΔE induced by the field. This justifies an approximation with a two level system in certain limits. In the other temperature scenario, where temperature is the dominant energy scale, one can evaluate and compare the data to high temperature expansion results.

4.2.1 Exact diagonalization

In this part it is shown, that the assumed model can describe the experimental results, at least for high fields. At this stage only the 1d results are considered and taken to compare with the experimental data for the specific heat. For this purpose numerical diagonalization using ALPS³³ was evaluated for systems of $L = 16$ sites in magnetic fields respectively for $L = 18$ if $B_x = 0$. This explicit calculation was also done by Breunig *et al.*³⁰ and there are several results obtained running this calculation. A basic question on such a calculation is if the experimental data is reproduced (see Fig. 4.3). Moreover one can extract the constants involved in the model, such as the intra chain coupling J or the g-factor. Kenzelmann *et al.*¹² proposed the first to be $J/k_B = 2.67\text{K}$, which can be almost reproduced by the numerical calculation providing $J/k_B = 2.6\text{K}$. The best fit for the g-factor provides a value of $g = 2.23$. Both values are calculated under the assumption of the anisotropy term $\Delta = 0.25$.

In Fig. 4.3 the experimental results as in Fig. 4.1 are compared to the results of the described exact diagonalization. The 3d effects are obviously not reproduced in this calculation, as the calculation is done on a 1d chain. In the lowest part of this figure (high field part) one can see nice agreement between theory and experiment, involving the gap mentioned above, which is increasing with increasing field. The intermediate

part show worse agreement and a tendency, besides the 3d effects, to underestimate the absolute value of the specific heat in comparison to the experiment. This becomes obvious in the first part of Fig.4.3, where the peak in the theoretical data is about ten percent lower compared to the experimental values.

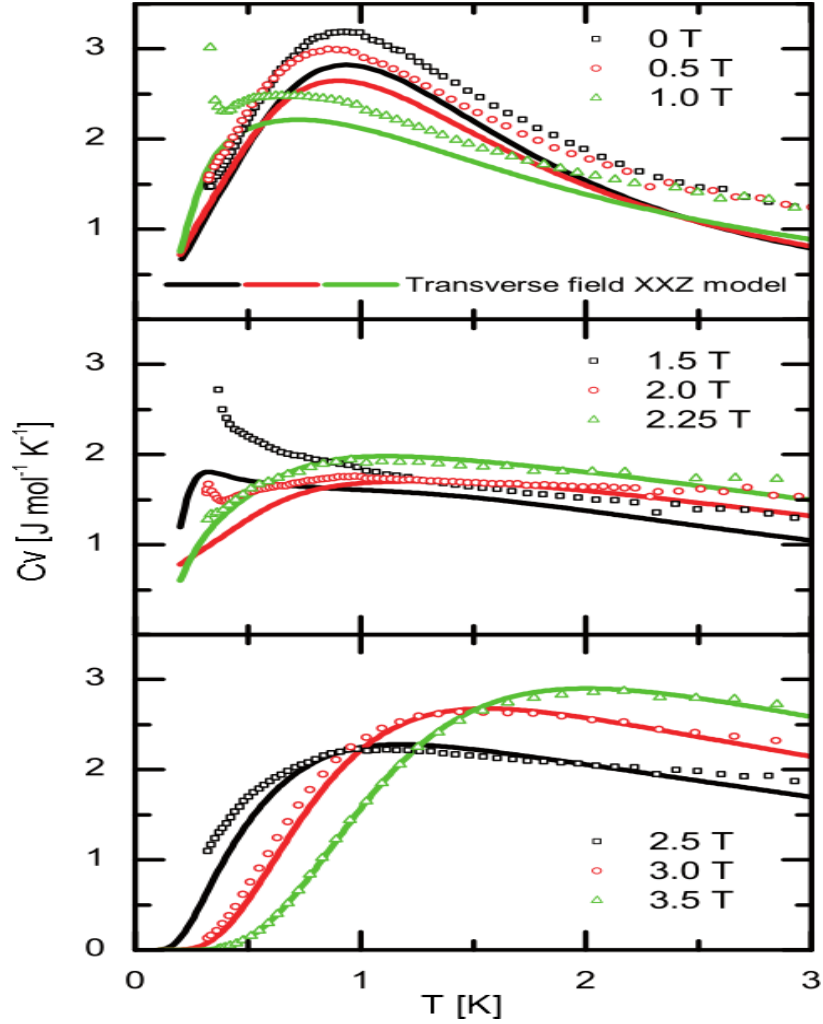


Figure 4.3: In these figures the specific heat is shown. The individual marks are data points obtained by measurements done by Breunig *et al.*³⁰. The solid lines are results of exact diagonalization. Further description can be found in Sec.4.2.1

4.2.2 Low temperature and high field

In the domain where the temperature is comparable low $T \ll J$ and for relatively high fields $B \gg J$, the system can be described as a two level system. The 3d degrees of freedom become neglectable in the high field limit concerning the excitation energy and the basic remaining excitation is a spin flip in a large field. Now one can compare the energy balance for adding one of this excitation. The initial and the excited state form a two level system with an energy gap ΔE . Assuming that the dispersion is constant $\omega = \Delta E$, one can calculate the energy expectation value

$$\langle E \rangle = \int_{-\pi}^{\pi} \frac{dk}{2\pi} \omega f[\omega[k]] = \frac{\Delta E}{e^{\frac{\Delta E}{T}} + 1}, \quad (4.1)$$

with $f[\omega] = 1/(e^{\omega/T} + 1)$ the Fermi distribution function. With the usual formula for the specific heat $C_V = \frac{\partial \langle E \rangle}{\partial T}$ one obtains the following formula for the specific heat:

$$C_{V,\Delta E} = \frac{\Delta E^2}{T^2} \frac{e^{\Delta E/T}}{(e^{\Delta E/T} + 1)^2}. \quad (4.2)$$

If one assumes, that the description of the system as a two level system is valid, one implicitly assumes, that $T \ll \Delta E$. In this limit the specific heat deforms into:

$$C_{V,\Delta E} \simeq \frac{\Delta E^2}{T^2} e^{\Delta E/T}. \quad (4.3)$$

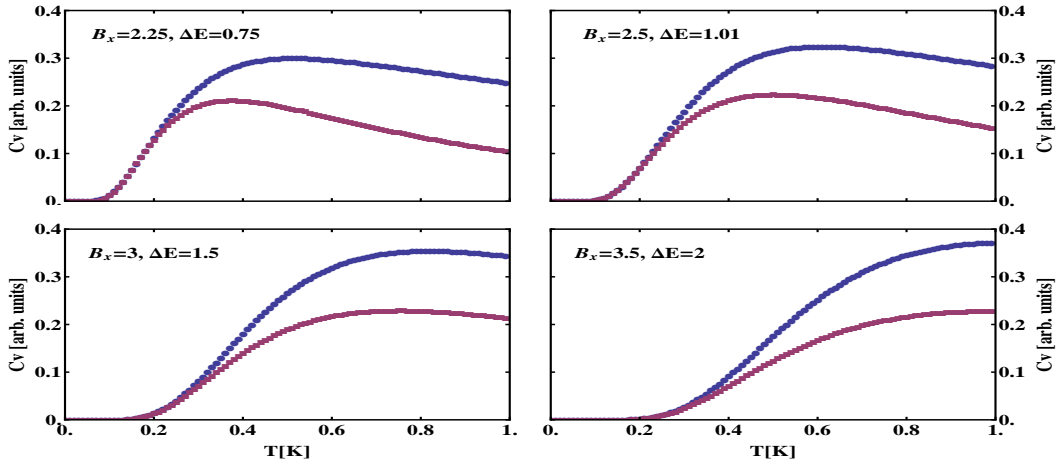


Figure 4.4: ● Exact Diagonalization; ■ Two level approximation

In these figures the specific heat results obtained by exact diagonalization are compared to corresponding results by considering a two level system. The specific energy gap ΔE for several magnetic fields B_x is indicated in each sub figure. The corresponding constant prefactors are $A = 0.39$, $A = 0.41$, $A = 0.42$ and $A = .42$ (from top left to bottom right). The agreement is obviously as better as smaller the temperature is. This reflects the fact that $T \ll \Delta E$ was used as a approximation.

Only for small temperatures, fitting adjustments presented in Fig. 4.4 show good agreement with the result of the exact diagonalization. For this purpose Eq. (4.3) was fitted with a constant prefactor A .

4.2.3 High temperature limit

In this part an estimate for the high temperature regime is derived. This estimate will be used to be compared with the exact diagonalization results.

The derivation starts from the partition sum written as a power series

$$\mathcal{Z} = \text{tr}[e^{-\mathcal{H}/T}] = \text{tr}[\mathbb{1}] - \frac{1}{T}\text{tr}[\mathcal{H}] + \frac{1}{2T^2}\text{tr}[\mathcal{H}^2] + \mathcal{O}\left(\frac{1}{T^3}\right) \quad (4.4)$$

in the small parameter T^{-1} and where \mathcal{H} is taken from Eq. (2.5). Inserting spin creation and annihilation operators one obtains the form (c.f. Eq. (3.29)):

$$\mathcal{H} = J \sum_i \left(\frac{1}{2} (S_i^- S_{i+1}^+ + S_i^+ S_{i+1}^-) + \Delta S_i^z S_{i+1}^z \right) - B \sum_i S_i^x. \quad (4.5)$$

where in this case the rotation is not performed (see Sec. 3.3.1).

The dimension of a Hilbert space for a spin- s spin chain of length L , is $(2s - 1)^L$. This induces for the spin-1/2 model a normalized trace operation $\text{tr} \rightarrow \text{tr}/2^L$, so that $\text{tr}[\mathbb{1}] = 1$. With this convention one can evaluate the several traces occurring in Eq. (4.4).

Linear order

The first two terms in Eq. (4.5) vanish under the trace operation, because there is no option for a term $\langle s_i s_{i+1} | S_i^\pm S_{i+1}^\mp | s_i s_{i+1} \rangle$ to be finite. Basically all term containing the creation and annihilation operators in linear order vanish. The contribution of the $S_i^z S_{i+1}^z$ term adds up to zero and the term coupling to the field is zero due to the same reason than the first terms are zero. This concludes to the fact, that $\text{tr}[\mathcal{H}] = 0$.

Second order

The first non trivial contribution to the partition sum arises from the term $\text{tr}[\mathcal{H}^2]$. With the observation again, that linear orders in the S^+ or S^- operators does not contribute, one can express the trace in the following way.

$$\begin{aligned} \text{tr}[\mathcal{H}^2] = \frac{1}{2^L} \text{tr} \left[\sum_{i,j}^L \left(\frac{J^2}{4} (S_i^+ S_{i+1}^- S_j^- S_{j+1}^+ + S_i^- S_{i+1}^+ S_j^+ S_{j+1}^-) \right. \right. \\ \left. \left. + J^2 \Delta^2 (S_i^z S_{i+1}^z S_j^z S_{j+1}^z) + \frac{B^2}{4} (S_i^+ S_j^- + S_i^- S_j^+) \right) \right] \end{aligned} \quad (4.6)$$

where all terms corresponding to $i \neq j$ are zero under the trace. Because the trace is an additive operation and only term involving two spins contribute one can rearrange the expression Eq. (4.6) to

$$\begin{aligned} \text{tr}[\mathcal{H}^2] = & \frac{J^2}{4} \frac{L2^{L-2}}{2^L} (\text{tr}_2[S_1^+ S_1^- S_2^- S_2^+] + \text{tr}_2[S_1^- S_1^+ S_2^+ S_2^-]) \\ & + J^2 \Delta^2 \frac{L2^{L-2}}{2^L} \text{tr}_2[(S_1^z S_2^z)^2] + \frac{B^2}{4} \frac{L2^{L-1}}{2^L} (\text{tr}_1[S_1^+ S_1^-] + \text{tr}_1[S_1^- S_1^+]). \end{aligned} \quad (4.7)$$

where $L = \sum_i$ and 2^{L-n} is the trace over $L - n$ spins. The reduced trace $\text{tr}_n[\]$ is defined over the reduced Hilbert space of n spins. The several reduced traces in Eq. (4.7) evaluate to: $\text{tr}_2[S_1^\pm S_1^\mp S_2^\mp S_2^\pm] = 1$, $\text{tr}_2[(S_1^z S_2^z)^2] = 1/4$ and $\text{tr}_1[S_1^\pm S_1^\mp] = 1$. This simplifies the result to

$$\frac{\text{tr}[\mathcal{H}^2]}{L} = J^2 \left(\frac{1}{8} + \frac{\Delta^2}{16} \right) + \frac{B^2}{4}. \quad (4.8)$$

With the usual formula, for the free energy $\mathcal{F} = -T \log \mathcal{Z}$ and for the specific heat Eq. (3.71), it reads in the high temperature limit:

$$C_V = -T \frac{\partial^2}{\partial T^2} \left(-T \log \left[1 + \frac{1}{2T^2} \text{tr}[\mathcal{H}^2] \right] \right) \simeq T \frac{\partial^2}{\partial T^2} \frac{1}{2T} \text{tr}[\mathcal{H}^2] = \text{tr}[\mathcal{H}^2] \frac{1}{T^2} \quad (4.9)$$

where $\log 1 + x \simeq x$ and $\frac{\partial^2 T^{-1}}{\partial T^2} = 2T^{-3}$ was used. With this result the temperature dependence of the specific heat in the concerned limit is:

$$C_V = J^2 \left(\frac{1}{8} + \frac{\Delta^2}{16} \right) \frac{1}{T^2} + \frac{B^2}{4} \frac{1}{T^2} + \mathcal{O} \left(\frac{1}{T^3} \right) \quad (4.10)$$

with correction of cubic order.

In Fig. 4.5 the resulting specific heat curves obtained from a $L = 10$ exact diagonalization and the evaluation of the presented high temperature expansion for the XXZ chain are shown. In the case of $B_x = 0.001$ the curves lie on top each other down to one Kelvin. With increasing field, the temperature at which the two theories start to diverge increases as well. But still the two curves and the corresponding theories seem to converge to the same prediction for $T \rightarrow \infty$. This coincides with the taken limit, at which for high temperatures the corresponding expansion becomes exact.

It was shown, that the XXZ chain model describes the physics, at least the 1d features are reproduced. Furthermore both temperature limits $T \rightarrow 0$ in high fields and $T \rightarrow \infty$ can be understood from the present theoretical point of view. To understand the small field and temperature regime, the 3d analysis has to be considered.

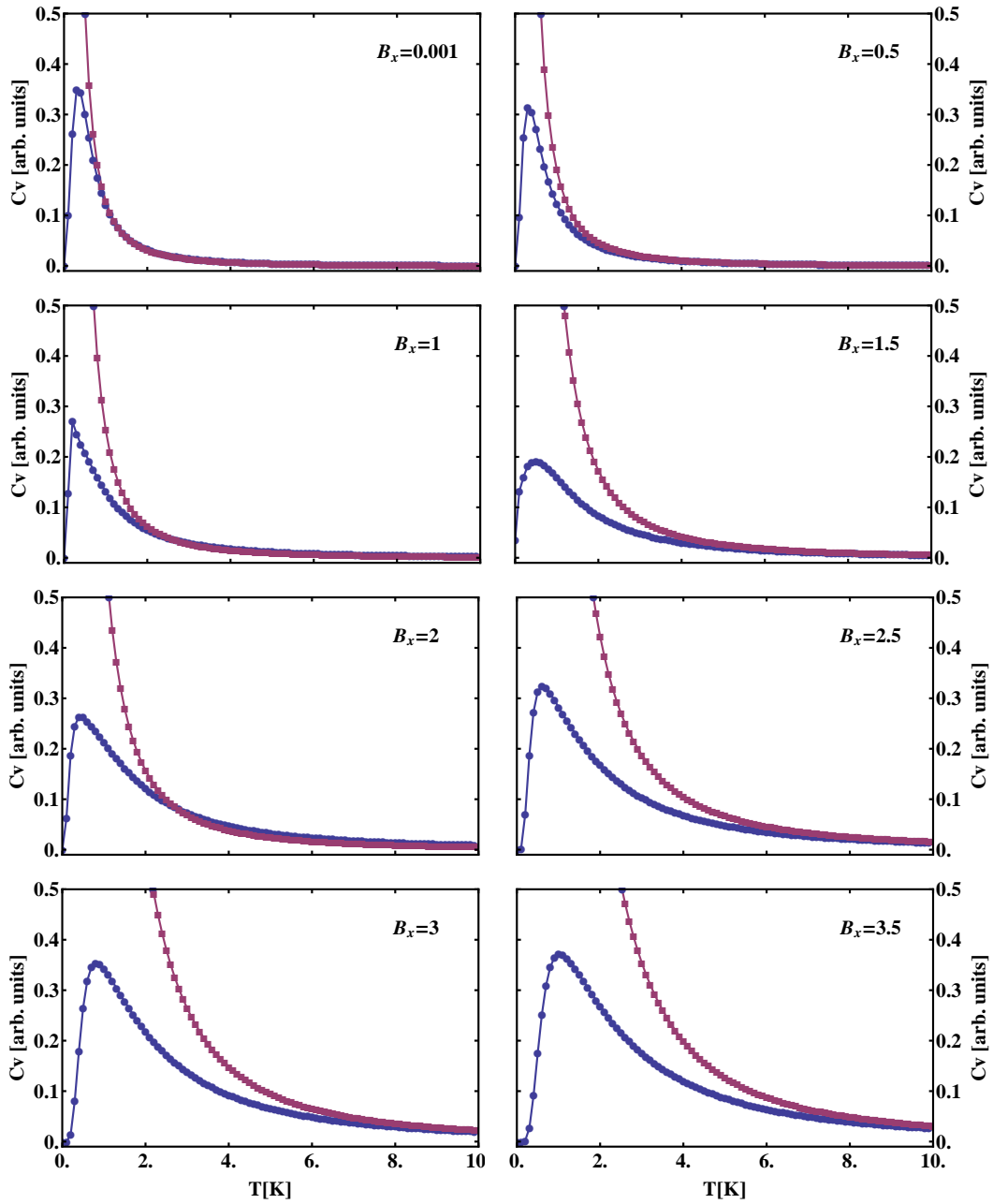


Figure 4.5: ● Exact Diagonalization; ■ High temperature expansion
 In these figures the high temperature results for the specific heat are compared with the corresponding exact diagonalization results for several magnetic fields. The coincidence for high temperatures can be seen clearly. Further explanation are given in the text in Sec. 4.2.3.

4.3 Calculation of C_V for the 1d system

In this section the Mf calculation of the specific heat and its major steps are presented. The obtained results are compared to similar exact diagonalization results as described in the previous section ($L = 10$, $J = 1$, $g = 2.2$). In the previous part it was shown, that the exact diagonalization provides, in certain limits, a good agreement with the experimental data. Performing the Mf approach in 1d only the 1d system can be described. Therefore one cannot expect a better result to the experimental data than from the exact diagonalization scheme. This justifies that the Mf calculation of the specific heat is only compared to the exact diagonalization results.

4.3.1 1d c_{++} Program

In Sec. 3.3 the theoretical concept to solve the given Hamiltonian Eq. (3.29) in the framework of Mf techniques was developed, resulting in the following equations:

$$\tilde{H} = H + 2M \quad \tilde{J}_+ = J_+ + 2K \quad \tilde{J}_- = J_- - 2P. \quad (4.11)$$

These equations are the heart of the calculation, as they describe the relation between the parameter in the initial model and those in the effective model which can be solved exactly. These equations were called the Mf equations, as they are the determining equations for the Mfs. The derivation of the dispersion relation of the effective Hamiltonian \mathcal{H}_{eff} was shown in Sec. 3.3.3 to be of the following form:

$$\omega[k, \tilde{H}, \tilde{J}_+, \tilde{J}_-] = \sqrt{[\tilde{J}_+ \cos k + \tilde{H}]^2 + \tilde{J}_-^2 \sin^2 k} \quad (4.12)$$

The central aspect is how to solve the Mf equations. As mentioned above it is equivalent to find the set of parameters $\tilde{H}_i \in \{\tilde{H}, \tilde{J}_+, \tilde{J}_-\}$ (defined in Eq. (3.60)) either by an iterative approach to the self-consistent solutions or by the minimization of the corresponding Mf free energy. In this part the latter option was used. In a first step the expectation values M_i are calculated for a given external field and for a initial set of parameters \tilde{H}_i^0 . This is done with the integral representation of the expectation values (c.f. Eq. (3.69)) using the dispersion relation. Then having those values, the free energy (Eq. (3.70)) corresponding to these expectation values is calculated. Having these expressions one can define a gradient $\nabla_i^{\tilde{H}}$ which contains the three derivatives with respect to the parameters \tilde{H}_i . Considering the free energy in the space of these three parameters one has by this a measure to find a local minima. Followingly the initial parameters \tilde{H}_i are updated with the following allocation:

$$\tilde{H}_i^{new} = \tilde{H}_i - \delta \nabla_i^{\tilde{H}} \tilde{H}_i \quad (4.13)$$

with a small constant $0 < \delta < 1$ to decrease the step size. With the updated set the expectation values and so forth are repeatedly calculated until the absolute value of the gradient becomes smaller as a predefined tolerance barrier. After this loop the \tilde{H}_i fulfill in certain error estimates the self-consistent equations and can be used for further analysis. Firstly one can consider the structure of the dispersion and whether

it is gapped or not, or at which field the gap closes. With this calculation the critical field of $B_c = 1.604J$ proposed by Löw *et al.*³¹ at which the gap closes is reproduced (see Fig. 4.6). From these parameters the specific heat (see Fig. 4.3.2) can be calculated, following Eq. (3.70) and Eq. (3.71)

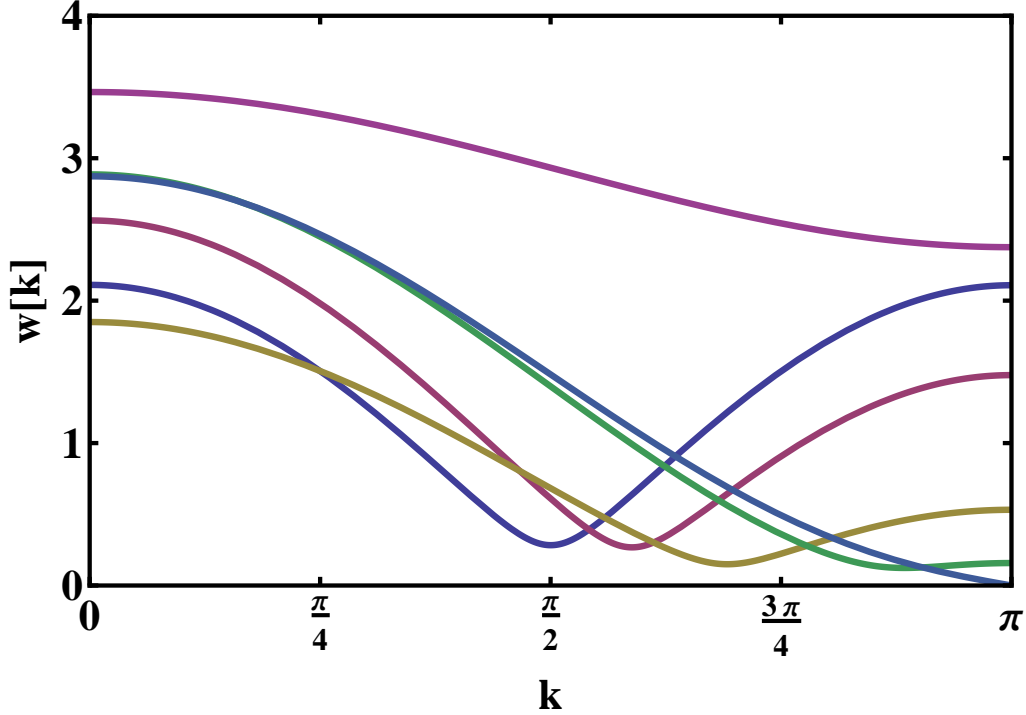


Figure 4.6: Shown is the dispersion relation $\omega[k]$ as function of momentum k in the 1d model for several magnetic fields $B_x \leq 2$. At $k = \pi$ the highest curve is at $B_x = 2J$ and the five dispersions below correspond to fields $B_x/J = 0.001$, 0.5 , 1.0 , 1.5 and 1.604 (top to bottom). One can observe, that for the proposed value for the external field $B_c = 1.604J$ ³¹ the gap closes. This curves are obtained using Eq. (4.12), where the parameters $\tilde{H}_i \in \{\tilde{H}, \tilde{J}_+, \tilde{J}_-\}$ are obtained using the minimization of the Mf free energy. Further specification can be found in the theoretical description (see 3.3) and in the text Sec. 4.3.

4.3.2 Exact diagonalization vs. Mean field

As argued in Sec. 4.3 the results of the Mf calculation can be compared the best to exact diagonalization results. This is done in Fig. 4.7 for the specific heat as function of T ($J = 1$, $g = 2.2$).

To focus on the disagreement for small fields, again the specific heat result for $B_x = 0.001$ is shown in Fig. 4.8. The low temperature tail coincides nicely, in contrast to the high temperature tail, that disagrees badly. In the limit $T \rightarrow \infty$ the high temperature expansion becomes exact and coincides with the exact diagonalization (considered in

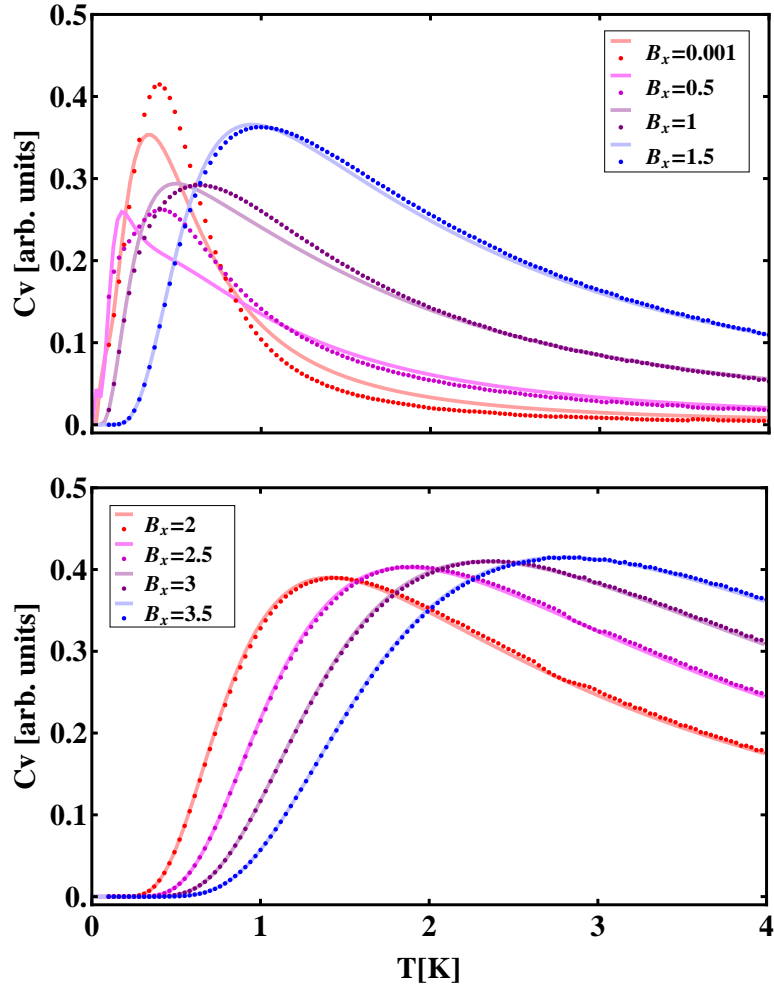


Figure 4.7: Shown is a comparison between Mf specific heat results (dotted) and exact diagonalization results (solid line) as function of temperature. Each pair of one colour is the result corresponding to the indicated external field. The results corresponding to higher fields, coincident more with the validated exact diagonalization. Especially the $B = 0.001$ case disagrees qualitatively with the exact diagonalization for temperatures above the peak. The reason why the Mf approach fails in this limit is, that it breaks the $U(1)$ symmetry of the XXZ model. This argument is further explained in the text of Sec. 4.3.2. The second sub figure show the high field range $B \gg J$, in which the coincidence between exact diagonalization and Mf solution is obvious.

Sec. 4.2.3). For temperatures in which the high temperature expansion is valid, the Mf specific heat is underestimated. Followingly at a specific temperature, it crosses the exact diagonalization specific heat and overestimates the specific heat. The reason for the disagreement in small field was given by Sebastian Caux *et al.*³¹. For $B_x = 0$ the model reduces to a critical XXZ spin chain with exponentially vanishing staggered magnetization. The 1d Mf Hamiltonian fails to describe the system in small magnetic field because the XXZ model has a $U(1)$ symmetry, which is broken by the applied Mffs. This imply that the Mf approach is not valid in the absence of a external magnetic field and therefore fails to describe the system in this case.

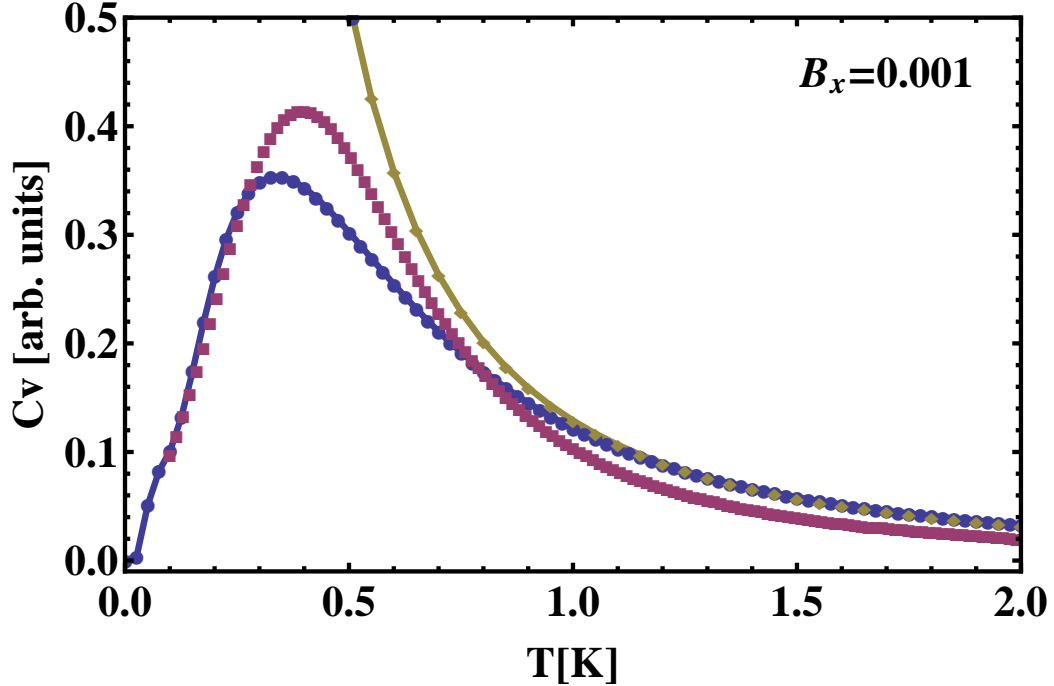


Figure 4.8: ● Exact Diag.; ■ Mf approx.; ◆ High temperature expansion

In this figure the specific heat is shown for $B_x = 0.001$. The Mf solution shows disagreement with the exact diagonalization which was counter checked in both limits (see Section 4.2.2 and 4.2.3). Basically for high temperatures the Mf calculation underestimates the specific heat. At a given temperature the Mf specific heat crosses the exact diagonalization result and followingly over estimates the mentioned quantity. Further explanation is given in the text 4.3.2.

It remains to emphasize, that for high fields and even intermediate fields, the description delivered by the Mf approach is surprisingly good (cf. Fig. 4.7). The presented data is one main result of this work, as the experimental data Fig. 4.1 was the conceptual starting point of the whole theoretical work on Cs_2CoCl_4 presented in this work. It was shown that for finite fields, the Mf approach is a decent method to describe the Cs_2CoCl_4 system in the light of spin chains. For high fields the experimental data could be reproduced quantitatively. The only restriction of the method is that the external field has to be finite due to symmetry reasons mentioned above.

4.4 Specific heat for coupled chains in the 3d setting

With the minimized free energy $\tilde{\mathcal{F}}$ one can calculate the corresponding specific heat using Eq. (3.71). The results are shown in Fig. 4.9. They show the typical Mf behaviour, as there is a jump in the specific heat curve at the critical temperature. Moreover the linear behaviour closed to the transition, with different slope is an indication for the Mf character of the transition. The results of the fitting is presented in Tab 4.4.1. This results can be compared to the experimental results.

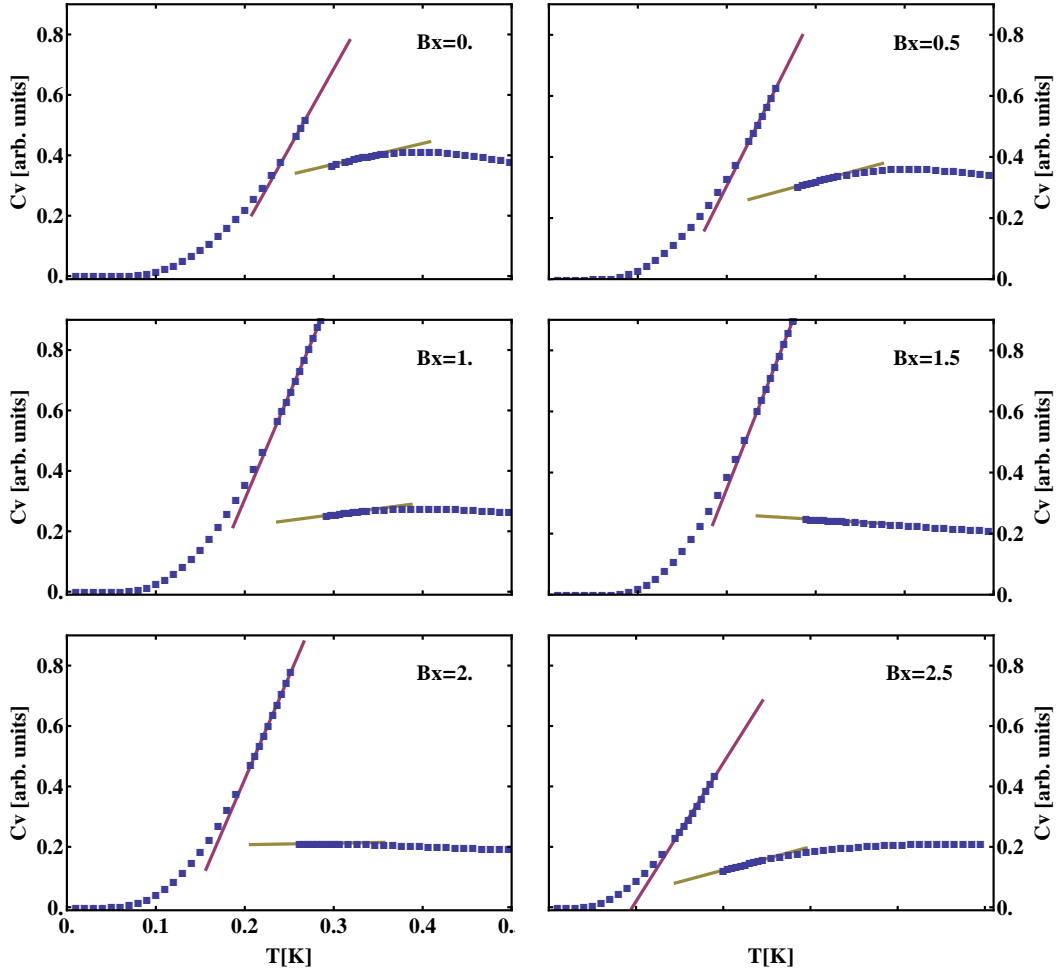


Figure 4.9: \blacksquare $C_{v,Mf}$; $\color{red}\rule{0.5pt}{1cm}$ and $\color{yellow}\rule{0.5pt}{1cm}$ Linear fits closed to the transition temperature
 Shown are the Mf specific heat results at external fields indicated inside each sub figure. The linear fits are executed for temperatures close to the transition temperature but either below or above. The jump as well as the linear behaviour close to the transition are clear indicates for a Mf transition. Further interpretation can be found in the text.

The numerical results for the slopes are

B_x	■ : a	b	◆ : a	b
0	-0.89	5.25	0.16	0.69
0.5	-0.85	5.79	0.08	0.79
1.0	-1.08	6.94	0.14	0.39
1.5	-1.14	7.42	0.30	-0.18
2.0	-0.95	6.84	0.20	0.05
2.5	-0.44	4.58	-0.03	0.77

Table 4.4.1: This table shows the results for the linear fits $a + bx$, on the specific heat close to the transition temperature. It is obvious that the slope above the critical temperature is about one order smaller than the slope below the critical temperature.

The transition temperatures, indicated with the Mf jump in the specific heat is analyzed in Sec. 4.5, as the same transition temperatures are found using the staggered susceptibility calculation.

4.5 Phase diagram for coupled chains

In this section the calculation of the phase diagram of coupled XXZ chains will be presented. The approximative tool is again the MF approach, where the external field acts as the tuning parameter. As the numerical value of the relative angle β between the different types of chains (see Sec. 3.4.2 and Fig. 3.9) is not clear β is varied. Because there are both kinds of phase transition, first and second order phase transition, different techniques to calculate the critical fields and temperatures are used. In Fig. 4.10

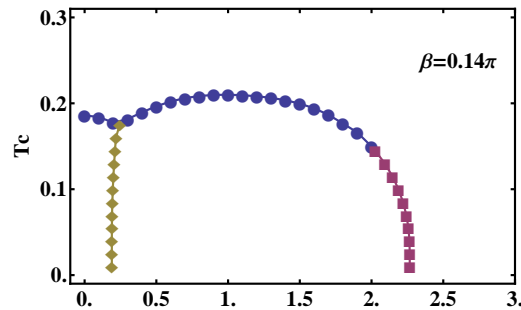


Figure 4.10: Exemplary phase diagram

an exemplary phase diagram is shown. Beside the special cases ($\beta = 0$ and $\beta = \pi$) the structure of the obtained diagrams is similar. There is the intermediate order to order phase transition (◆). Here the free energy for staggered magnetization in x -respectively y -direction was used to examine the transition points. The curve separating the ordered from the non ordered region is found with the aid of the staggered susceptibility. Either the field was kept fixed and the temperature was varied (χ_T , ●) or the opposite (χ_{B_x} , ■). In the following sections the main steps of the calculations for the phase diagram are presented. In this part of the work not the minimization of the free energy was used to solve the self consistent equation but rather an iterative approach.

4.5.1 Staggered magnetization and Iteration

Conceptually the first major part of the program is the exact diagonalization of a 1d chain of specific type (A or B) and its usage to calculate expectation values. Given the fields \mathbf{H}_{un} and \mathbf{H}_{st} and having the eigenstates which correspond to those fields, one can calculate expectation values of spin operators. Those expectation values (defined in Eq. (3.9)) are identified with the corresponding magnetizations (for definitions and derivation see Eq. (3.102)). From these magnetizations again the additional Mffs are calculated until a certain convergence in specific errors is reached.

By setting up the iteration one has to break the symmetry by hand. In Fig. 3.5 it is visible, that the staggered component of chains of different type in the ab -plane are always negative relative to each other. One has to choose arbitrarily one of the two to be the negative of the other. Concretely this means, to initialize the staggered fields with opposite sign, where the uniform fields have the same initial value (see also Sec. 4.5.2). Having the first set of magnetizations a loop follows, which is evaluated until the largest difference between updated magnetization and old one is below an convergence criteria. In the figures Fig. 4.11 and Fig. 4.12 the resulting staggered (x and y) and uniform (x) magnetizations for the fixed temperature $T = 0.2$ are given. This plots provide a first insight where which phase transition will occur. The inter order phase transition, from the Néel to the Ising phase, will happen at the specific field at which the main contribution to the staggered magnetization changes ($M_{st}^x \rightarrow M_{st}^y$). This will happen for fields below $B_x < 0.75J$. For the second order phase transition no indication as clear as for the first order transition can be found. It was argued, that for $\beta = 0$ and $B_x = 0$ both contributions are equal ($M_{st}^x = M_{st}^y$), which can be seen at the very left of the first sub figure. Than still for $\beta = 0$ but at finite field, there is only staggered magnetization in the y direction, and for $\beta = \pi/2$ the opposite applies. The second figure Fig. 4.12 shows the same quantities for a narrow angle interval, especially at which the two magnetizations are separated. This fact indicates, that the critical temperature will have a minimum as a function of external field. This can be seen in Fig. 4.16.

Having the magnetizations or the fields respectively one can go one step further and calculate the corresponding susceptibility (introduced in Eq. (3.113)). Conceptually one can restrict the 'Mf solver' to uniform Mf fields and calculate the susceptibility until the first eigenvalue becomes on, by reducing temperature or magnetic field. At this point the system undergoes a phase transition into an ordered phase, where staggered magnetization is present. The solution obtained by the restricted 'solver' is only valid until the transition temperature or field is reached. More characteristics and fundamental description can be found in the theoretical foundation of this work (cf. 2.1)

In conclusion, the calculation of the susceptibility provide the possibility to calculate the outer T_c line (● and ■ in Fig. 4.10) for a given temperature. The remaining part is the interior first order phase transition, which goes from order (staggered magnetization in x direction) into different order (staggered magnetization mainly in y direction). This transition can be defined through the free energy of the corresponding phases (◆ in Fig. 4.10).

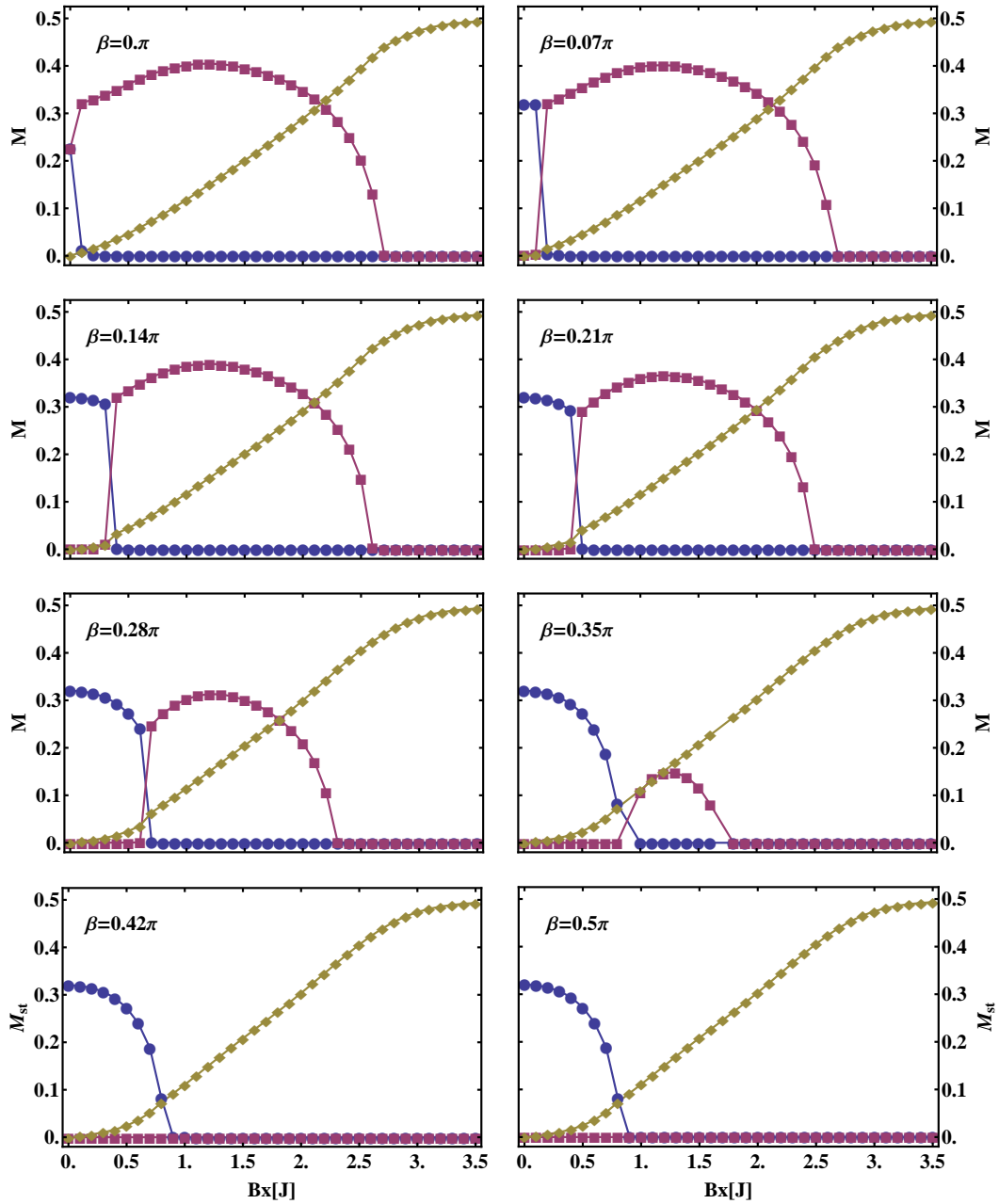


Figure 4.11: ● M_{st}^x , ■ M_{st}^y , ◆ M_{un}^x

Shown are plots of the uniform magnetization (x) and staggered magnetizations (x and y) as function of the external field B_x for several easy-plane angles β at the temperature $T = 0.2$. The 'holes', e.g. for high angles below $B_x = 1.25$ or at fields closed to those at which M_{st}^x vanishes and M_{st}^y emerges, are points where the iteration process does not find a converged solution.

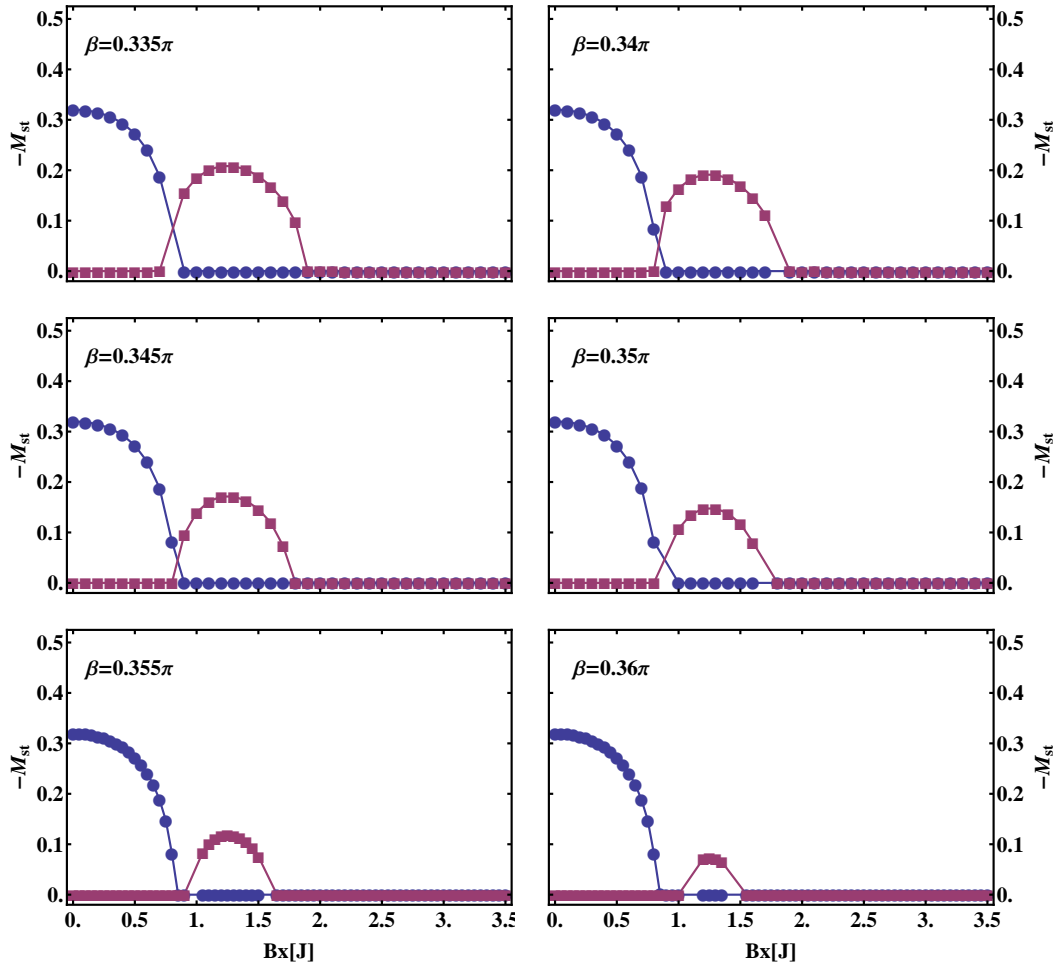


Figure 4.12: ● M_{st}^x ; ■ M_{st}^y

Here a small angle range at which the staggered magnetizations (for description see caption of Fig.4.11), separate is shown, again for $T = 0.2$. In short this fact indicates, that at the intermediate field, the system already is in the non ordered phase, where below and above there is still order. For more detailed description see Sec. 4.5.1.

4.5.2 Free energy

One has to keep in mind, that this solution depends on the initial magnetic fields.

First of all the basic feature of the spontaneous symmetry breaking mentioned above should be made explicit. One main aspect of this fact is, that the free energy has two minima for temperatures below the transition temperature. With the artificial breaking of the symmetry in the staggered magnetization (see Sec. 4.5.1) one chooses one of the two minima in the free energy. This induces the fact, that there should be an coexistence region in which both phases M_{st}^x and M_{st}^y can be finite. This region is not been investigated, but the transition field B_{c1} is examined at which the Mf free energies of the two phases cross as function of external field.

For this purpose consider the Fig.4.14 where the level crossing for different angles β is shown. The several curves are obtained by a restriction of the Mf solution to the specific phases. The statement of these curves is, that the Mf solution, or the iterative approach can not decide at every point which of the two minima is the global minima. This is the case at each curve where both free energies do not coincide. Both curves represent solutions to the Mf equations, but the corresponding free energies does not coincide generally. The difference is induced through different initial fields, favouring staggered magnetization either in x or y -direction.

In Fig. 4.14 ($\beta = 0.2\pi$, $\beta = 0.25\pi$) at a finite distance to the critical field the free energy of the higher level falls down on the ground state free energy. This are the points at which the Mf solution finally converges to the right solution, namely the minimal free energy solution. If one would zoom in, one would find the crossing of the corresponding Mf free energies up to an angle $\beta = \pi/2$. In the special case, where $\beta = 0$ only for zero field the system forms staggered magnetization in x -direction. The reason for this fact is, that for $\beta = 0$ there is no compensation process for the anti parallel aligned spins, which constitute the Néel _{x} phase.

Concluding it is shown, how one can determine the expected phase transition line in the given model of coupled anisotropic Heisenberg chains. It was calculated the susceptibility and additionally the Mf free energies to extract the transition lines.

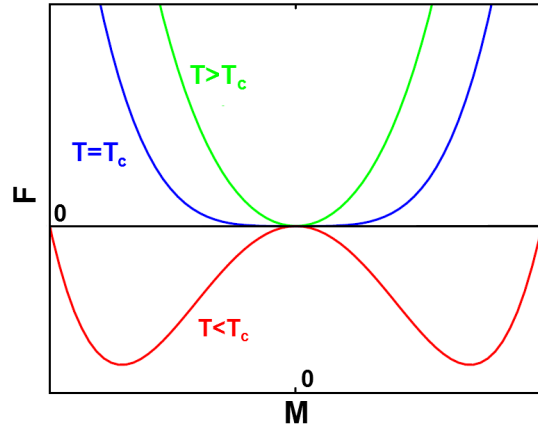


Figure 4.13: Shown is the free energy as function of magnetization for the temperature being above $T > T_c$, exactly $T = T_c$ and below $T < T_c$ the critical temperature. The Mf approach artificially produces two minimas in the free energy¹⁶

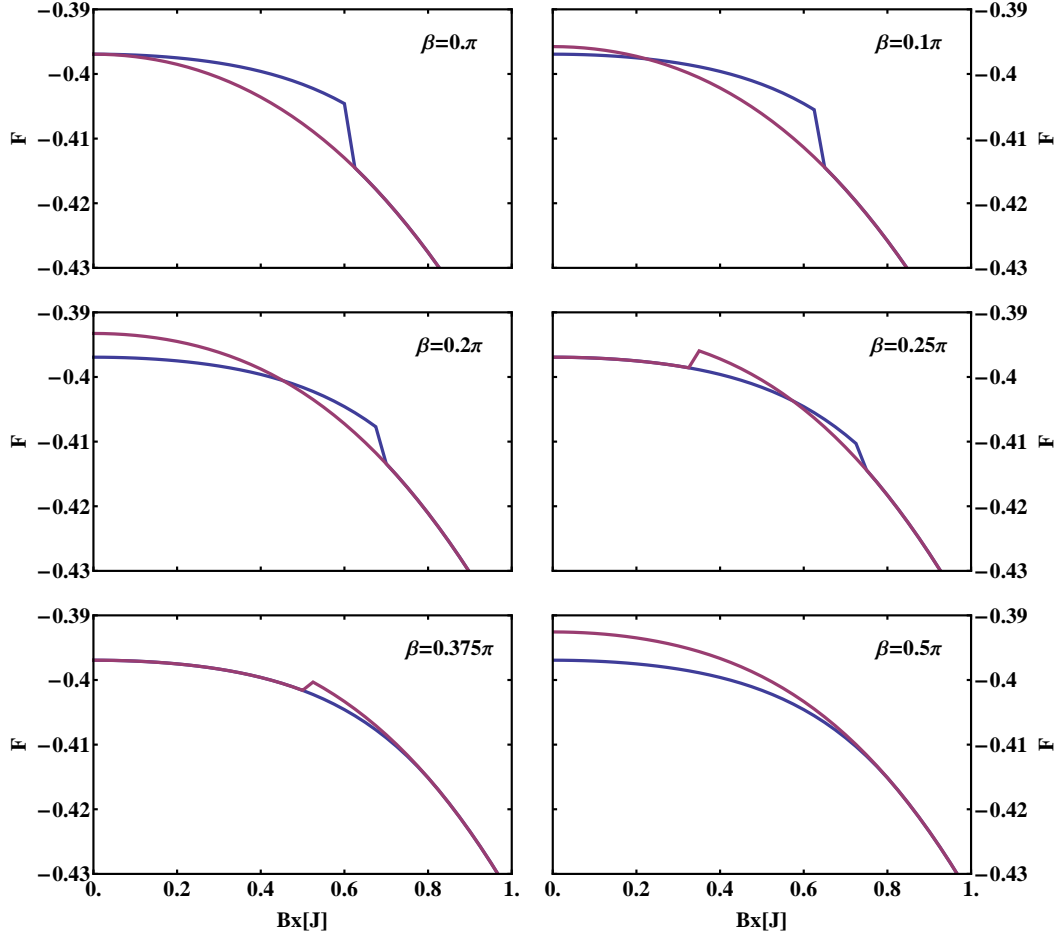


Figure 4.14: M_{st}^x ; M_{st}^y
 Shown are the free energies of the two phases as function of external magnetic field, the M_{st}^x and the M_{st}^y phase. The specific shape of the curves is explained in the text of Sec. 4.5.2. The central aspect for each curve is the point of level crossing, e.g. for $\beta = 0.25\pi$ at $B_x \simeq 0.6$, showing that the ground state changes.

4.5.3 Phase diagrams

In this section the resulting phase diagrams are presented and classified in a more general context.

The relative angle between the easy-planes is varied to be $0 \leq \beta \leq \pi/2$. For an angle of $\beta = 0$ the system immediately is in the yz staggered phase, also called spin flop phase. As mentioned above an angle of $\beta = \pi/2$ is the point at which the antiferromagnetic phase is the ground state for all external fields, up to the critical field which induce the paramagnetic order. The case of $\beta > \pi/2$ is represented in the mentioned interval, and thus the two limits $\beta = 0$ and $\beta = \pi/2$ are the limits to consider. From Sec. 4.5.2 one can see, that one does not have to calculate at these borders the order to order phase transition, as the system is either in the spin flopped phase ($\beta = 0$) or in the antiferromagnetic phase ($\beta = \pi/2$). Another aspect concerning numerical values of parameters is the absolute value of the inter chain coupling. In the paper from Dmitriev *et al.*¹⁹ it was proposed that the inter chain coupling is about $10^{-2}J$, namely $J'' = 0.0147J$. The difference to the presented work is, that for this proposition, parallel chains of equal type were assumed. This in contrast to two types of chains, which are coupled frustrated and non frustrated in the presented work. In the paper of Starykh *et al.*²⁹ concerning the material Cs_2CuCl_4 , it is claimed, that $J' \simeq 0.34J$ and $J'' \simeq 0.05J$. In the calculation done for the presented work the two parameters were set equal $J' = J''$. Due to finite size effects, only inter chain couplings of around $J' \simeq 0.3J$ could be accessed. For smaller values the Mf equations and their iterative solution does not generate staggered magnetizations. This is related to a gap which is induced by the finite length of the considered chain and has to be overcome by the inter chain coupling. This is only fulfilled for $J' > J/L$. This certainly restricts the considered inter chain coupling from below to certain values.

There are several limitations related to calculation time and file size. As in every iteration step the mentioned expectation values are calculated (by means of numerical diagonalization techniques) the calculation had a time constrained by this. Moreover only systems of the size of $L = 6, 8$ could be calculated, due to the mentioned reasons. At this stage it would be meaningful to redo the calculation with a `c++` program to enable calculation for system sizes such as $L = 12$. As there is a temperature scale defined through the system size, the interchain coupling itself is restricted to certain values. This is the reason why only such unrealistic values for J' were accessible.

The diagrams obtained by the procedure described above are presented in Fig. 4.16. Except the special cases $\beta = 0$ and $\beta = \pi/2$ the diagrams show the following qualitative behaviour. Coming from $B_x = 0$, the critical temperature decreases with increasing magnetic field until a local minimum of the critical temperature is reached. The transition line (\blacklozenge) separating the two ordered phases end at this minimum. At this point one can ask how the three lines touch, which could be examined using a Ginzburg-Landau theory. Moreover the critical temperature has a maximum in the Ising ordered phase at a finite field $B_{c1} < B_x < B_{c2}$. Above the critical field B_{c2} there is no order anymore. Additionally one can examine how the critical field in between the two ordered phases, behaves as function of β and J'' . This qualitative behaviour will analysed and checked for convenience in Sec. 4.5.4.

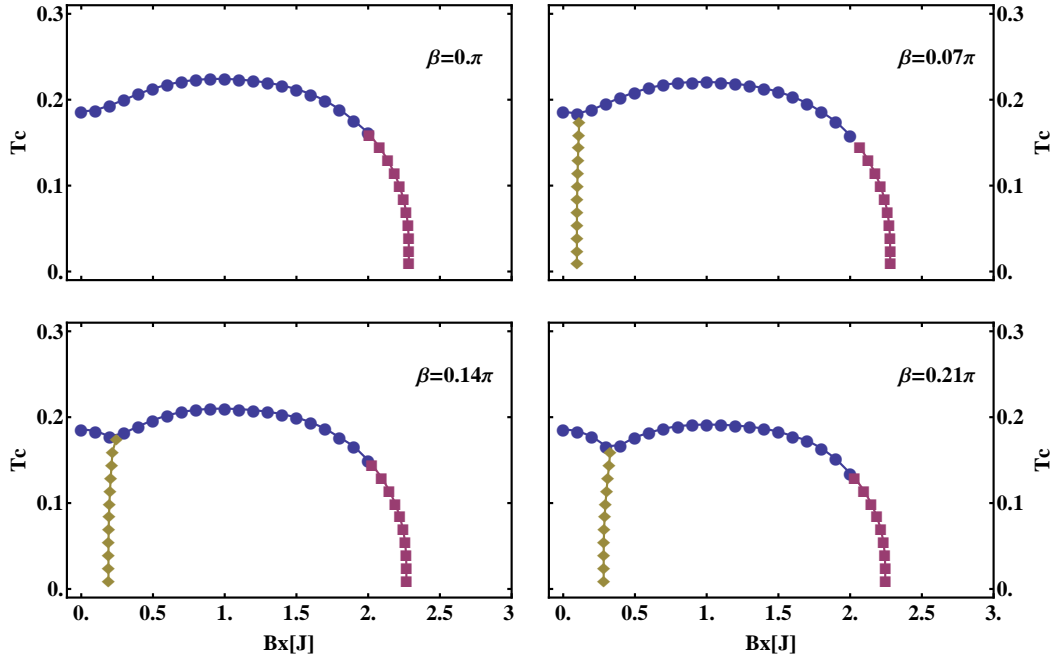


Figure 4.15: $\bullet \chi_{st}[T] \stackrel{!}{=} 1$; $\blacksquare \chi_{st}[B_x] \stackrel{!}{=} 1$; $\blacklozenge \tilde{\mathcal{F}}_x \stackrel{!}{=} \tilde{\mathcal{F}}_y$
 In this figure the phase diagram of the coupled XXZ chain in an transverse field for varying angle β is shown. The inter chain coupling is set to $J' = J'' = 0.3J$. This is the smallest numerical value, allowing staggered order to develop. One can see nicely the maximum in the critical temperature, which is explained in Sec. 4.5.4.

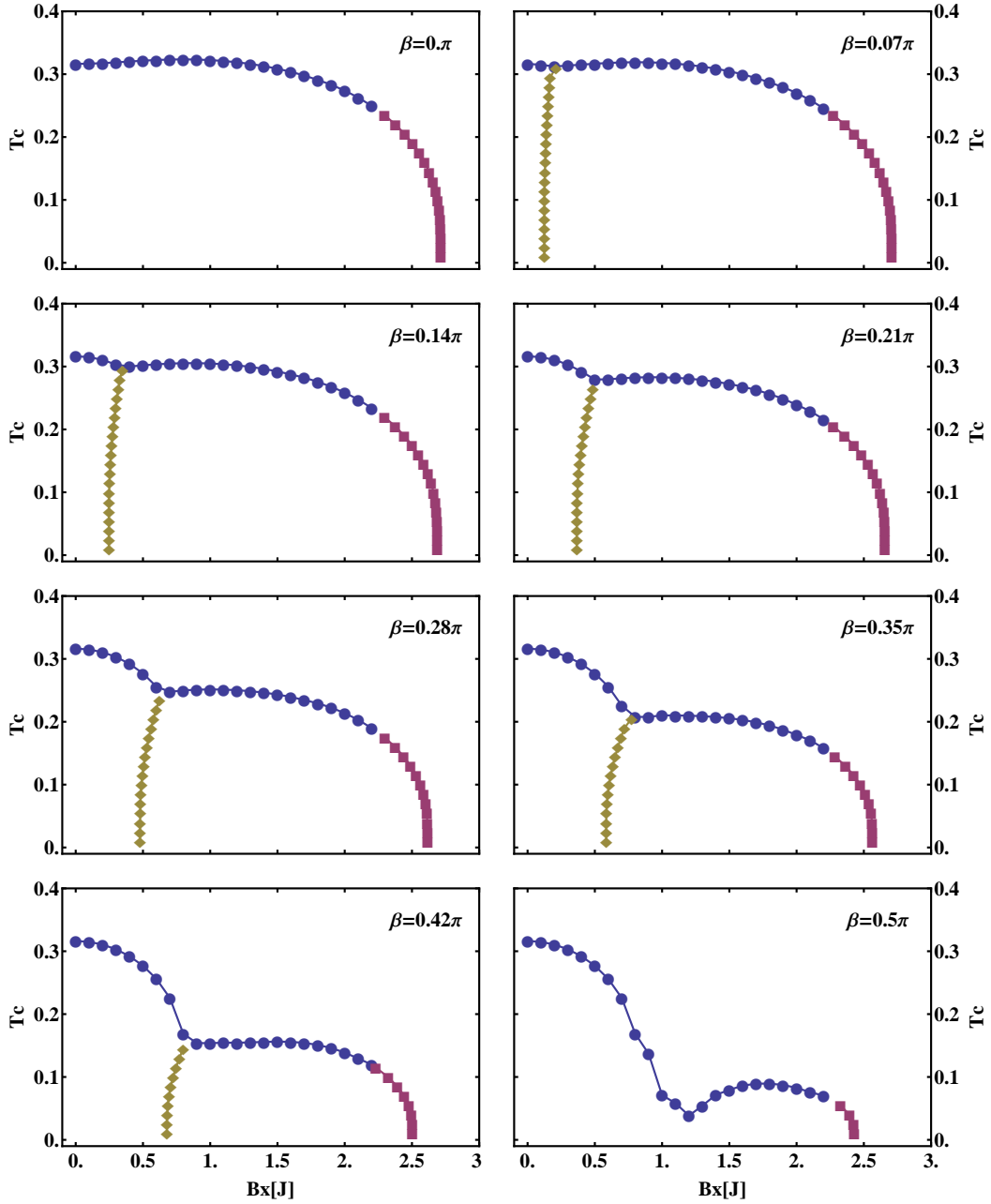


Figure 4.16: ● $\chi_{st}[T] \stackrel{!}{=} 1$; ■ $\chi_{st}[B_x] \stackrel{!}{=} 1$; ◆ $\tilde{\mathcal{F}}_x \stackrel{!}{=} \tilde{\mathcal{F}}_y$

In this figure the phase diagram of the coupled XXZ chain for a fixed the inter chain coupling $J' = J'' = 0.5J$ and varying angle β is plotted. In contrast to Fig. 4.15 the maximum in the critical temperature is mostly suppressed. In general all critical quantities (temperature and field) is shifted to larger values in comparison with the results for smaller J'' . Because one has to set the interchain coupling to such values (finite size effect) one can not compare quantitatively the critical fields obtained by the numerical approach with the experimental data.

An other aspect is the comparison with the experimental phase diagram. The phase diagram shown in Fig. 4.2 contains much more structure than the XXZ model can explain under the condition it was considered. Possible explanations for the emergence of the phases I and II were given in Sec. 4.1.2. To make a comparison between the numerical and experimental results, one has to make several identifications. One can identify the $T = 0$ critical fields B_{c1} and B_{c2} in Fig. 3.11 with the critical fields in the theoretical results Fig. 4.16. In turn this fields correspond in the following relation to the fields in Fig. 4.2:

$$\text{AF} \leftrightarrow \text{SF}: \quad H_{c0} = H_{c1} \rightarrow B_{c1} \quad (4.14)$$

$$\text{SF} \leftrightarrow \text{PM}: \quad H_{c3} = H_{c2} \rightarrow B_{c2}. \quad (4.15)$$

The equalities $H_{c0} = H_{c1}$ and $H_{c3} = H_{c2}$ occur because the used Mf approach cannot distinct the mentioned phases I and II (described in Sec. 4.1.2). From a quantitative comparison of the mentioned fields one can not expect much insight. As the critical quantities depend strongly on the chosen interchain coupling (cf. Fig. 4.15 and Fig. 4.16). Because this parameter had to be chosen in a unrealistic regime one can not assume to reproduce realistic quantitative results.

Behaviour of the spin flop field B_{c1}

One can verify, that the spin flop field B_{c1} is linear in the angle β as proposed in Eq. (3.97) in Sec. 3.4.3. For this purpose for a fixed arbitrary temperature $T = 0.085$ the critical field B_{c1} obtained by the free energy calculations is shown in Fig. 4.17. A

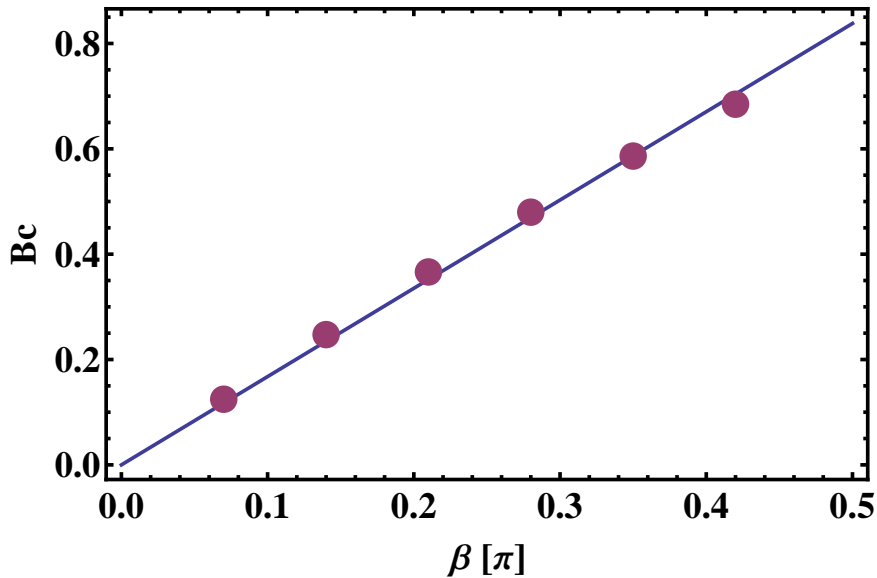


Figure 4.17: ● B_{c1} ; — Linear fit

Shown are the critical fields B_{c1} for several angles β at the temperature of $T = 0.085\text{K}$. A line fit shows the almost perfect linear behaviour as derived in Eq. (3.97)

numerical fit gives the following result:

$$B_{c1} \simeq 1.68\beta, \quad (4.16)$$

for $J'' = 0.5J$. This result is comparable, there is a deviation of 6% with the result of the linearised equation 3.97 which gives $B_{c1} \simeq 1.58\beta$ for $z = 2$. In principle using this formula one could give an estimate for the angle manifested in the material. This estimate would work, if a realistic inter chain coupling could be chosen, which is obviously not the case for the system sizes considered in the calculation.

4.5.4 Scaling estimates

In this section, scaling estimates will be used to classify the characteristics in the obtained phase diagrams, mentioned in the previous section. In certain limits the coupled XXZ model maps onto different known models. One specific limit is the case where the angle between the easy-planes is zero. Here the two limits $1.B = 0$: quasi long range order (qAF) and $2.0 < B \leq B_{c2}$: SF or Ising phase (see Fig. 3.11) are considered. In the paper of Dmitriev *et al.*¹⁹ beside other things a similar analysis can be found. In a third regime, the AF or Néel_x phase: $\beta \neq 0$ and $0 < B_x \leq B_{c1}$, with staggered magnetization along the x -direction, is studied.

qAF: $\beta = 0$ and $B_x = 0$

In the case where $B_x = 0$ the XXZ system can be described by a Luttinger liquid theory, shown by Peschel *et al.*³⁴. This can be used to show, that the critical temperature is finite in the vicinity of small fields, or more exactly that the system has a finite $B_x = 0$ transition temperature. In the Luttinger liquid model the spin-spin correlation functions, in the limit $|i - j| \rightarrow \infty$, have the following asymptotics³⁵:

$$\langle S_i^{x(y)} S_j^{x(y)} \rangle = \frac{A_1}{|i - j|^{\vartheta+1/\vartheta}} + \frac{(-1)^{i-j} A_2}{|i - j|^\vartheta} \quad (4.17)$$

$$\langle S_i^z S_j^z \rangle = \frac{A_3}{|i - j|^2} + \frac{(-1)^{i-j} A_4}{|i - j|^{1/\vartheta}} \quad (4.18)$$

Where the A_1 and A_2 are constants, and the exponent ϑ is given exactly to be:

$$\vartheta = 1 - \frac{\arccos \Delta}{\pi} \quad \text{with } \Delta = 0.25 \quad \vartheta \simeq 0.580. \quad (4.19)$$

All parameters have to be thought as function of the anisotropy Δ . In the following all stated numerical values of certain parameters are evaluated for $\Delta = 0.25$. The parameter ϑ is connected to the Luttinger parameter $K = (2\vartheta)^{-1} \simeq 0.861$. The non alternating term in Eq. (4.17) provides scaling dimensions for the spin operator S^x to be $d = \frac{1}{2}(\vartheta + \vartheta^{-1})$. In the book of Gogolin *et al.*³⁶ a formula for the mass gap as function of external field is given to be:

$$m[B] \sim B_x^\nu \quad \text{where} \quad \nu = \frac{1}{2-d} = \frac{2}{4-\vartheta-\vartheta^{-1}} \simeq 1.179 \quad (4.20)$$

Moreover Dmitriev *et al.*¹⁵ state that the staggered magnetization in the y direction behaves as:

$$\langle S_i^y \rangle \sim (-1)^i m^{\vartheta/2} \quad \text{with Eq. (4.20):} \quad \langle S_i^y \rangle \sim (-1)^i B_x^{\frac{\vartheta}{4-\vartheta-\vartheta^{-1}}} \quad (4.21)$$

Now one can think of a small perturbation δH to the Luttinger liquid theory created by the staggered fields. Especially the staggered magnetization $M_{st}^y \equiv L^{-1} \sum_i \langle S_{st,i}^y \rangle$ will be used. A staggered spin operator is defined through $S_{st,i}^y = (-1)^i S_{st}^y$. This staggered magnetization enters the Hamiltonian via the Mf treatment of J'' described in Sec. 3.2 using Eq. (4.17):

$$\delta H = J' M_{st}^y \frac{1}{L} \sum_i S_{st,i}^y \sim \langle S_{st,i}^y S_{st,j}^y \rangle = (-1)^{i+j} \langle S_{st}^y S_{st}^y \rangle \quad (4.22)$$

With Eq. (4.17) and taking only the alternating or staggered part one obtains, that $\delta H \sim |i-j|^{-\vartheta}$. Now one can use the notation of Peschel *et al.*³⁴ where the correlation functions are written time dependent. Basically the absolute value of the difference appearing in Eq. (4.17) is written to be $|i-j|$. Followingly one uses the definition of the staggered susceptibility, which is in this notation:

$$\chi_{st} = \int \langle S_{st,i}^y S_{st,j}^y \rangle dx dt \sim -\frac{|i-j|^{2-\vartheta}}{1-3\vartheta+\vartheta^2} \quad (4.23)$$

With the new exponent $\vartheta' = 2 - \vartheta$ this reads in the initial notation:

$$\chi_{st} \sim |i-j|^{\vartheta'} \quad \vartheta' = 1 + \frac{\arccos \Delta}{\pi} \simeq 1.420 \quad (4.24)$$

Via the length scale $a|i-j| \sim T^{-1}$ on can introduce temperature in Eq. (4.24):

$$\chi_{st} \sim \left(\frac{1}{T}\right)^{\vartheta'} \sim \frac{1}{J} \left(\frac{J}{T}\right)^{\vartheta'} \quad (4.25)$$

Where J was introduced due to dimensional reasons and as there is only this energy scale available. As mentioned above, at the critical temperature the product of inter-chain coupling and susceptibility becomes unity $J'' \chi_{st} = 1$. Using this fact with Eq. (4.25) one obtains an expression for the critical temperature:

$$\frac{T_c}{J} = \left(\frac{J''}{J}\right)^\alpha \quad \text{with} \quad \alpha \equiv \frac{1}{\vartheta'} \simeq 0.704 \quad (4.26)$$

This derivation provides an expression for the critical temperature for the Néel_x phase. The evaluation of Eq. (4.26) for the above mentioned value of the interchain coupling $J'' = 0.0147J$ results in the critical temperature of: $T_c/J = 0.039$. This derivation shows, that the critical temperature is finite for $B_x = 0$.

Ising: $\beta = 0$, $\mathbf{B}_x \neq 0$ and $\beta \neq 0$, $\mathbf{B}_{c1} < \mathbf{B}_x < \mathbf{B}_{c2}$

If there is a finite angle one can still think of the Ising phase to be realized for field values: $B_{c1} < B_x < B_{c2}$. In this phase the system gains energy from tilting the spins towards the field direction. In contrast to this it loses energy, because partially they are parallel in conflict with the favoured antiferromagnetic ordering. Starting at B_{c1} , the external field suppresses fluctuations and thus it is obvious that the critical temperature firstly increases with increasing field. At a specific field the gain due to the suppression of fluctuations is overcome by the loss due to the parallel alignment. At this point the critical temperature is maximal and followingly decreases. This can be concluded to the fact that the critical temperature firstly increases in the Ising phase until a maximum is reached. Secondly it decreases with increasing field. At a specific field the spins are totally aligned parallel and thus no long range order except the mentioned paramagnetic order is present and thus the transition temperature vanishes.

Assuming the system to be deep in the Ising phase it will be shown that the critical temperature has a maximum as function of external field. In this phase the staggered susceptibility is given as an exponential of the massgap $m[B_x]$:

$$\chi_{st} = e^{m[B_x]/T} \quad (4.27)$$

depending itself on the external field. This formula provides the proof that there is a maximum in the critical temperature. The susceptibility in Eq.(4.25) depends on T as a power law, but in Eq.(4.27) it depends exponentially on temperature. Thus the susceptibility in the Ising phase becomes unity for higher temperatures than in the qAF phase. Again with the dimensionality argument and the criticality condition $J'\chi_{st} = 1$ one obtains the critical temperature for the Ising phase:

$$\frac{T_c}{J} = \frac{m[B_x]}{\log J/J'} \quad \text{with } J \sim m \quad \frac{T_c}{J} \simeq 0.217 \quad (4.28)$$

This last value is about five times larger than the zero field Néel temperature of $T_c/J = 0.039$. Exactly this fact explains the maximum in the phase diagrams.

AF: $\beta \neq 0$ and $\mathbf{B}_x < \mathbf{B}_{c1}$

In this regime, one expects the critical temperature firstly to decrease until the external critical field $B_x = B_{c1}$ is reached. This fact can be understood in the light of an energy balance. The spins per chain gain energy by their antiparallel alignment (AF). Simultaneously there is an energy loss, due to every second spin pointing against the field. This loss is overcome by the finite angle β and in order to that, by the gain of antiferromagnetic energy by interchain coupling. It is obvious, that with increasing external field, the energy loss increases as well. In other words, the energy scale at which the system stays in the ordered phase becomes smaller with increasing field. This can explain, why the critical temperature, as a measure of the fundamental energy scale decreases with the field strength.

4 Numerical solutions

The same applies for the Ising phase and the decrease of the critical temperature reaching the critical field B_{c2} . Here as well the energy scale for which the ordered phase survives is reduced by approaching the critical field.

The previous section can be summarized by the following statements. It was shown, that the obtained phase diagrams reproduce the features occurring in the experimental data. The critical temperatures have the right order. Moreover the theoretical scaling estimates provide a full agreement between the theoretic limits and their integration in the obtained numerical results.

5 Summary

Summary

In the presented work the Cs_2CoCl_4 system was used as a starting point for several theoretical considerations. Experimental data obtained by Breunig were a motivation to calculate the specific heat of the mentioned system. Furthermore the phase diagram was calculated and compared to experimental data. In this summary the used concepts and their results should be presented.

The mentioned physical system Cs_2CoCl_4 can be described as a compound of weakly coupled spin chains. First of all the picture of local spin-spin interactions on a one dimensional chain was developed. This considerations were related to several Heisenberg chains with varying anisotropy term Δ . The influence of such terms as well as the effects of a coupled external magnetic field was considered. At this stage it is fundamentally important to distinguish between longitudinal and transversal fields. The different ground states of this several models are discussed in dependence on Δ , β and B_x .

In the second chapter of this work the principle of Mf theory for specific cases is developed. This principle was used to describe the behaviour of the spins in the chain, as well as to describe the effects occurring through the coupling of those chains. One central aspect of the work is the Bogoliubov inequality $\mathcal{F} \leq \tilde{\mathcal{F}} \equiv \mathcal{F}_{\text{Mf}} + \langle \mathcal{H} - \mathcal{H}_{\text{Mf}} \rangle_{\text{Mf}}$. It gives an upper bound of the free energy for a well chosen reference system \mathcal{H}_{Mf} . It was necessary to develop certain approximations such as the used Mf approach to solve the considered models. Two particle terms are decoupled using the evaluation of expectations values with respect to \mathcal{H}_{Mf} . With the definition of a reference system new parameters were introduced. This so called Mf fields or parameters can be determined as follows. First of all, there can be found a relation between the new parameters and the expectation value of involved operators. This is done using the minimum condition of the Mf free energy $\tilde{\mathcal{F}}$, where this is used as a approximation to the free energy. From this self consistent equations arise, which can be solved iteratively or equivalently by minimization of the free energy with respect to such parameters.

This values obtained by the mentioned techniques can be used e.g. to calculate thermodynamic quantities. The comparison of the numerical data with the experimental data show surprisingly good coincidence for high fields. For small fields there is a discrepancy which can be understood considering a symmetry argument.

Basically in the same way, self consistent equations were derived in the case of coupled chains. In contrast to further works on this material, different chain types are considered. The specific type is defined through the orientation of the corresponding easy-plane. The self consistent equations derived by this, are solved iteratively to obtain

5 Summary

the phase diagram. It was possible to qualitatively reproduce the theoretical predicted response of the material. For fields below B_{c1} the system orders antiferromagnetically in the field direction, this phase is called Néel_x or simply antiferromagnetic phase. With increasing field (temperature) the system undergoes a first order quantum phase transition into the so called spin flop (SF) or Ising like (paramagnetic (PM)) phase. In the SF-phase all moments have a finite staggered component perpendicular to the field direction and in addition they are tilted towards the field, which result in a finite uniform magnetization. The basic difference between the first phase and the SF- or PM-phase with finite magnetization in the same direction induces, that the phase transition has to be first order. The SF-phase is additionally bounded by a second order phase transition line. For fields above B_{c2} and temperatures above the given critical temperature the system transits into the paramagnetic phase.

Further remarks

With larger system sizes the described features of the phase diagram are expected to be more pronounced. This is because J' can be chosen more realistic. Moreover one can use a cluster calculation to obtain the real lowest upper bound for the free energy, where the presented calculation only calculates a free energy approximation for the length L system. Moreover without the restriction to two types of chains (A and B \rightarrow {1,2,3 and 4} sites) one could introduce realistic effects by an spin-orbit term. This would allow a interaction of the staggered moments between the planes and thus it is expected, that the phase I in Fig. 4.2 can be reproduced.

Deutsche Zusammenfassung

In der vorliegenden Arbeit wurde das Cs_2CoCl_4 System als Ausgangspunkt theoretischer Betrachtungen benutzt. Die experimentellen Daten, welche von Breunig gemessen wurden, waren eine Motivation die spezifische Wärmekapazität auf theoretische Art und Weise herzuleiten. Weiterhin wurden ermittelte Phasendiagramme mit ebenfalls gemessenen verglichen. In der hier angefertigten Zusammenfassung sollen die verwendeten inhaltlichen Konzepte dargestellt werden. Weiterhin soll beschrieben werden, mit welcher Zielsetzung und welchen Ergebnissen diese entwickelt und ausgewertet werden konnten.

Das betrachtete physikalische System lässt sich als schwach gekoppelte anisotrope Spin Ketten beschreiben. Zunächst wurde das Bild der lokalen Spin-Spin Wechselwirkung im Sinne von in eine Richtung gekoppelte Atome im Allgemeinen betrachtet. Diese Betrachtung bezog sich auf verschiedene Heisenberg Modelle, mit einem variierenden Anisotropie term Δ . Es wurden sowohl die verschiedenen Einflüsse dessen beschrieben, als auch die unterschiedlichen Effekte, die ein angekoppeltes Magnetfeld B_x haben kann betrachtet. Hier ist es von entscheidender Wichtigkeit, zu unterscheiden, ob das Feld longitudinal oder transversal in Relation zum Anisotropieterm ist. Aus diesen allgemeinen Betrachtungen wurden die verschiedenen Grundzustände der sich ergebenden Modelle (in Abhängigkeit von Δ , β und B_x) beschrieben.

Im zweiten Abschnitt der Arbeit wurde das Prinzip der Mean field Theorie für die entsprechenden Fälle entwickelt. Das genannte Prinzip wurde genutzt, um sowohl das Verhalten der Spins innerhalb der Ketten zu beschreiben als auch die Effekte, die aus der Kopplung der Ketten entspringen, aufzuspüren. Als ein zentraler Aspekt dieser Arbeit kann die Bogoliubov Ungleichung $\mathcal{F} \leq \tilde{\mathcal{F}} \equiv \mathcal{F}_{\text{Mf}} + \langle \mathcal{H} - \mathcal{H}_{\text{Mf}} \rangle_{\text{Mf}}$ betrachtet werden. Sie gibt eine Obergrenze der freien Energie an, wobei ein geschickt gewähltes Referenzsystem \mathcal{H}_{Mf} gewählt werden muss. Da das untersuchte System nicht exakt lösbar ist, wurden Näherungsmethoden, die der Mf Theorie zugeschrieben werden, benutzt. So werden nicht lokale Operatoren beziehungsweise zwei Teilchenterme durch die Bildung des Erwartungswertes bezüglich \mathcal{H}_{Mf} entkoppelt. Mit der Definition und Festlegung eines Referenzsystems werden auch neue Parameter eingeführt. Diese sogenannten Mf Felder oder Parameter im Allgemeinen, können wie folgt bestimmt werden: Zunächst lässt sich ein formaler Zusammenhang zwischen den neu eingeführten Parametern und entsprechenden Erwartungswerten über die Minimums Bedingung des Ausdrucks F_{MF} finden. Die sich so ergebenden selbstkonsistenten Gleichungen lassen sich entweder iterativ oder durch die Minimierung des genannten Ausdrucks in Bezug auf die erhaltenen Parameter lösen.

Die auf diese Art gefundenen Parameter können genutzt werden, um z.B. thermodynamische Größen zu bestimmen. Der Vergleich mit den experimentellen Daten zeigte

überraschend gute Übereinstimmung mit den numerischen Daten für hohe Felder.

Im Prinzip wurden auf dieselbe Weise selbstkonsistente Gleichungen für den Fall von gekoppelten Ketten hergeleitet. Anders als in bereits erschienenen Arbeiten, wurden hier verschiedene Arten von Ketten gekoppelt. Die Verschiedenheit ist über die Ausrichtung der Easyplane der entsprechenden Kette definiert. Die so erhaltenen Mf Gleichungen wurden iterativ gelöst, mit dem Ziel der Berechnung des Phasendiagramms. Theoretisch erwartet und numerisch bestätigt wurde, dass das Material zunächst antiferromagnetisch (in Feld Richtung!) reagiert. Diese erste Phase, welche bis zu einem endlichen kritischen Feld B_{c1} und einer kritischen Temperatur T_c Bestand hat, wurde als antiferromagnetische Phase bezeichnet. In Abhängigkeit vom externen Feld (Temperatur) findet ein Quantenphasenübergang erster Ordnung statt. Der Grundzustand ändert sich abrupt in die SF- (PM-)Phase, in welcher sich die Momente senkrecht zum Feld ausrichten. In der SF-Phase können sich, im Gegensatz zur ersten Phase, endliche Magnetisierungen in Feldrichtung ergeben. Allerdings sind die Komponenten der Momente in der Ebene senkrecht zur Feldrichtung antiparallel ausgerichtet. Die Tatsache, dass der Phasenübergang zwischen der ersten Phase (antiparallele Ausrichtung der Momente in Feldrichtung) und der SF- oder PM-Phase (endliche uniforme Magnetisierung in Feldrichtung) stattfindet, macht deutlich, dass es sich hier um einen Übergang erster Ordnung handeln muss. Des Weiteren wird die SF-Phase von einem Quanten Phasenübergang zweiter Ordnung begrenzt. Für entsprechende Felder oder Temperaturen, geht das System in den, als paramagnetische (PM) Phase bezeichneten Zustand, in welchem nur uniforme Magnetisierung in Feld Richtung erzeugt wird.

Da in jedem Iterationsschritt die Erwartungswerte mit Hilfe numerischer Diagonalisierung berechnet wurden, waren die Berechnung durch Laufzeiten und Speicherkapazitäten stark limitiert. Es konnten nur kleine Systemgrößen $L = 6, 8$ betrachtet werden. An dieser Stelle wäre es sicherlich sinnvoll, die bestehende Rechnung in einem c_{++} Programm zu wiederholen. Hier wären Systemgrößen bis $L = 12$ sicherlich möglich. Da durch die Systemgröße auch eine Temperaturskala definiert ist, wird somit auch die Zwischenkettenkopplung auf einen bestimmten Wertebereich festgelegt. Dies erklärt, warum nur unrealistisch große Werte für J' genutzt wurden. Mit der Berechnung der Phasendiagramme für größere Systeme kann erwartet werden, dass auch die beschriebenen Eigenschaften deutlicher werden, da J' realistischer gewählt werden kann. Weiterhin ist es möglich ohne die Beschränkung auf zwei Kettentypen (A und B $\rightarrow \{1,2,3$ und $4\}$ sites) realitivistische Effekte über einen Spin-Bahn Term einzuführen. Dieser würde eine Wechselwirkung zwischen den gestaggerten Momenten verschiedener Ebenen erlauben. Dies wiederum könnte die mit I in Fig. 4.2 bezeichnete Phase reproduzieren.

Acknowledgements

During the time of working and writing on my Master thesis, many people supported me. First of all I would like to thank my supervisors Eran Sela and Achim Rosch. Without their deep insight in the physics I considered this work would not exist. The possibility to discuss at any time and this with patience was a strong support I could not imagine.

Moreover I would like to thank everybody whom I could ask for help concerning the every day issues.

Also I would like to thank all the people I live together supporting me during the last months.

Declaration

I hereby certify that the work presented here was accomplished by myself and without the use of illegitimate means or support, and that no sources and tools were used than those cited.

Cologne, the August 21, 2012

Hiermit versichere ich, dass ich die vorliegende Arbeit selbstständig verfasst und außer den angegebenen Quellen keine weiteren Hilfsmittel verwendet habe. Alle Zitate habe ich kenntlich gemacht.

Köln, den 22. August 2012

List of Figures

2.1	Phase diagram ¹⁵ of the Heisenberg chain in a transverse field	12
3.1	Crystal structure of Cs ₂ CoCl ₄	14
3.2	Tetrahedral surrounding of Co ²⁺ ions by Cl ⁻	15
3.3	Term diagram of the Co ²⁺ ions	16
3.4	Introduction of the relative plane angle β	17
3.5	Magnetic structure results using neutron scattering ¹² of Cs ₂ CoCl ₄ for $B_x = 0$	18
3.6	Geometrical setup for the numerical calculation in 3d	20
3.7	ab - and bc -plane	21
3.8	Fig. 3.4	31
3.9	Definition of the relative angle β	32
3.10	Classical spin	34
3.11	Symbolic phase diagram for coupled chains	35
4.1	Experimental results ³⁰	42
4.2	Phase diagram of Cs ₂ CoCl ₄ ³⁰	43
4.3	Specific heat: experimental results vs. exact diagonalization ³⁰	45
4.4	Two level comparison	46
4.5	High temperature expansion vs. exact diagonalization specific heat	49
4.6	Numerically obtained dispersion relation	51
4.7	Mf Specific heat results	52
4.8	Low field inconsistency between exact diagonalization and Mf	53
4.9	Mf specific heat results	54
4.10	Exemplary phase diagram	55
4.11	Staggered magnetization curves at $T = 0.2$ I	57
4.12	Staggered magnetization curves at $T = 0.2$ II	58
4.13	Mf artifact: Two free energy minima	59
4.14	Comparison of the free energies	60
4.15	Phase diagram for certain parameters	62
4.16	Phase diagram for certain parameters	63
4.17	Linearity of the critical field B_{c1}	64

Bibliography

- [1] W. Heisenberg, *Zeitschrift für Physik A Hadrons and Nuclei* **49**, 619 (1928), ISSN 0939-7922, 10.1007/BF01328601, URL <http://dx.doi.org/10.1007/BF01328601>.
- [2] P. A. M. Dirac, *Proceedings of the Royal Society of London. Series A, Containing Papers of a Mathematical and Physical Character* **112**, pp. 661 (1926), ISSN 09501207, URL <http://www.jstor.org/stable/94692>.
- [3] H. E. Stanley, *Introduction to phase transitions and critical phenomena* (Oxford Univ. Pr., New York [u.a.], 1987), ISBN 0-19-505316-8.
- [4] R. P. Feynman, *Statistical mechanics*, *Frontiers in physics* (Benjamin, 1972), ISBN 0-8053-2509-3, 0-8053-2508-5.
- [5] H. Algra, L. de Jongh, H. Blöte, W. Huiskamp, and R. Carlin, *Physica B+C* **82**, 239 (1976), ISSN 0378-4363, URL <http://www.sciencedirect.com/science/article/pii/0378436376901868>.
- [6] C. N. Yang and C. P. Yang, *Phys. Rev.* **150**, 321 (1966), URL <http://link.aps.org/doi/10.1103/PhysRev.150.321>.
- [7] D. Dmitriev, V. Krivnov, A. Ovchinnikov, and A. Langari, *Journal of Experimental and Theoretical Physics* **95**, 538 (2002), ISSN 1063-7761, 10.1134/1.1513828, URL <http://dx.doi.org/10.1134/1.1513828>.
- [8] J. Kurmann, H. Thomas, and G. MÄ¶ller, *Physica A: Statistical Mechanics and its Applications* **112**, 235 (1982), ISSN 0378-4371, URL <http://www.sciencedirect.com/science/article/pii/0378437182902175>.
- [9] J. Kurmann, G. Muller, H. Thomas, M. W. Puga, and H. Beck, *Journal of Applied Physics* **52**, 1968 (1981), URL <http://link.aip.org/link/?JAP/52/1968/1>.
- [10] G. Lagmago Kamta and A. F. Starace, *Phys. Rev. Lett.* **88**, 107901 (2002), URL <http://link.aps.org/doi/10.1103/PhysRevLett.88.107901>.
- [11] E. Lieb, T. Schultz, and D. Mattis, *Annals of Physics* **16**, 407 (1961), ISSN 0003-4916, URL <http://www.sciencedirect.com/science/article/pii/0003491661901154>.
- [12] M. Kenzelmann, R. Coldea, D. A. Tennant, D. Visser, M. Hofmann, P. Smeibidl, and Z. Tylczynski, *Phys. Rev. B* **65**, 144432 (2002).
- [13] Z. N.-C. Ha, *Quantum Many-Body Systems in One Dimension* - (World Scientific, Singapur, 1996), ISBN 978-9-810-22275-8.

Bibliography

- [14] C. N. Yang and C. P. Yang, Phys. Rev. **150**, 327 (1966), URL <http://link.aps.org/doi/10.1103/PhysRev.150.327>.
- [15] D. V. Dmitriev, V. Y. Krivnov, and A. A. Ovchinnikov, Phys. Rev. B **65**, 172409 (2002), URL <http://link.aps.org/doi/10.1103/PhysRevB.65.172409>.
- [16] S. Sachdev, *Quantum phase transitions* (Cambridge Univ. Press, New York [u.a.], 2011), ISBN 978-0-521-51468-2, 0-521-51468-1.
- [17] P. Jordan and E. Wigner, Zeitschrift für Physik A Hadrons and Nuclei **47**, 631 (1928), ISSN 0939-7922, 10.1007/BF01331938, URL <http://dx.doi.org/10.1007/BF01331938>.
- [18] S. Mori, J.-J. Kim, and I. Harada, Journal of the Physical Society of Japan **64**, 3409 (1995), URL <http://jpsj.ipap.jp/link?JPSJ/64/3409/>.
- [19] D. Dmitriev and V. Krivnov, JETP Letters **80**, 303 (2004), ISSN 0021-3640, 10.1134/1.1825110, URL <http://dx.doi.org/10.1134/1.1825110>.
- [20] F. C. Alcaraz and A. L. Malvezzi, Journal of Physics A: Mathematical and General **28**, 1521 (1995), URL <http://stacks.iop.org/0305-4470/28/i=6/a=009>.
- [21] M. Tsukano and K. Nomura, Journal of the Physical Society of Japan **67**, 302 (1998), URL <http://jpsj.ipap.jp/link?JPSJ/67/302/>.
- [22] B. N. Figgis, M. Gerloch, and R. Mason, Proceedings of the Royal Society of London. Series A. Mathematical and Physical Sciences **279**, 210 (1964), <http://rspa.royalsocietypublishing.org/content/279/1377/210.full.pdf+html>, URL <http://rspa.royalsocietypublishing.org/content/279/1377/210.abstract>.
- [23] P. A. Reynolds, B. N. Figgis, J. Bruce Forsyth, and F. Tasset, J. Chem. Soc., Dalton Trans. pp. 1447–1454 (1997), URL <http://dx.doi.org/10.1039/A607650E>.
- [24] H. Yoshizawa, G. Shirane, H. Shiba, and K. Hirakawa, Phys. Rev. B **28**, 3904 (1983), URL <http://link.aps.org/doi/10.1103/PhysRevB.28.3904>.
- [25] J. N. McElearney, S. Merchant, G. E. Shankle, and R. L. Carlin, The Journal of Chemical Physics **66**, 450 (1977), URL <http://link.aip.org/link/?JCP/66/450/1>.
- [26] Y. Xu, S. Carlson, K. Söderberg, and R. Norrestam, Journal of Solid State Chemistry **153**, 212 (2000), ISSN 0022-4596, URL <http://www.sciencedirect.com/science/article/pii/S0022459600987449>.
- [27] J. N. McElearney, S. Merchant, G. E. Shankle, and R. L. Carlin, The Journal of Chemical Physics **66**, 450 (1977), URL <http://link.aip.org/link/?JCP/66/450/1>.
- [28] Richard L. Carlin and Ramon Burriel and Fernando Palacio and Rachel A. Carlin and S. F. Keij and David W. Carnegie, Jr., Journal of Applied Physics **57**, 3351 (1985), URL <http://link.aip.org/link/?JAP/57/3351/1>.

- [29] O. A. Starykh, H. Katsura, and L. Balents, Phys. Rev. B **82**, 014421 (2010), URL <http://link.aps.org/doi/10.1103/PhysRevB.82.014421>.
- [30] O. Breunig, Diploma thesis, Universitaet zu Koeln, II. Physikalisches Institut (2011).
- [31] J.-S. Caux, F. H. L. Essler, and U. Löw, Phys. Rev. B **68**, 134431 (2003).
- [32] A. Altland and B. Simons, *Condensed matter field theory* (Cambridge Univ. Press, Cambridge [u.a.], 2010), ISBN 978-0-521-76975-4.
- [33] B. Bauer, L. D. Carr, H. G. Evertz, A. Feiguin, J. Freire, S. Fuchs, L. Gamper, J. Gukelberger, E. Gull, S. Guertler, et al., Journal of Statistical Mechanics: Theory and Experiment **2011**, P05001 (2011), URL <http://stacks.iop.org/1742-5468/2011/i=05/a=P05001>.
- [34] A. Luther and I. Peschel, Phys. Rev. B **12**, 3908 (1975), URL <http://link.aps.org/doi/10.1103/PhysRevB.12.3908>.
- [35] T. Giamarchi, *Quantum physics in one dimension*, International series of monographs on physics ; 121 (Clarendon Press, 2007), ISBN 978-0-19-852500-4.
- [36] A. O. Gogolin, A. A. Nersesyan, and A. M. Tsvelik, *Bosonization and strongly correlated systems* (Cambridge Univ. Press, Cambridge [u.a.], 2004), ISBN 0-521-61719-7, 0-521-59031-0.